Dr. Eng. Thesis

Development of Amorphous RuO_2-Ta_2O_5/Ti Anode for Oxygen Evolution in Electrowinning

TIAN ZHANG

Supervisor: Prof. Masatsugu Morimitsu

Department of Science of Environment and Mathematical Modeling

Graduate School of Science and Engineering

Doshisha University

September 2015

Acknowledgements

First of all, I would like to express my deep sense of appreciation to my supervisor, Prof. Masatsugu Morimitsu, for his insightful guidance, strong support, great help, fruitful discussions, and supervision throughout my Ph.D. study. I am extremely proud I could work together with such a knowledgeable supervisor.

I would also express my appreciation to Assistant Prof. Kenji Kawaguchi, for his helpful discussions and comments.

I am also grateful to all members of Environmental Systems Engineering Laboratory of Doshisha University, including alumni and alumnae, for their cooperation and continuing encouragement.

Finally, I would like to thank my parents and sister for their deep understanding, support, and love.

June 2015

Tian Zhang

Abstract

Electrowinning is one of the most important metal production processes, consuming significant amounts of electric energy worldwide. The total energy consumed by electrowinning in U.S.A is the order of 1-2 % of the total energy consumption, and this high energy consumption is caused by a high voltage of the electrolysis, which is mainly due to oxygen evolution reaction; it is the anodic reaction in electrowinning using sulfuric acid based solutions. In case of copper electrowinning, the overpotential of oxygen evolution is approximately 10 times larger than that of the cathodic reaction, *i.e.*, metal deposition, and accounts for 25-40 % of the total cell voltage, when the anode comprises lead alloys which have been employed for a long time. In addition, the electrowinning solutions contain metal ions such as Pb(II), Mn(II), or Co(II) ions as a minor component, and these ions are also oxidized on lead alloy anodes, which are unwanted side reactions and result in anodic deposition of PbO_2, MnOOH or CoOOH. Such oxide depositions further increase oxygen overpotential and reduce the anode's lifetime, since the deposited oxides have a low conductivity and a low catalytic activity for oxygen evolution. Therefore, reduction in oxygen overpotential and suppression of anodic metal oxide deposition are much important to realize a more energy-efficient electrowinning process which can reduce the energy consumption and less metal oxide sludge originated from deposited metal oxides.

Ruthenium oxide (RuO_2) is known as the most active metal oxide for oxygen evolution in aqueous solutions, and RuO_2-based coatings have been widely investigated as an oxygen evolution catalyst, in which thermal decomposition of a precursor solution is usually used to prepare such oxide coatings on a titanium substrate. While RuO_2-based oxide coated titanium electrode is known to be highly catalytic for oxygen evolution in acidic media, there has been no practical applications of the electrode in electrowinning. In addition, the effects of thermal decomposition temperature on the RuO_2-based coatings have hardly been examined. From the background mentioned above, I aimed in this thesis to investigate the characterization and performance of

RuO_2-Ta_2O_5 coated titanium anodes prepared at different thermal decomposition temperatures and Ru:Ta mole ratios for electrowinning applications. The suppression effects to the anodic metal oxide deposition and the durability for oxygen evolution on these anodes were also studied.

RuO_2-Ta_2O_5/Ti anodes were prepared by thermal decomposition of precursor solutions containing Ru (III) and Ta (V). The temperature ranged from 260 ^oC to 500 ^oC, and the Ru:Ta ratio ranged from 30:70 mol% to 90:10 mol%. The characterization of the coatings was done with XRD, SEM and EDX. Voltammetric measurements were performed to obtain double layer charge, polarization curves, and Tafel slope in acidic aqueous solutions. Constant current electrolysis was conducted to measure the cell voltage during electrowinning of zinc, copper, nickel and cobalt and to evaluate the durability for oxygen evolution in continuous electrolysis.

The catalytic coatings prepared consisted of a mixture of amorphous RuO_2 and Ta_2O_5, when the thermal decomposition temperature was 280 ^oC or less. SEM observation revealed that the oxide coating comprised nano particles of RuO_2 uniformly dispersed in amorphous Ta_2O_5 matrix. One of the most specialized points of such amorphous oxides was that nano RuO_2 particles induced the increase in effective surface area and change in rate determining step for oxygen evolution, resulting in a significant decrease in oxygen overpotential. The amorphous RuO_2-Ta_2O_5/Ti electrode prepared at 80 mol% Ru and at 260 ^oC was found to be the best performance for oxygen evolution; the oxygen overpotential was 0.20 V lower than that prepared at 30 mol% Ru and at 500 ^oC, the amorphous oxide anode showed the increase in overpotential of PbO_2 deposition. As a result, the difference between the onset potentials of oxygen evolution and PbO_2 deposition reached 0.58 V with amorphous RuO_2-Ta_2O_5/Ti anode, and it was revealed that the overpotentials of these two reactions occurring on the same anode were individually controlled; amorphous RuO_2 works to accelerate oxygen evolution and suppress PbO_2 deposition. The amorphous oxide anode further demonstrated that the cell voltage of zinc or copper electrowinning was successfully reduced by 0.7 V in

maximum compared to lead alloy anode and showed a high durability for oxygen evolution even at a high current density like 5,000 A m^{-2}. In conclusion, the amorphous RuO_2-Ta_2O_5/Ti anode has a high possibility for a significant electric energy saving, suppression of anodic metal oxide deposition and a long lifetime in various kinds of electrowinning processes in which the anodic reaction is oxygen evolution.

Contents

Chapter 1

Introduction

1.1 Electrowinning

Electrowinning (EW) is carried out in an electrolytic cell with a metal cathode and an insoluble anode and is the final process in production of non-ferrous metals such as zinc, copper, nickel and cobalt, of which the typical electrolytic cell is shown in Figure 1.1 [1,2]. A pair of electrodes (anode and cathode) is immersed alternately in an acidic aqueous solution containing metal ions extracted from ore, and all anodes and cathodes in the cell are connected in parallel. During electrolysis, the electrolyte is pumped through a series of cells and is circulated slowly, in which metal ions are electrodeposited on the cathode and oxygen evolution occurs on the anode, when acidic sulfate solutions are used.

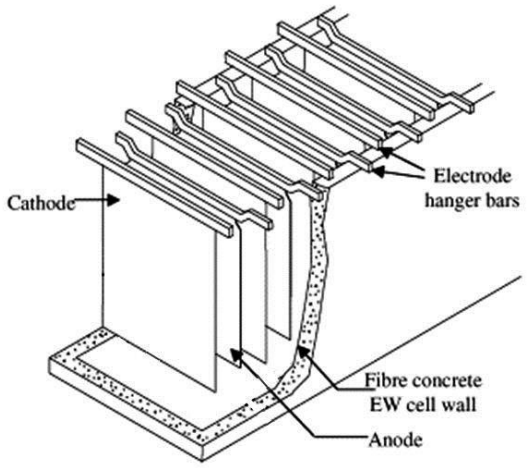

Figure 1.1 Cross-section of an electrowinning cell [1].

The reactions on the cathode and the anode and their standard potentials, E^o, referred to normal hydrogen electrode (NHE) in EW are given below:

Cathode

Zinc EW	$Zn^{2+} + 2e^- \rightarrow Zn$	$E^o = -0.763$ V	(1-1)
Copper EW	$Cu^{2+} + 2e^- \rightarrow Cu$	$E^o = 0.337$ V	(1-2)
Nickel EW	$Ni^{2+} + 2e^- \rightarrow Ni$	$E^o = -0.23$ V	(1-3)
Cobalt EW	$Co^{2+} + 2e^- \rightarrow Co$	$E^o = -0.277$ V	(1-4)

Anode

$$2H_2O \rightarrow O_2 + 4H^+ + 4e^- \qquad E^o = 1.229\ V \qquad (1\text{-}5)$$

Although E^o of zinc, nickel, and cobalt are more negative than that of hydrogen evolution (E^o=0), the current efficiency of metal deposition on the cathode is high (90-98%) [3-6], because the overpotential of hydrogen evolution is very high on such metals deposited on aluminum or titanium substrates [6], so that the reduction of metal ions to metal occurs preferentially to hydrogen evolution, resulting in the high current efficiency.

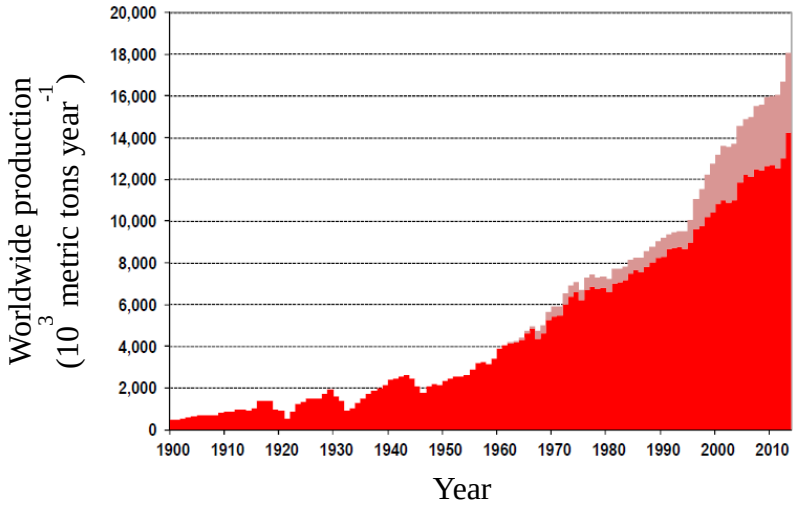

Figure 1.2 World copper mine production by concentrates (■) and SX/EW (■) between 1900 and 2013 [8].

Zinc EW produces 90 % or more of the world's zinc and a high purity (>99.99 %) of zinc metal can be obtained at reasonable cost [7]. The production of copper by EW has become increasingly important in recent years, and The International Copper Study Group (ICSD) [8] has reported the transition of world copper mine production by concentrates and solvent extraction/electrowinning (SX/EW) between 1900 and 2013, as shown in Figure 1.2; copper EW process was not performed before 1960s, while the world copper production by EW increased from *ca*. 10 % in 1990 to *ca*.

20 % in 2013. There are some reasons for this; in EW, simplified flow sheets, diverse process integration options, and more size flexibility compared to electrorefining [9]. ICSD has also reported that the copper mining capacity is estimated to reach 27.5 million tonnes in 2017, with 21 % by EW production [10]. This will be around 30 % higher than 21.0 million tonnes of copper produced in 2013. It seems that the volume and fraction of metal produced by EW are expected to more increase.

1.2 Energy consumption

One of the issues of modern EW processes is high energy consumption, and this is becoming more significant with increasing demand of metal production and rising energy costs. Table 1.1 shows the production and energy consumption of zinc and copper EW, in which the total refined zinc and copper in 2013 were 13,000 kt [11] and 21,000 kt [12] and copper produced by EW process is about 20% of total copper. Among EW processes, zinc EW consumes the largest electrical energy amounting to 3,000-3,500 kWh t^{-1} [3,6,13-16]. Compared to this, the energy consumption of copper EW is 2,000-2,160 kWh t^{-1} [6,13,15], although copper EW needs more energy than the other copper production process, *i.e.*, electrorefining (300~340 kW t^{-1}) [13,15]. The annual energy consumption of zinc and copper EW processes in the world calculated by the data given above are 45,500 GWh for zinc and 9,072 GWh for copper with the conditions that the unit energy consumption for zinc and copper is assumed 3,500 kWh t^{-1} and 2,160 kWh t^{-1}, respectively [6,11-13,15]. These values correspond to 4,200,000 households and 837,000 households of electricity consumption in U.S.A. (the average annual electricity consumption is 10,837 kWh per household in U.S.A. [17]), and it is estimated that the consumption of the electricity by EW in U.S.A is the order of 1 to 2% of total electric energy produced [18]. Therefore, it is crucially important to explore energy reduction technologies for current energy intensive EW processes.

Table 1.1 Production and energy consumption of Zn and Cu EW in 2013 [3,6,11-16].

	Total production in 2013 (kt)	Energy (kWh/t)	Energy (GWh)	Energy (household)
Zinc	13,200	3,000-3,500	46,200	4,260,000
Copper	21,000 (*ca.* 20 % by EW)	2,000-2,160	9,070	837,000

The most effective approach to suppress the energy consumption of EW is to reduce the cell voltage, because the cell voltage is directly proportional to the energy consumption which accounts for 60-80 % of the energy requirement of a refinery [4,16]. The cell voltage of EW can be expressed as:

$$E_{cell} = \Delta E_{eq} + \eta_a + \eta_c + IR_{solution} + IR_{other} \quad (1\text{-}6)$$

where E_{cell} is the cell voltage, ΔE_{eq} is the equilibrium potential difference between the anodic and cathodic reactions, η_a and η_c are the overpotential associated with the anode and cathode, $IR_{solution}$ is the voltage drop in the electrolyte, and IR_{other} is the resistance other than the solution resistance, such as the contact resistance between the bus bar and the electrodes.

Table 1.2 shows the contents of the components of the cell voltage for zinc and copper EW [15,16,19-22]. For zinc EW, the overpotential of the anodic reaction is approximately 4 times larger on average than that of the cathodic reaction [16], and the anodic overpotential is 18-30 % of total cell voltage when the cell voltage is 3.3 V [7,15] which is a typical value. The anodic overpotential in copper EW is 10 times larger than the cathodic overpotential in maximum and account for 25-40 % of the total cell voltage which is usually around 2.0 V [13,19]. All these data insist that the reduction of the anodic overpotential is extremely important for reducing the energy consumption in the EW processes.

Table 1.2 Distribution of electric energy in Zn and Cu EW [15,16,19-22].

	i (A m^{-2})	ΔE_{eq} (V)	η_a (V)	η_c (V)	$IR_{solution}$ (V)	IR_{other} (V)
Zinc	400-700	1.99	0.60-1.0	0.15-0.30	0.30-0.40	0.05-0.10
Copper	200-300	0.89	0.50-0.80	0.05-0.10	0.10-0.50	0.05-0.15

Furtheremore, there are also EW plants in least developed countries such as Africa and Sotheast Asia, in which refining companies have an important industry to surpport these area. Development of the technology for energy saving and low environmental impact will also play a significant role in national construction of the conflict countries in Middle East that is rich in metal resources, while it is imppossible to produce the metals in such area due to the political uncertainty now.

1.3 Lead alloy anodes

The high overpotential for the anodic reaction as mentioned above is due to low catalytic activity for oxygen evolution on lead alloys which have been employed as the anode's material of commercial EW processes for about a century; the typical material is the alloys with several percent of antimony [23-29]. To decrease the oxygen overpotential of lead alloys, many researches on the composition and performance have been continuously performed. Clancy [23] summarized the influences of alloying elements on electrochemistry of lead anodes and reported the properties of 45 types of lead alloy anodes. The representative examples are Pb-Ag [21,22,24,25,30-33], Pb-Ca [24,25,34], Pb-Ca-Sn [24,27,35-37], Pb-Sr-Sn [25] and Pb-Co_3O_4 anodes [27,28,31-33,38]. Hrussanova demonstrated that the oxygen evolution potential of Pb-Co_3O_4 anode was *ca.* 40 mV lower than that of Pb-Sb anode and *ca.* 70 mV lower than that of Pb-Ca-Sn anode [27], although the corrosion rate of Pb-Co_3O_4 anode was

6.7 times lower than that of Pb-Sb anode [28]. The alloy with addition of silver such as Pb-Ca-Sn-Ag was found to prolong the service life [39] and the cobalt-added alloy, Pb-Ca-Sn-Co, was reported to improve the anode performance for oxygen evolution [24]. Some recent studies have also shown that Pb-RuO_2 anode [40] and Pb-Co_3O_4 coated titanium anode with SnO_2-Sb_2O_3 interlayer [41] have lower anode potential than other Pb alloy anodes without such metal oxides. However, the overpotential for oxygen evolution is still high and a large portion of cell voltage, as described in the previous section. In addition, there are some disadvantages of lead alloy anodes; anodic deposition of metal oxide, low durability, contamination of dissolved Pb(II) ions to the electrolyte and the cathode deposit, and generation of hazardous by-products on the anode. Especially, the anodic deposition of metal oxide on the anode is required to suppress for EW processes [13,29,42].

1.4 Metal oxide deposition on anode

In copper and nickel EW, the electrolyte contains Pb(II) ions as an impurity, and Pb(II) ions are oxidized on the anode and are converted to PbO_2 [25,43], as given below.

$$Pb^{2+} + 2H_2O \rightarrow PbO_2 + 4H^+ + 2e^- \qquad E^o = 1.455 \text{ V vs. NHE} \qquad (1\text{-}7)$$

There is also a case that PbO_2 deposited on the anode is reduced to non-conductive $PbSO_4$ because of a local electrochemical cell reaction when the electrolysis is stopped, in which PbO_2 is reduced to $PbSO_4$ as below,

$$PbO_2 + SO_4^{2-} + 4H^+ + 2e^- \rightarrow PbSO_4 + 2H_2O \qquad E^o = 1.685 \text{ V vs. NHE} \qquad (1\text{-}8)$$

The deposition of metal oxide is also known in zinc and cobalt EW. Zinc EW solutions usually contain Mn(II) ions as a minor component, because MnO_2 or $KMnO_4$ are added

as the oxidizer for dissolving $ZnO \cdot Fe_2O_3$ generated in Zn(II) extraction process. Mn(II) ions are oxidized on the anode, resulting in manganese oxide (MnO_2, MnOOH) deposition [43-45]. Cobalt oxide (CoOOH) deposition is observed in cobalt EW, and Co(II) ions which should be reduced on the cathode are also oxidized on the anode, which induces CoOOH generation and unwanted consumption of Co(II) ions [46]. These manganese oxide or cobalt oxide depositions are expressed as,

Zinc EW

$$Mn^{2+} \rightarrow Mn^{3+} + e^- \qquad E^o = 1.51 \text{ V vs. NHE} \qquad (1\text{-}9)$$

$$Mn^{3+} + 2H_2O \rightarrow MnOOH + 3H^+ \qquad (1\text{-}10)$$

$$MnOOH \rightarrow MnO_2 + H^+ + e^- \qquad (1\text{-}11)$$

Cobalt EW

$$Co^{2+} \rightarrow Co^{3+} + e^- \qquad E^o = 1.82 \text{ V vs. NHE} \qquad (1\text{-}12)$$

$$Co^{3+} + 3H_2O \rightarrow CoOOH \cdot H_2O + 3H^+ \qquad (1\text{-}13)$$

The reason why metal oxide deposition occurs is that the onset potential of oxidation of metal ions on the lead alloy anode is lower than that of oxygen evolution due to high oxygen overpotential. The deposition of metal oxide results in an increase in cell voltage during the electrolysis, the shortening of the anode's lifetime, and the production of hazardous by-products and wastes. Therefore, it is needed to develop a highly catalytic anode for oxygen evolution, which replacing the existing lead alloy anode in view of energy and environment for EW industry.

1.5 Oxide coated titanium anodes

Metal oxide coated titanium electrodes have been widely investigated for insoluble oxygen or chlorine evolution anodes and have been used in industrial electrochemical processes such as chlor-alkali electrolysis, metal electrowinning, metal

recovery, electroplating, electrolytic foil production, electrosynthesis, water treatment and water electrolysis [47-77] since the two patents invented by Beer were issued in 1960s [78,79], for which Lee [80] recently reported the history on the development of electrocatalysts for oxygen evolution from its basic studies to current industrial processes. Among metal oxides for oxygen electrocatalyst examined, Trasatti concluded that iridium oxide (IrO_2) or ruthenium oxide (RuO_2) have higher electrocatalytic activity than other metal oxides [81,82]. These anodes can be prepared by a variety of processes such as, sol-gel method [47,83-99], Pechini method [100-104], electrodeposition [105-108], metal organic chemical vapor deposition [109,110], and sputtering [111-113]. However, commercially utilizing anodes are currently prepared by thermal decomposition of aqueous or alcohol-based precursor solutions containing metal ions on titanium as the substrate because of its high production efficiency compared to others.

1.5.1 IrO_2-based anodes

IrO_2-based anode represents the titanium electrode covered with binary or ternary oxides comprising IrO_2, of which the typical one is a mixture of IrO_2 and Ta_2O_5. Comninellis and his co-workers [114,115] investigated the catalytic activity of IrO_2-Ta_2O_5/Ti anodes for oxygen evolution with a wide range of Ir ratio from 10 mol% to 100 mol% and revealed that the IrO_2-Ta_2O_5 coating at 70 mol% Ir showed the highest activity. This composition is now one of the standards for industrial applications of the anode. On the other hand, the electrocatalytic activity and durability of the anode are strongly affected by preparation procedure and parameters, such as pretreatment of the substrate, solvent, concentration, and application method of the precursor solution, combination of mixed oxides, thickness of the prepared oxide, and thermal decomposition temperature [50-58,72,87,94,102,103,116-139]. For example, Angelinetta [139] reported that IrO_2-based anodes prepared from organic solvent showed better performance than those from aqueous solutions, and Krysa [116] demonstrated that the service life of the anode was proportional to the weight of Ir in the mixed oxide.

Commercially available IrO_2-Ta_2O_5/Ti anodes for practical applications are prepared by thermal decomposition at a temperature of 450 ^oC or more and the obtained mixed oxide coating consists of crystalline IrO_2 and amorphous Ta_2O_5, having lower oxygen overpotential than lead alloy anodes [25,29,60,105,140,141]. Msindo [25] examined the anode potentials of IrO_2-Ta_2O_5/Ti anodes and traditional Pb-6%Sb anodes during copper electrodeposition by chronopotentiometry at a current density of 190 A m^{-2} and the comparison indicated that the anode potential of the IrO_2-Ta_2O_5/Ti anode was *ca.* 20 % lower than that of the lead alloy anode. However, previously reported IrO_2-Ta_2O_5/Ti anodes have been also found to be impossible to suppress the metal oxide deposition explained in Section 1.4.

Prof. Morimitsu [142-161], my supervisor, has investigated the effect of crystallographic structure of IrO_2-Ta_2O_5 coatings prepared by thermal decomposition method and revealed that reducing thermal decomposition temperature makes IrO_2 amorphous or less crystalline with SEM observation that the coating surface shows generation of ordered nano IrO_2 particles of 5-10 nm. It has also demonstrated that such amorphous coatings have very high catalytic activity for not only oxygen but also chlorine evolution, so that the anode potential or the cell voltage in EW can be significantly decreased compared to the crystalline coatings. The reason for the activity enhancement is that nano IrO_2 particles induce an increase in effective surface area for oxygen or chlorine evolution, although the effective surface area for unwanted side reactions, *i.e.*, metal oxide deposition, is unchanged, thereby the anodic depositions of lead oxide, manganese oxide and cobalt oxide are suppressed. These effects bring stable and constant cell voltage, no sludge generation, and prolongation of the anode's lifetime.

1.5.2 RuO_2-based anodes

Another popular example of oxide coated titanium anode is RuO_2-based anode, especially the titanium electrode coated with a ruthenium and titanium composite oxide,

$Ru_xTi_{1-x}O_2$/Ti (or expressed as RuO_2-TiO_2/Ti), which is the commercial anode of chloro-alkali electrolysis (brine electrolysis) and its excellent catalytic activity and stability for chorine evolution has been proven [47,48,81,82,89,108,162-169]. While the anode for chloro-alkali electrolysis uses crystalline oxide coatings, Prof. Morimitsu has revealed that the amorphous RuO_2-TiO_2/Ti anode prepared at low temperature thermal decomposition has lower chorine evolution potential than the crystalline one and can suppress CoOOH deposition in cobalt EW electrolytes [170].

Besides for chlorine evolution, RuO_2 has been well known as the most active oxide for oxygen evolution. The relationship between the overpotential of oxygen evolution and the standard enthalpy of some metal oxides was first analyzed by Trassatti, and the result shown in Figure 1.3 indicated that the oxygen overpotential, η, of RuO_2 is the lowest one among them [81].

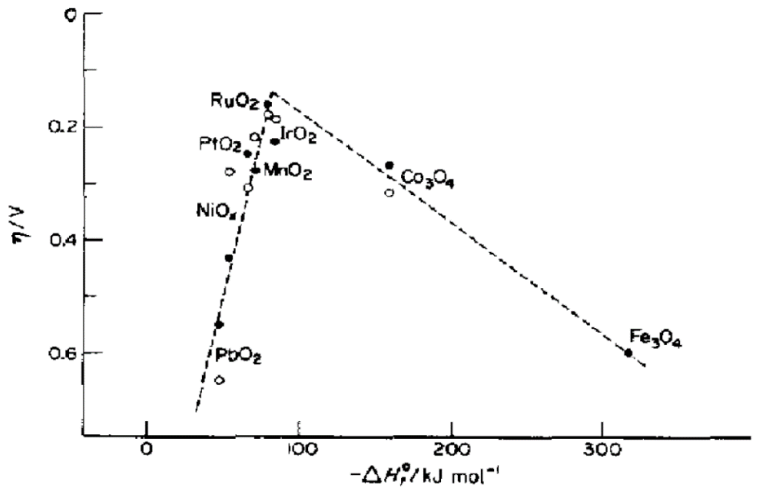

Figure 1.3 Electrochemical activity for oxygen evolution at various metal oxides as a function of the enthalpy in acid (●) and alkaline (○) solutions [81].

Rosmeisl and his co-workers also investigated the theoretical overpotential of a number of metal oxides using density functional theory (DFT) calculation [171-173], and reported the data of the overpotential as a function of standard free energy as shown in Figure 1.4 [173]. The result predicted that Co_3O_4 is slightly more active for oxygen

evolution than RuO_2, although it was revealed that in practice, RuO_2 has higher activity than Co_3O_4 [91,174].

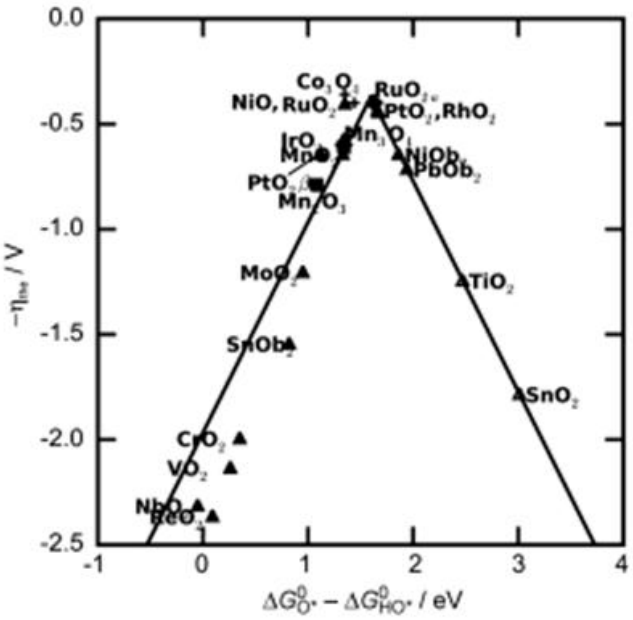

Figure 1.4 Oxygen evolution activity trends towards for various metal oxides as volcano plot of theoretical overpotential vs. standard free energy of the step [173].

On the other hand, the stability of RuO_2 for oxygen evolution in acidic media is lower than that of IrO_2, and pure RuO_2 is drastically deteriorated and loses its activity during oxygen evolution [175,176]. The reason seems to be the phase transition from RuO_2 to soluble RuO_4 at high potentials [178-189].

Therefore, various types of metal oxides including RuO_2 have been tested to improve the stability and activity for oxygen evolution and are summarized in Table 1.3. In addition, the physic-chemical properties of RuO_2 [113], RuO_2-TiO_2 [85,85], RuO_2-Ta_2O_5 [237-239], RuO_2-SnO_2 [92,97], RuO_2-IrO_2-TiO_2 [107] and RuO_2-TiO_2-IrO_2-Ta_2O_5 [240] were investigated by X-ray diffraction (XRD), scanning electron microscopy (SEM), X-ray photoelectron spectroscopy (XPS), Rutherford backscattering spectrometry (RBS), elastic recoil detection (ERD), thermogravimetry (TG) and differential thermal analysis (DTA).

Table 1.3 RuO_2-based coatings studied in the previous works.

Oxide	Electrolyte	References
RuO_2	H_2SO_4	61, 66, 68, 70, 98, 165, 175, 178-189, 191
	$HClO_4$	102, 106, 163-165, 178
	NaCl	75, 76, 165
	NaOH	182, 190, 192
	KOH	93, 180, 193
	Na_2SO_4	75, 76
RuO_2-TiO_2	H_2SO_4	99, 108, 114, 165, 194, 195, 197, 199-201
	NaCl	89, 90, 99, 108, 165, 166, 168, 177, 197, 190
	$HClO_4$	165, 177, 196, 200
	HCl	170
	NaOH	200
	$NaClO_3$	166, 168
	$NaNO_3$, Na_2SO_4	200
RuO_2-IrO_2	H_2SO_4	73, 86, 104, 176, 186, 189, 191-204
	NaOH	191
RuO_2-Ta_2O_5	H_2SO_4	114, 189, 205-210
RuO_2-ZrO_2	H_2SO_4	112, 209
RuO_2-SnO_2	H_2SO_4	190, 196, 212-215
	$HClO_4$	216
	NaOH	190, 217

Table 1.3 (*Continued*)

Oxide	Electrolyte	References
RuO_2-Nb_2O_5	$HClO_4$	100
RuO_2-RhO_2	H_2SO_4	218
RuO_2-Co_3O_4	H_2SO_4	174
RuO_2-MnO_2	H_2SO_4	63
RuO_2-NiO	NaOH	192, 220-222
	KOH	219
RuO_2-SiO_2	H_2SO_4	98
RuO_2-PbO_2	H_2SO_4	41, 223
$RuO_{0.3}Pt_xTi_{0.7-x}O_2$	NaCl	224
RuO_2-IrO_2-TiO_2	NaCl	65, 74, 108, 226
	$HClO_4$	226, 227
RuO_2-IrO_2-Ta_2O_5	H_2SO_4	187
RuO_2-IrO_2-SnO_2	H_2SO_4	230
	HCl, $HClO_4$, NaCl, Na_2SO_4	229
	KCl	228
RuO_2-TiO_2-SnO_2	H_2SO_4	77
	NaCl	77, 233
	$HClO_4$	231, 234
RuO_2-Sb_2O_5-SnO_2	H_2SO_4	234
RuO_2-TiO_2-CeO_2	NaOH	235

Table 1.3 (*Continued*)

Oxide	Electrolyte	References
RuO_2-Co_3O_4-CeO_2	KOH	236
RuO_2-IrO_2-SnO_2-TiO_2	H_2SO_4	76

Among the oxide combinations in Table 1.3, RuO_2-Ta_2O_5 has received much attention since Ta_2O_5 is chemically stable in acidic aqueous solutions and has some merits for prohibiting the detachment of the catalytic coating and suppressing passivation of titanium substrate [241,242]. It is noted that thin Ta_2O_5 films also have other applications such as dynamic memory capacitors, solid state ion sensors, and metal oxide semiconductor transistors [243-247] due to its wide band gap (4.3 eV).

Yeo [189] suggested that the stability of RuO_2 for oxygen evolution is improved by combination with Ta_2O_5 which prevents the oxidation of RuO_2 and showed that RuO_2-IrO_2-Ta_2O_5 has higher catalytic activity than pure RuO_2. Ribeiro and Andrade [205] demonstrated that RuO_2-Ta_2O_5/Ti anodes (Ru:Ta = 80:20 atom%) prepared at 450 ^oC are much stable than RuO_2-TiO_2/Ti anodes (Ru:Ti = 50:50 atom%) for oxygen evolution at 750 A m^{-2} in 0.5 mol dm^{-3} H_2SO_4 solution. They also found that the catalytic activity and durability of the RuO_2-Ta_2O_5/Ti anode prepared sol-gel (Pechini) method is better than that prepared by conventional thermal decomposition method [207]. However, all those studies were done with the mixed oxide mainly prepared at high temperature, by which RuO_2 is crystalline. RuO_2 and its composite or mixed oxides have been explored in supercapacitor applications; RuO_2 [93,111,184,186-188] RuO_2-Ta_2O_5 [209,210,238], RuO_2-IrO_2 [186], RuO_2-SnO_2 [212]. Jow and his co-workers [209] examined the stability and capacitance of RuO_2-Ta_2O_5 films prepared by heat treatment at a low temperature of 220-300 ^oC and showed that high capacitance and stability were obtained with the films prepared at *ca.* 250 ^oC.

On the other hand, Trasatti and his co-workers [180,183] studied the electrocatalysis for oxygen evolution on RuO_2/Ti electrodes prepared by thermal decomposition of Ru chloride or Ru nitrate solutions at a range of 260-550 ^oC and indicated that the double layer charge (DLC) increased with decreasing thermal decomposition temperature, especially in a range of 260-300 ^oC, which means that the effective surface area increases for oxygen evolution, and that the nitrate precursor showed more effective surface area than the nitrate precursor irrespective of thermal decomposition temperature; *e.g.*, the former presented more than 10 times larger DLC than the later when the decomposition temperature was 300 ^oC.

Ma [68] and Melsheimer [175] each investigated the catalytic activity of RuO_2 coatings using nitrate or chloride precursor solutions in the temperature range of 300 ^oC to 550 ^oC. Those results also proved that lower temperature was effective to increase the effective surface area with small RuO_2 particles and enhance the catalytic activity. Tsuji [106] prepared RuO_2 coatings on SnO_2 coated glasses by electrodeposition and thermal decomposition at 200 ^oC, 300 ^oC or 400 ^oC. As a result, RuO_2 became amorphous at 200 ^oC and amorphous RuO_2 had higher activity for oxygen evolution than crystalline RuO_2 prepared at 300 ^oC or 400 ^oC.

While some works have been done on the effect of thermal decomposition temperature on electrocatalytic activity of pure RuO_2 coatings, as indicated above, there is little information on amorphous RuO_2-based binary coatings formed on titanium prepared by thermal decomposition method. Moreover, the effects of the crystallographic structure and surface morphology of such RuO_2-based coatings on the catalytic activity and durability for oxygen evolution has not been systematically investigated.

1.6 Aim of this thesis

The main aim of this thesis is to develop a novel oxygen evolution anode with low overpotential for electrowinning applications. For this purpose, RuO_2-Ta_2O_5 coated titanium anodes were prepared at different thermal decomposition temperatures and Ru:Ta mole ratios, and the characterization and performance were studied with focusing on the relationship between the crystallographic structure and surface morphology and the catalytic coating performance for oxygen evolution. The suppression effects to unwanted side reactions and durability of the amorphous anodes were also investigated.

This thesis consists of the following chapters:

Chapter 1, the present chapter, describes the background and the purpose of this thesis.

Chapter 2 shows the preparation of the anodes and experimental details.

Chapter 3 mentions the effect of crystallographic structure and surface morphology of RuO_2-Ta_2O_5 coatings prepared at different thermal decomposition temperatures on the catalytic activity for oxygen evolution. The cell voltages of zinc, copper, nickel or cobalt EW are also reported.

Chapter 4 mentions the effect of Ru:Ta mole ratio of the amorphous coatings on catalytic activity for oxygen evolution. The pure RuO_2/Ti anode is also used for comparison.

Chapter 5 presents the suppression effect on anodic deposition of metal oxides on amorphous RuO_2-Ta_2O_5/Ti anodes.

Chapter 6 describes the long-term stability of amorphous RuO_2-Ta_2O_5/Ti anodes for oxygen evolution and its dependence on the preparation condition.

Chapter 7 gives the general conclusions from Chapter 3 to Chapter 6.

1.7 References

[1] G.D. Rigby, P.E. Grazier, A.D. Stuart, E.P. Smithson, "Gus bubble induced mixing in electrowinning baths", Chemical Engineering Science, **56** (2001) 6329-6336.

[2] T. Robinson, K.C. Sole, M.S. Moats, F.K. Crundwell, M. Morimitsu, L. Palmu, "Developments in base metal electrowinning cellhouse design", Proc. of Electrometallurgy 2012, TMS (2012) 147-156.

[3] H. Huang, J.Y. Zhou, B.M. Chen, Z.C. Guo, "Polyaniline anode for zinc electrowinning from sulfate electrolytes", Trans. Nonferrous Met. Soc. China, **20** (2010) s288-s292.

[4] G.W. Barton, A.C. Scott, "A validated mathematical model for a zinc electrowinning cell", J. Appl. Electrochem., **22** (1992) 104-115.

[5] A.C. Scott, R.M. Pitblado, G.W. Barton, "A mathematical model of a zinc electrowinning Cell", **2** (1987) 51-62.

[6] D.R. Sadoway, "Electrometallurgy", Encyclopedia of materials science and engineering, M.B. Bever, editor, Pergamon Press, Oxford (1986) 1444-1447.

[7] International Zinc Association, Zinc Production - From Ore to Metal, http://www.zinc.org/basics/zinc_production.

[8] International Copper Study Group, "The World Copper Factbook 2014" (2014) 8.

[9] M. Moats, M. Free, "A bright future for copper electrowinning", JOM, **59** (2007) 34-36.

[10] International Copper Study Group, "The World Copper Factbook 2014" (2014) 11.

[11] International Lead and Zinc Study Group, "Lead and Zinc Statistics", http://www.ilzsg.org/static/statistics.aspx?from=1.

[12] International Copper Study Group, "The World Copper Factbook 2014" (2014) 6.

[13] M. Free, M. Moats, T. Robinson, N. Neelameggham, G. Houlachi, M. Ginatta, D. Creber and G. Holywell, "Electrometallurgy – Now and in the Future", Proc. of Electrometallurgy 2012, TMS (2012) 3-27.

[14] T. Yoshida, "Technological overviews of the zinc industry – now and future", Proc. T.T. Chen Honorary Symposium on Hydrometallurgy and Materials Characterization, TMS (2012) 23-37.

[15] P. Paunovic, S.H. Jordanov, "Electrometallurgy: electrochemical economic and environmental (3E) aspects", Macedonian J. Chemistry and Chemical Engineering, **30** (2011) 75-83.

[16] F.T. Parada, E. Asselin, "Reducing power consumption in zinc electrowinning", JOM**, 61** (2009) 54-58.

[17] U.S. Energy Information Administration, http://www.eia.gov/tools/faqs/faq.cfm?id=97&t=3.

[18] D. Steingart, "Electrowinning principles and practice: a brief introduction to the

electrochemistry and engineering behind modern electrowinning Plants", 2012 Annual Meeting of American Institute of Chemical Engineers, Pittsburgh (2012).

[19] G. Cifuentes, J. Simpson, F. Lobos, L. Briones, A. Morales, "An alternative copper electrowinning process based on reactive electrodialysis (RED)", J. the Chilean Chemical Society, **54** (2009) 334-338.

[20] J.H. Gibbons, "Copper: Technology and Competitiveness", U.S. Congress, Office of Technology Assessment (1988) 151-158.

[21] Y.J. Lai, L.X. Jiang, S.P. Zhong, X.J. Lu, H.J. Peng, Y.X. Liu, "A novel porous Pb-Ag anode for energy-saving in zinc electrowinning Part I: Laboratory preparation and properties", Hydrometallurgy, **102** (2010) 73-80.

[22] Y.J. Lai, L.X. Jiang, S.P. Zhong, X.J. Lu, H.J. Peng, Y.X. Liu, "A novel porous Pb-Ag anode for energy-saving in zinc electrowinning Part II: Preparation and pilot plant tests of large size anode", Hydrometallurgy, **102** (2010) 81-86.

[23] M. Clancy, C.J. Bettles, A. Stuart, N. Birbilis, "The influence of alloying elements on the electrochemistry of lead anodes for electrowinning of metals: A review", Hydrometallurgy, **131-132** (2013) 144-157.

[24] A. Felder, R. Prengaman, "Lead alloy for permanent anodes in the nonferrous metals industry", JOM, **58** (2006) 28-31.

[25] Z.S. Msindo, V. Sibanda, J.H. Potgieter, "Electrochemical and physical characterisation of lead-based anodes in comparison to Ti-(70%) IrO_2/(30%) Ta_2O_5 dimensionally stable anodes for use in copper electrowinning", J. Appl. Electrochem., **40** (2009) 691-699.

[26] A. Hrussanova, L. Mirkova, T. Dobrev, S. Vasilev, "Influence of temperature and current density on oxygen overpotential and corrosion rate of Pb-Co_3O_4, Pb-Ca-Sn, and Pb-Sb anodes for copper electrowinning: Part I", Hydrometallurgy, **72** (2004) 205-213.

[27] A. Hrussanova, L. Mirkova, T. Dobrev, "Influence of additives on the corrosion rate and oxygen overpotential of Pb-Co_3O_4, Pb-Ca-Sn and Pb-Sb anodes for copper electrowinning: Part II", Hydrometallurgy, **72** (2004) 215-224.

[28] A. Hrussanova, L. Mirkova, T. Dobrev, "Anodic behaviour of the Pb-Co_3O_4 composite coating in copper electrowinning", Hydrometallurgy, **60** (2001) 199-213.

[29] K. Kinoshita, "Electrometallurgy", Electrochemical Oxygen Technology, The Electrochemical Society Series (1992) 376-379.

[30] H. Hui, Y.Y. Wang, L.Y. Chai, H.J. Xiao, F. Pei, Y.D. Shu, "Effect of impurities in recycling water on Pb-Ag anode passivation in zinc electrowinning process", Trans. Nonferrous Met. Soc. China, **21** (2011) 1665-1672.

[31] St. Rashkov, Ts. Dobrev, Z. Noncheva, Y. Stefanov, B. Rashkova, M. Petrova, "Lead-cobalt anodes for electrowinning of zinc from sulphate electrolytes",

Hydrometallurgy, **52** (1999) 223-230.

[32] I. Ivanov, Y. Stefanov, Z. Noncheva, M. Petrova, T. Dobrev, L. Mirkova, R. Vermeersch, J.P. Demaerel, "Insoluble anodes used in Hydrometallurgy Part I: Corrosion resistance of lead and lead alloy anodes", Hydrometallurgy, **57** (2000) 109-124.

[33] I. Ivanov, Y. Stefanov, Z. Noncheva, M. Petrova, T. Dobrev, L. Mirkova, R. Vermeersch, J.P. Demaerel, "Insoluble anodes used in Hydrometallurgy Part II: Anodic behavior of lead and lead alloy anodes", Hydrometallurgy, **57** (2000) 125-139.

[34] F. Mohammadi, M. Tunnicliffe, P. Nesbitt, A. Alfantazi, "Lead anodes performance in nickel electrowinning", Proc. of Electrometallurgy 2012, TMS (2012) 77-85.

[35] R.D. Prengaman, T.W. Ellis, A.H. Mirza, "New lead anode for copper electrowinning", Hydroprocess 2010, International Workshop on Process Hydrometallurgy, Chile (2010).

[36] R.D. Prengaman, A. Siegmund, "Improved copper electrowinning operations using wrought Pb-Ca-Sn anodes", Copper 99-Cobre 99 International Symposium (1999) 1-11.

[37] R.D. Prengaman, "New insoluble lead anodes for copper electrowinning", Proc. of The Electrorefining and Winning of Copper, TMS (1987) 457-467.

[38] Y. Stefanov, Ts. Dobrev, "Potentiodynamic and electron microscopy investigations of lead–cobalt alloy coated lead composite anodes for zinc electrowinning", **83** (2005) 296-299.

[39] M. Stelter, H. Bombach, P. Saltykov, "Use of lead alloy anodes in electrowinning of metals", Proc. of European Metallurgical Conference (2003) 561-571.

[40] M. Taguchi, M. Nagai, T. Sawao, H. Takahashi, K. Suzuki, R. Sato, "Pb-based insoluble anode with dispersed catalyst powders of low oxygen evolution overpotential for zinc electrowinning", J. MMIJ, **130** (2014) 434-440. (in Japanese)

[41] M.J. Barmi, A.N. Nikoloski, "Alternative low-cost composite coated anodes for base metal electrowinning. In: Proceedings of the Materials Science & Technology MS&T'13 Conference", Canada (2013).

[42] M. Moats, "Will lead-based anodes ever be replaced in aqueous electrowinning", JOM, **60** (2008) 46-49.

[43] S. Sandoval, C. Clayton, E. Gebrehiwot, J. Morgan, "Tankhouse parameters for transition from lead to alternative anodes", Hydroprocess 2013, 5th International Seminar on Process Hydrometallurgy (2013).

[44] S. Nijjer, J. Thonstad, G. M. Haarberg, "Oxidation of manganese (II) and reduction of manganese dioxide in sulphuric acid", Electrochimica Acta, **46** (2000) 395-399.

[45] S. Nijjer, J. Thonstad, G. M. Haarberg, "Cyclic and linear voltammetry on Ti/IrO_2-Ta_2O_5-MnO_x electrodes in sulfuric acid containing Mn^{2+} ions", Electrochimica Acta, **46** (2001) 3503-3508.

[46] T. Akre, G.M. Haarberg, S. Haarberg, J. Thonstad, O.M. Dotterud, "The anode process in cobalt electrowinning", Proc. of ECS, PV 2004-18 (2005) 276-287.

[47] S. Trasatti, "Electrocatalysis: understanding the success of DSA®", Electrochim. Acta, **45** (2000) 2377-2385.

[48] K. Kinoshita, "Electrode structure", Electrochemical Oxygen Technology, The Electrochemical Society Series (1992) 130-139.

[49] M. Panizza, L. Ouattara, E. Baranova, C. Comninellis, "DSA-type anode based on conductive porous p-silicon substrate", Electrochem. commun., **5** (2003) 365-368.

[50] R. Otogawa, K. Soda, S. Yamauchi, Y. Nagatoishi, M. Morimitsu, M. Matsunaga, "Morphological deterioration of iridium oxide-tantalum oxide anode by oxygen evolution", Denki Kagaku, **65** (1997) 987-991.

[51] R. Otogawa, K. Soda, H. Shimizu, T. Ikeda, M. Morimitsu, M. Matsunaga, "Effects of cathodizing on the durability of an IrO_2-based anode in an electrogalvanizing", Tetsu to Hagane, **84** (1998) 785-789. (in Japanese)

[52] H. Meng, M. Morimitsu, M. Matsunaga, R. Otogawa, "Effects of SnO_2 on the oxidation of PSA on IrO_2-based anodes", Denki Kagaku, **66** (1998) 1148-1149.

[53] R. Otogawa, H. Shimizu, T. Inoue, M. Morimitsu, M. Matsunaga, "Improved properties of IrO_2-based anodes for HCD electroplating", Proc. of 9th Continuous Steel Strip Plating Symp., AESF (1999) 11-16.

[54] T. Kunihiro, M. Morimitsu, M. Matsunaga, "Comparison of platinum with IrO_2-Ta_2O_5 system for the stannous ion consumption in methane sulfonic acid baths with and without catechol", J. Appl. Electrochem., **30** (2000) 359-364.

[55] R. Otogawa, M. Morimitsu, M. Matsunaga, "Development of a highly durable anode for electrogalvanizing lines", Nippon Kagaku Kaishi, **5** (2000) 299-350. (in Japanese)

[56] M. Morimitsu, H. Tamura, M. Matsunaga, R. Otogawa, "Polarization behavior and lifetime of IrO_2-Ta_2O_5-SnO_2/Ti anodes in p-phenolsulfonic acid solution for tin plating", J. Appl. Electrochem., **30** (2000) 511-514.

[57] M. Morimitsu, R. Otogawa, M. Matsunaga, "Effects of cathodizing on the morphology and composition of IrO_2-Ta_2O_5/Ti anodes", Electrochim. Acta, **46** (1997) 401-406.

[58] H. Higobashi, R. Otogawa, H. Shimizu, "Production method of metal foil", JP Patent application No. 2002-88495 (2002).

[59] H. Higobashi, "Highly-durable iridium oxide anode", J. Surface Finishing Soc. of Japan, **66** (2015) 3-5. (in Japanese)

[60] S. Kulandaisamy, J.P. Rethinaraj, S.C. Chockalingam, S. Visvanathan, K.V.

Venkateswaran, P. Ramachandran, V. Nandakumar, "Performance of catalytically activated anodes in the electrowinning of metals", J. Appl. Electrochem., **27** (1997) 579-583.

[61] M.G. Pavlovic, A. Dekanski, "On the use of platinized and activated titanium anodes in some electrodeposition processes", J. Solid State Electrochem., **1** (1997) 208-214.

[62] T. Subbaiah, P. Singh, G. Hefter, D. Muir, R.P. Das, "Sulphurous acid as anodic depolarizer in copper electrowinning Part II", **30** (2000) 181-214.

[63] B. Panda, S.C. Das, "Electrowinning of copper from sulfate electrolyte in presence of sulfurous acid", Hydrometallurgy, **59** (2001) 55-67.

[64] L. Cifuentes, R. Glasner, J.M. Casas, "Aspects of the development of a copper electrowinning cell based on reactive electrodialysis", Chemical Engineering Science, **59** (2004) 1087-1101.

[65] Z. Yi, C. Kangning, W. Wei, J. Wang, S. Lee, "Effect of IrO_2 loading on RuO_2-IrO_2-TiO_2 anodes: A study of microstructure and working life for the chlorine evolution reaction", Ceram. Int., **33** (2007) 1087-1091.

[66] Y. Takasu, N. Yoshinaga, W. Sugimoto, "Oxygen reduction behavior of RuO_2/Ti, IrO_2/Ti and IrM (M: Ru, Mo, W, V) O_x/Ti binary oxide electrodes in a sulfuric acid solution", Electrochem. commun., **10** (2008) 668-672.

[67] R. Tolba, M. Tian, J. Wen, Z.H. Jiang, A. Chen, "Electrochemical oxidation of lignin at IrO_2-based oxide electrodes", J. Electroanal. Chem., **649** (2010) 9-15.

[68] H. Ma, C. Liu, J. Liao, Y. Su, X. Xue, W. Xing, "Study of ruthenium oxide catalyst for electrocatalytic performance in oxygen evolution", J. Mol. Catal. A Chem., **247** (2006) 7-13.

[69] A. Marshall, S. Sunde, M. Tsypkin, R. Tunold, "Performance of a PEM water electrolysis cell using $Ir_xRu_yTa_zO_2$ electrocatalysts for the oxygen evolution electrode", Int. J. Hydrogen Energy, **32** (2007) 2320-2324.

[70] J.C. Cruz, S. Siracusano, V. Antonucci, A.S. Aricò, R. Ornelas, L. Ortiz-Frade, G. Osorio-Monreal, S. M. Durón-Torres, L.G. Arriaga, "Preparation and characterization of RuO_2 catalysts for oxygen evolution in a solid polymer electrolyte", Int. J. Electrochem. Sci., **6** (2011) 6607-6619.

[71] W. Simka, J. Piotrowski, G. Nawrat, "Influence of anode material on electrochemical decomposition of urea", Electrochim. Acta, **52** (2007) 5696-5703.

[72] Y. Kamegaya, K. Sasaki, M. Ogumi, T. Asaki, H. Kobayashi, T. Mitamura, "Improved durability of iridium oxide coated titanium anode with interlayers for oxygen evolution at high current densities", Electrochim. Acta, **40** (1995) 889-895.

[73] J.M. Roller, M.J Arellano-Jimenez, R. Jain, H. Yu, C.B. Carter, R. Maric. "Oxygen evolution during water electrolysis from thin films using bimetallic oxides of Ir-Pt and Ir-Ru", J. Electrochem. Soc., **160** (2013) F716-F730.

[74] N. Fan, Z. Li, L. Zhao, N. Wu, T. Zhou, "Electrochemical denitrification and kinetics study using Ti/IrO_2-TiO_2-RuO_2 as the anode and Cu/Zn as the cathode", Chemical Engineering Journal, **214** (2013) 83-90.

[75] S. Kim, S.K. Choi, B.Y. Yoon, S.K. Lim, H. Park, "Effects of electrolyte on the electrocatalytic activities of RuO_2/Ti and Sb-SnO_2/Ti anodes for water treatment", Applied Catalysis B: Environmental, **97** (2010) 135-141.

[76] S. Chellammal, P. Kalaiselvi, P. Ganapathy, G. Subramanian, "Anodic incineration of phthalic anhydride using RuO_2-IrO_2-SnO_2-TiO_2 coated on Ti anode", Arabian J. Chem., (2012).

[77] X. Zeng, M. Zhang, X. Wang, X. Chen, X. Su, W. Tang, "Effects of Sn content on Ti/RuO_2-SnO_2-TiO_2 anodes used in the generation of electrolyzed oxidizing water", J. Electroanal. Chem., **677-680** (2012) 133-138.

[78] H.B. Beer, G. B. Patent, 1, 147, 422A (1965).

[79] H.B. Beer, G. B. Patent, 1, 195, 871A (1969).

[80] J. Lee, B. Jeong, J.D. Ocon, "Oxygen electrocatalysis in chemical energy conversion and storage technologies", Curr. Appl. Phys., **13** (2013) 309-321.

[81] S. Trasatti, "Electrocatalysis in the anodic evolution of oxygen and chlorine", Electrochim. Acta, **29** (1984) 1503-1512.

[82] S. Trasatti, "Physical electrochemistry of ceramic oxides", Electrochim. Acta, **36** (1991) 225-241.

[83] S. Ardizzone, C.L. Bianchi, G. Cappelletti, M. Ionita, A. Minguzzi, S. Rondinini, A. Vertova, "Composite ternary SnO_2-IrO_2-Ta_2O_5 oxide electrocatalysts", J. Electroanal. Chem., **589** (2006) 160-166.

[84] Y. Liu, Z. Li, J. Li, "IrO_2/SnO_2 electrodes: prepared by sol–gel process and their electrocatalytic for pyrocatechol", Acta Materialia, **52** (2004) 721-727.

[85] V. Panić, A. Dekanski, G. Wang, M. Fedoroff, S. Milonjić, B. Nikolić, "Morphology of RuO_2-TiO_2 coatings and TEM characterization of oxide sols used for their preparation", J. Colloid and Interface Science, **263** (2003) 68-73.

[86] F.I. Mattos-Costa, P. de Lima-Neto, S.A.S. Machado, L.A. Avaca, "Characterisation of surfaces modified by sol-gel derived $Ru_xIr_{1-x}O_2$ coatings for oxygen evolution in acid medium", Electrochim. Acta, **44** (1998) 1515-1523.

[87] L. Xu, Y. Xin, J. Wang, "A comparative study on IrO_2-Ta_2O_5 coated titanium electrodes prepared with different methods", Electrochim. Acta, **54** (2009) 1820-1825.

[88] M. Guglielmi, P. Colombo, V. Rigato, G. Battaglin, A. Boscolo-Boscoletto, A. De Battisti, "Compositional and microstructural characterization of RuO_2-TiO_2 catalysts synthesized by the sol‐gel method", J. Electrochem. Soc., **139** (1992) 1655-1661.

[89] V. Panić, A. Dekanski, S. K. Milonjić, R.T. Atanasoski, B.Ž. Nikolić, "RuO_2-TiO_2

coated titanium anodes obtained by the sol–gel procedure and their electrochemical behaviour in the chlorine evolution reaction", Colloids Surfaces A: Physicochem. Eng. Asp., **157** (1999) 269-274.

[90] V. Panić, A. Dekanski, S. Milonjić, R. Atanasoski, B. Nikolić, "The influence of the aging time of RuO_2 and TiO_2 sols on the electrochemical properties and behavior for the chlorine evolution reaction of activated titanium anodes obtained by the sol-gel procedure", Electrochimica Acta, **46** (2000) 415-421.

[91] G. Spinolo, S. Ardizzone, S. Trasatti, "Surface characterization of Co_3O_4 electrodes prepared by the sol-gel method", J. Electroanal. Chem., **423** (1997) 49-57.

[92] X. Wang, D. Tang, J. Zhou, "Microstructure, morphology and electrochemical property of $RuO_2$70$SnO_2$30mol% and $RuO_2$30$SnO_2$70mol% coatings", J. Alloys Compd., **430** (2007) 60-66.

[93] Y. Su, F. Wu, L. Bao, Z. Yang, "RuO_2/activated carbon composites as a positive electrode in an alkaline electrochemical capacitor," New Carbon Mater., **22** (2007) 53-58.

[94] J. Kristóf, T. Szilágyi, E. Horváth, A. De Battisti, R.L. Frost, Á. Rédey, "Investigation of IrO_2/Ta_2O_5 thin film evolution", Thermochim. Acta, **413** (2004) 93-99.

[95] Y. Murakami, H. Ohkawauchi, M. Ito, K. Yahikozawa, Y. Takasu, "Preparations of ultrafine IrO_2-SnO_2 binary oxide particles by a sol-gel process", Electrochimica Acta, **39** (1994) 2551-2554.

[96] Y. Murakami, S. Tsuchiya, K. Yahikozawa, Y. Takasu, "Preparation of ultrafine IrO_2-Ta_2O_5 binary oxide particles by a sol-gel process", Electrochim. Acta, **39** (1994) 651-654.

[97] M. Ito, Y. Murakami, H. Kaji, H. Ohkawauchi, K. Yahikozawa, Y. Takasu, "Preparation of ultrafine RuO_2-SnO_2 binary oxide particles by a sol-gel process", J. Electrochem. Soc., **141** (1994) 1243-1245.

[98] I. Paseka, "Hydrogen evolution reaction on RuO_2-3SiO_2 electrodes prepared by the sol-gel process", Hemijska industrija, **54** (2000) 133-139.

[99] V.V. Panić, V.M. Jovanović, S.I. Terzić, M.W. Barsoum, V.D. Jović, A.B. Dekanski, "The properties of electroactive ruthenium oxide coatings supported by titanium-based ternary carbides", Surface and Coating Technology, **202** (2007) 319-324.

[100] A.J. Terezo, E.C. Pereira, "Preparation and characterization of Ti/RuO_2-Nb_2O_5 electrodes obtained by polymeric precursor method", Electrochim. Acta, **44** (1999) 4507-4513.

[101] A.J Terezo, E.C Pereira, "Fractional factorial design applied to investigate properties of Ti/IrO_2-Nb_2O_5 electrodes", Electrochimica Acta, **45** (2000)

4351-4358.

[102] A.J. Terezo, E.C. Pereira, "Preparation and characterization of Ti/RuO_2 anodes obtained sol-gel and conventional method", Materials Letters, **53** (2002) 339-345.

[103] A. de Oliveira-Sousa, M.A.S. da Silva, S.A.S. Machado, L.A. Avaca, P. de Lima-Neto, "Influence of the preparation method on the morphological and electrochemical properties of Ti/IrO_2-coated electrodes", Electrochimica Acta, **45** (2000) 4467-4473.

[104] N. Mamaca, E. Mayousse, S. Arrii-Clacens, T.W. Napporn, K. Servat, N. Guillet, K.B. Kokoh, "Electrochemical activity of ruthenium and iridium based catalysts for oxygen evolution reaction", Applied Catalysis B: Environmental, **111-112** (2012) 376-380.

[105] A.J. Scarpellino, G.L. Fisher, "The development of an energy-efficient insoluble anode for nickel electrowinning", J. Electrochem. Soc., **129** (1982) 515-521.

[106] E. Tsuji, A. Imanishi, K. Fukui, Y. Nakato, "Electrocatalytic activity of amorphous RuO_2 electrode for oxygen evolution in an aqueous solution", Electrochim. Acta, **56** (2011) 2009-2016.

[107] M. Yousefpour, A. Shokuhy, "Electrodeposition of TiO_2-RuO_2-IrO_2 coating on titanium substrate", Superlattices and Microstructures, **51** (2012) 842-853.

[108] V, Trieu, B. Schley, H. Natter, J. Kintrup, A. Bulan, R. Hempelmann, "RuO_2-based anodes with tailored surface morphology for improved chlorine electro-activity", Electrochim. Acta, **78** (2012) 188-194.

[109] J.R. Brown, P.W. Haycock, L.M. Smith, A.C. Jones, E.W. Williams, "Response behaviour of tin oxide thin film gas sensors grown by MOCVD", Sensors and Actuators B, **63** (2000) 109-114.

[110] A.K. Mukhopadhyay, P. Mitra, A.P. Chatterjee, H.S. Maiti, "Tin dioxide thin film gas sensor", Ceramics International, **26** (2000) 123-132.

[111] A. Barbu, V. Plichon, "Voltammetry of thermally prepared ruthenium oxide films and flux detection at the electrolyte interface", Electrochim. Acta, **42** (1997) 489-492.

[112] R. Kötz, S. Stucki, "Stabilization of RuO_2 by IrO_2 for anodic oxygen evolution in acid media", Electrochim. Acta, **31** (1986) 1311-1316.

[113] R. Kötz, H.J. Lewerenz, S. Stucki, "XPS Studies of Oxygen Evolution on Ru and RuO_2 Anodes", J. Electrochem. Soc., **130** (1983) 825-829.

[114] Ch. Comninellis. G.P. Vercesi, "Characterization of DSA®-type oxygen evolving electrodes: choice of a coating", J. Appl. Electrochem., **21** (1991) 335-345.

[115] G.P. Vercesi, J. Rolewicz, Ch. Comninellis, J. Hinder, "Characterization of DSA-type oxygen evolving electrodes. Choice of base metal", Thermochim. Acta,

176 (1991) 31-47.

[116] J. Krysa, L. Kule, R. Mraz, I. Rousar, "Effect of coating thickness and surface-treatment of titanium on the properties of IrO_2-Ta_2O_5 anodes", J. Appl. Electrochem., **26** (1996) 999-1005.

[117] J. Krysa, J. Maixner, R. Mraz, I. Rousar, "Effect of coating thickness on the properties of IrO_2-Ta_2O_5 anodes", J. Appl. Electrochem., **28** (1998) 369-372.

[118] G.P. Vercesi, J.Y. Salamin, Ch. Comninellis, "Morphological and microstructural study of the Ti/IrO_2-Ta_2O_5 electrode: effect of the preparation temperature", Electrochimica Acta, **36** (1991) 991-998.

[119] G. Foti, C. Mousty, V. Reid, C. Comninellis, "Characterization of DSA type electrodes prepared by rapid thermal decomposition of the metal precursor", Electrochim. Acta, **44** (1998) 813-818.

[120] C. Mousty, G. Foti, C. Comninellis, V. Reid, "Electrochemical behavior of DSA type electrodes prepared by induction heating", Electrochim. Acta, **45** (1999) 451-456.

[121] C.P. de Pauli, S. Trasatti, "Composite materials for electrocatalysis of O_2 evolution: IrO_2+SnO_2 in acid solution", J. Electroanal. Chem., **538-539** (2002) 145-151.

[122] G.N. Martelli, R. Ornelas, G. Faita, "Deactivation mechanisms of oxygen evolving anodes at high current densities", Electrochimica Acta, **39** (1994) 1551-1558.

[123] J.M. Hu, J.Q. Zhang, H.M. Meng, C.N. Cao, "Microstructure, electrochemical surface and electrocatalytic properties of IrO_2 + Ta_2O_5", **38** (2003) 705-712.

[124] J.M. Hu, J.Q. Zhang, C.N Cao, "Thermolytic formation and microstructure of IrO_2 + Ta_2O_5 mixed oxide anodes from chloride precursors", Thermochimica Acta, **403** (2003) 257-266.

[125] J.M. Hu, J.Q. Zhang, C.N. Cao, "Oxygen evolution reaction on IrO_2-based DSA® type electrodes: kinetics analysis of Tafel lines and EIS", Int. J. Hydrogen Energy, **29** (2004) 791-797.

[126] L.K Xu, J.D Scantlebury, "A study on the deactivation of an IrO_2-Ta_2O_5 coated titanium anode", Corrosion Science, **45** (2003) 2729-2740.

[127] L.K. Xu, J.D. Scantlebury, "Electrochemical surface characterization of IrO_2-Ta_2O_5 coated titanium electrodes in Na_2SO_4 solution", J. Electrochem. Soc., **150** (2003) B288-B293.

[128] L.K. Xu, J.D. Scantlebury, "Microstructure and electrochemical properties of IrO_2-Ta_2O_5-coated titanium anodes", J. Electrochem. Soc., **150** (2003) B254-B261.

[129] X. Chen, G. Chen, "Investigation of Ti/IrO_2-Sb_2O_5-SnO_2 electrodes for O_2 evolution: calcination temperature and precursor composition effects", J. Electrochem. Soc., **152** (2005) J59-J64.

[130] E. Mahé, D. Devilliers, "Surface modification of titanium substrates for the preparation of noble metal coated anodes", Electrochim. Acta, **46** (2000) 629-636.

[131] B.S. Li, A. Lin, F.X. Gan, "Preparation and electrocatalytic properties of Ti/IrO_2-Ta_2O_5 anodes for oxygen evolution", Trans. Nonferrous Met. Soc. China, **16** (2006) 1193-1199.

[132] J.Y. Lee, D.K. Kang, K.H. Lee, D.Y. Chang, "An investigation on the electrochemical characteristics of Ta_2O_5-IrO_2 anodes for the application of electrolysis process", Mater. Sci. Appl., **2** (2011) 237-243.

[133] Z. Yan, H. Meng, "Effect of Different shapes of the titanium based IrO_2-Ta_2O_5 coatings anode on electrochemical properties", Rare Metal Materials and Engineering, **41** (2012) 772-775.

[134] H.B. Xu, Y.H. Lu, C.H. Li, J.Z. Hu, "A novel IrO_2 electrode with iridium-titanium oxide interlayers from a mixture of TiN nanoparticle and H_2IrCl_6 solution", J. Appl. Electrochem., **40** (2009) 719-727.

[135] S. Sandoval, C. Clayton, M. Garshasb, "Development of lead and arsenic free copper stock for electrical conductors via the electrowinning process", Wire Journal International, **44** (2011) 62-71.

[136] S. Sandoval, C. Clayton, S. Dominguez, C. Unger, T. Robinson, "Development and commercialization of an alternative anode for copper electrowinning", Proc. Cu 2010 (2010) 1-13.

[137] J. Rolewicz, Ch. Comninellis, E. Plattner, J. Hinden, "Charactérisation des électrodes de type DSA pour le dégagement de O_2. L'électrode Ti/IrO_2-Ta_2O_5", Electrochimica Acta, **33** (1988) 573-580.

[138] R. Otogawa, M. Morimitsu, M. Matsunaga, "Effects of microstructure of IrO_2-based anodes on electrocatalytic properties", Electrochim. Acta, **44** (1998) 1509-1513.

[139] C. Angelinetta, S. Trasatti, Lj.D. Atanasoska, Z.S. Minevski, R.T. Atanasoski, "Effect of preparation on the surface and electrocatalytic properties of RuO_2+IrO_2 mixed oxide electrodes", Materials Chemistry and Physics, **22** (1989) 231-247.

[140] P. Ramachandran, V. Nandakumar, N. Sathaiyan, "Electrolytic recovery of zinc from zinc ash using a catalytic anode", J. Chem. Tech. Biotechnol, **79** (2004) 578-583.

[141] A.L. Antozzi, C.W. Brown, Jr., A. Calderara, "Novel DSA® anode for electrowinning of non-ferrous metals", Proc. of Electrometallurgy 2012, TMS (2012) 35-40.

[142] M. Morimitsu, "Anodes for zinc electrowinning and electrowinning method", JP patent application No. 2008-151007 (JP PAT 4516617).

[143] M. Morimitsu, "Anodes for cobalt electrowinning and electrowinning method", JP patent application No. 2008-163714 (JP PAT 4516618).

[144] M. Morimitsu, "Anode for metal electrowinning and electrowinning Method", JP patent application No. 2009-278607 (JP PAT 5013438).

[145] M. Morimitsu, "Electrowinning anode and electrowinning Method", JP patent application No. 2011-067365 (JP PAT 4916040).

[146] M. Morimitsu, "Anode for chlorine evolution", JP patent application No. 2011-199257 (JP PAT 5008043).

[147] M. Morimitsu, "Anode for zinc and cobalt electrowinning and electrowinning method", WIPO international patent application PCT/JP2009/060504.

[148] M. Morimitsu, "Metal electrowinning system and method", WIPO international patent application PCT/JP2010/70809.

[149] M. Morimitsu, N. Oshiumi, "Accelerated oxygen evolution and suppressed MnOOH deposition on amorphous IrO_2-Ta_2O_5 coatings", Chemistry Letters, **38** (2009) 822-823.

[150] M. Morimitsu, K. Uno, "A novel electrode for cobalt electrowinning to suppress CoOOH deposition", Proc. of Hydrometallurgy of Nickel and Cobalt 2009 (2009) 571-580.

[151] M. Morimitsu, N. Oshiumi, N. Wada, "Smart anodes for electrochemical processing of copper production", Proc. of Copper 2010, Electrowinning and – refining, **4** (2010) 1511-1520.

[152] M. Morimitsu, N. Oshiumi, T. Yamaguchi, "Amorphous oxide coated anode for energy saving of zinc electrowinning", Proc. of Lead-Zinc 2010 (2010) 813-818.

[153] M. Morimitsu, T. Yamaguchi, N. Oshiumi, T. Zhang, "Energy-efficient electrowinning process with smart anode comprising nano-oxide catalyst", Proc. of European Metallurgical Conference 2011, **3** (2011) 975-984.

[154] M. Morimitsu, "Development of a novel smart anode for environmentally friendly electrowinning process", Prof. ALTA 2011 Ni/Co/Cu Conference (2011) 260-265.

[155] M. Morimitsu, "New technology of oxygen evolution anodes for electrowinning", Proc. New Technology Implementation in Metallurgical Processes CIM (2011) 313-320.

[156] M. Morimitsu, "Performance and commercialization of the smart anode, MSA^{TM}, for environmentally friendly electrometallurgical process", Proc. Electrometallurgy 2012, TMS (2012) 49-54.

[157] M. Morimitsu, "Oxide coated titanium electrode for oxygen evolution", J. MMIJ, **130** (2014) 415-420. (in Japanese)

[158] K. Kawaguchi, G.M. Haarberg, M. Morimitsu, "Control of amorphization of IrO_2-Ta_2O_5/Ti electrodes to suppress unwanted side reactions", ECS Transactions, **16** (2009) 41-47.

[159] K. Kawaguchi, G.M. Haarberg, M. Morimitsu, "Ordered nano particles in

amorphous IrO_2-Ta_2O_5 coatings detected by SEM detected by low accelerated incident electrons acidic solutions", Electrochemistry, **77** (2009) 879-881.

[160] K. Kawaguchi, G.M. Haarberg, M. Morimitsu, "Nano-architecture on the mud-cracked surface of IrO_2-Ta_2O_5 binary system", ECS Transactions, **25** (2010) 67-73.

[161] K. Kawaguchi, G.M. Haarberg, M. Morimitsu, "Suppression of PbO_2 deposition on nano-structure surface of IrO_2-Ta_2O_5/Ti anodes in acidic solutions", ECS Transactions, **50** (2013) 75-85.

[162] K. Kinoshita, "Chlor-alkali technology", Electrochemical Oxygen Technology, The Electrochemical Society Series (1992) 339-348.

[163] S. Trasatti, G. Buzzanca, "Ruthenium dioxide: A new interesting electrode material. Solid state structure and electrochemical behaviour", J. Electroanal. Chem., **29** (1971) A1-A5.

[164] D. Galizzioli, F. Tantardini, S. Trasatti, "Ruthenium dioxide: a new electrode material. I. Behaviour in acid solutions of inert electrolytes", J. Appl. Electrochem., **4** (1974) 57-67.

[165] T. Arikawa, Y. Murakami, Y. Takasu, "Simultaneous determination of chlorine and oxygen evolving at RuO_2/Ti and RuO_2-TiO_2/Ti anodes by differential electrochemical mass spectroscopy", J. Appl. Electrochem., **28** (1988) 511-516.

[166] V.I. Eberil', N.S. Fedotova, E.A. Novikov, A.F. Mazanko, "Studying the link between the potential of a metal-oxide anode, the current efficiency for chlorate, and the current losses for the oxygen and chlorine evolution in a wide range of the chlorate electrolysis conditions", Russian J. Electrochem., **36** (2000) 1463-1470.

[167] S.W. Evdokimov, "Electrochemical and corrosion behavior of dimensionally stable anodes in chlorate electrolysis: efficiency of the sodium chlorate production at elevated temperatures", Elektrokhimiya **37** (2001) 363-371.

[168] A. Cornell, B. Håkansson, G. Lindbergh, "Ruthenium based DSA® in chlorate electrolysis-critical anode potential and reaction kinetics", Electrochim. Acta, **48** (2003) 473-481.

[169] A. Cornell, "Electrode reactions in the chlorate process", PhD thesis, Royal Institute of Technology, Stockholm (2002).

[170] M. Morimitsu, K. Kawaguchi, "A novel bifunctionality of RuO_2-TiO_2 electrocatalyst prepared by low temperature thermal decomposition", J. Surface Finishing Society of Japan, **60** (2009) 817-819.

[171] J. Rossmeisl, A. Logadottir, J.K. Nørskov, "Electrolysis of water on (oxidized) metal surfaces", chemical Physics, **319** (2005) 178-184.

[172] J. Rossmeisl, Z.W. Qu, H. Zhu, G.J. Kroes, J.K. Nørskov, "Electrolysis of water on oxide surfaces", J. Electroanalytical Chemistry, **607** (2007) 83-89.

[173] I.C. Man, H.Y. Su, F. Calle-Vallejo, H.A. Hansen, J.I. Martínez, N.G. Inoglu, J.

Kitchin, T.F. Jaramillo, J.K. Nørskov, J. Rossmeisl, "Universality in Oxygen Evolution Electrocatalysis on Oxide Surfaces", ChemCatChem, **3** (2011) 1159-1165.

[174] L.M. Da Silva, J.F.C. Boodts, L.A. De Faria, "Oxygen evolution at $RuO_2(x)+Co_3O_4(1-x)$ electrodes from acid solution", Electrochim. Acta, **46** (2001) 1369-1375.

[175] J. Melsheimer, D. Ziegler, "The oxygen electrode reaction in acid solutions on RuO_2 electrodes prepared by the thermal decomposition method", Thin Solid Films, **163** (1988) 301-308.

[176] J. Cheng, H. Zhang, G. Chen, Y. Zhang, "Study of $Ir_xRu_{1-x}O_2$ oxides as anodic electrocatalysts for solid polymer electrolyte water electrolysis", Electrochim. Acta, **54** (2009) 6250-6256.

[177] F. Hine, M. Yasuda, T. Noda, T. Yoshida, J. Okuda, "Electrochemical Behavior of the Oxide‐Coated Metal Anodes", J. Electrochem. Soc., **126** (1979) 1439-1445.

[178] G. Lodi, E. Sivieri, A. De Battisti, S. Trasatti, "Ruthenium dioxide-based film electrodes", J. Appl. Electrochem., **8** (1978) 135-143.

[179] R. Kötz, S. Stucki, D. Scherson, D.M. Kolb, "In-situ identification of RuO_4 as the corrosion product during oxygen evolution on ruthenium in acid media", J. Electroanalytical Chemistry and Interfacial Electrochemistry, **172** (1984) 211-219.

[180] S. Ardizzone, M. Falciola, S. Trasatti, "Effect of the Nature of the Precursor on the Electrocatalytic Properties of Thermally Prepared Ruthenium Oxide", J. Electrochem. Soc., **136** (1989) 1545-1550.

[181] Lj.M. Gajić-Krstajić, T.Lj. Trišović, N.V. Krstajić, "Spectrophotometric study of the anodic corrosion of Ti/RuO_2 electrode in acid sulfate solution", Corrosion Science, **46** (2004) 65-74.

[182] T.E. Lister, Y. Chu, W. Cullen, H. You, R.M. Yonco, J.F. Mitchell, Z. Nagy, "Electrochemical and X-ray scattering study of well defined RuO_2 single crystal surfaces", J. Electroanalytical Chemistry, **524-525** (2002) 201-218.

[183] E. Fachinotti, E. Guerrini, A.C. Tavares, S. Trasatti, "Electrocatalysis of H_2 evolution by thermally prepared ruthenium oxide: Effect of precursors: Nitrate vs. chloride", J. Electroanal. Chem., **600** (2007) 103-112.

[184] W.C. Fang, J.H. Huang, L.C. Chen, Y.L.O. Su, K.H. Chen, "Effect of temperature annealing on capacitive and structural properties of hydrous ruthenium oxides", J. Power Sources, **160** (2006) 1506-1510.

[185] S. Ardizzone, G. Fregonara, S. Trasatti, "Inner" and "outer" active surface of RuO_2 electrodes, Electrochimica Acta, **35** (1990) 263-267.

[186] C.C. Hu, Y.H. Huang, K.H. Chang, "Annealing effects on the physicochemical characteristics of hydrous ruthenium and ruthenium–iridium oxides for

electrochemical supercapacitors", J. Power Sources, **108** (2002) 117-127.

[187] Y.Y. Liang, H.L. Li, X.G. Zhang, "Solid state synthesis of hydrous ruthenium oxide for supercapacitors", J. Power Sources, **173** (2007) 599-605.

[188] L.M. Huang, H.Z. Lin, T.C. Wen, A. Gopalan, "Highly dispersed hydrous ruthenium oxide in poly (3,4-ethylenedioxythiophene) – poly (styrene sulfonic acid) for supercapacitor electrode", Electrochimica Acta, **52** (2006) 1058-1063.

[189] R.S. Yeo, J. Orehotsky, W. Visscher, S. Srinivasan, "Ruthenium-based mixed oxides as electrocatalysts for oxygen evolution in acid electrolytes", J. Electrochem. Soc., **128** (1981) 1900-1904.

[190] M.E.G. Lyons, L.D. Burke, "Mechanism of oxygen reactions at porous oxide electrodes. Part 1-Oxygen evolution at RuO_2 and $Ru_xSn_{1-x}O_2$ electrodes in alkaline solution under vigorous electrolysis conditions", J. Chem. Soc., Faraday Trans., **1** (1987) 299-321.

[191] M.E.G. Lyons, S. Floquet, "Mechanism of oxygen reactions at porous oxide electrodes. Part 2-Oxygen evolution at RuO_2, IrO_2 and $Ir_xRu_{1-x}O_2$ electrodes in aqueous acid and alkaline solution", Phys. Chem. Chem. Phys., **13** (2011) 5314-5335.

[192] D. Miousse, A. Lasia, "Hydrogen evolution reaction on RuO_2 electrodes in alkaline solutions", J. New Mat. Electrochem. Sys., **2** (1999) 71-78.

[193] H. Wendt, V. Plzak, "Electrocatalytic and thermal activation of anodic oxygen- and cathodic hydrogen-evolution in alkaline water electrolysis", Electrochimica Acta, **28** (1983) 27-34.

[194] B. Børresen, G. Hagen, R. Tunold, "Hydrogen evolution on $Ru_xTi_{1-x}O_2$ in 0.5 M H_2SO_4", Electrochim. Acta, **47** (2002) 1819-1827.

[195] J. Aromaa, O. Forsén, "Evaluation of the electrochemical activity of a Ti-RuO_2-TiO_2 permanent anode", Electrochim. Acta, **51** (2006) 6104-6110.

[196] P.D.P. Alves, M. Spagnol, G. Treiliosi-Filho, A.R. de Andrade, "Investigation of the influence of the anode composition of DSA-type electrodes on the electrocatalytic oxidation of phenol in neutral medium", J. Braz. Chem. Soc., **15** (2004) 626-634.

[197] M. Spasojević, L. Ribić-Zelenović, P. Spasojević, "Microstructure of new composite electrocatalyst and its anodic behavior for chlorine and oxygen evolution", Ceram. Int., **38** (2012) 5827-5833.

[198] A.R. Zeradjanin, F.L Mantia, J. Masa, W. Schuhmann, "Utilization of the catalyst layer of dimensionally stable anodes - Interplay of morphology and active surface area", Electrochim. Acta, **82** (2012) 408-414.

[199] J.C. Forti, A. Manzo-Robledo, K.B. Kokoh, A.R. de Andrade, N. Alonso-Vante, "Electrooxidation of acetaldehyde on platinum-modified Ti/$Ru_{0.3}Ti_{0.7}O_2$ electrodes", Electrochim. Acta, **51** (2006) 2800-2808.

[200] G.R.P. Malpass, D.W. Miwa, S.A.S. Machado, P. Olivi, A.J. Motheo, "Oxidation of the pesticide atrazine at DSA electrodes", J. Hazard. Mater., **137** (2006) 565-572.

[201] G.R.P. Malpass, R.S. Neves, A.J. Motheo, "A comparative study of commercial and laboratory-made Ti/$Ru_{0.3}Ti_{0.7}O_2$ DSA® electrodes: "In situ" and "ex situ" surface characterisation and organic oxidation activity", Electrochim. Acta, **52** (2006) 936-944.

[202] D. Čukman, M. Vuković, M. Milun, "Enhanced oxygen evolution on an electrodeposited ruthenium + iridium coating on titanium", J. Electroanal. Chem., **389** (1995) 209-213.

[203] L.E. Owe, M. Tsypkin, K.S. Wallwork, R.G. Haverkamp, S. Sunde, "Iridium-ruthenium single phase mixed oxides for oxygen evolution: Composition dependence of electrocatalytic activity", Electrochim. Acta, **70** (2012) 158-164.

[204] J.C. Cruz, A.R. Hernández, M.G. Balcazar, A.U. Chávez-Ramirez, J.L. García, L.G. Arriaga, "Electrochemical evaluation of a Ir-Ru binary oxide for oxygen evolution reaction", Int. J. Electrochem. Sci., **7** (2012) 7866-7876.

[205] J. Ribeiro, A.R. de Andrade, "Characterization of RuO_2-Ta_2O_5 coated titanium electrode microstructure, morphology, and electrochemical investigation", J. Electrochem. Soc., **151** (2004) D106-D112.

[206] J. Ribeiro, A.R. de Andrade, "Investigation of the electrical properties, charging process, and passivation of RuO_2-Ta_2O_5 oxide films", J. Electroanal. Chem., **592** (2006) 153-162.

[207] J. Ribeiro, M.S. Moats, A.R. de Andrade, "Morphological and electrochemical investigation of RuO_2-Ta_2O_5 oxide films prepared by the Pechini-Adams method", J. Appl. Electrochem., **38** (2008) 767-775.

[208] J. Ribeiro, F.L.S. Purgato, K.B. Kokoh, J.M. Léger, A.R. de Andrade, "Application of Ti/RuO_2-Ta_2O_5 electrodes in the electrooxidation of ethanol and derivants: Reactivity versus electrocatalytic efficiency", Electrochim. Acta, **53** (2008) 7845-7851.

[209] J.J. Jow, H.H. Lai, H.R. Chen, C.C. Wang, M.S. Wu, T.R. Ling, "Effect of hydrothermal treatment on the performance of RuO_2-Ta_2O_5/Ti electrodes for use in supercapacitors", Electrochimica Acta, **55** (2010) 2793-2798.

[210] H.R. Chen, H.H. Lai, J.J. Jow, "Annealing effect on the performance of RuO_2-Ta_2O_5/Ti electrodes for use in supercapacitors", Materials Chemistry and Physics, **125** (2011) 652-655.

[211] O.R. Camara, S. Trasatti, "Surface electrochemical properties of Ti/(RuO_2+ZrO_2) electrodes", Electrochim. Acta, **41** (1996) 419-427.

[212] C.C. Hu, K.H. Chang, C.C. Wang, "Two-step hydrothermal synthesis of Ru-Sn oxide composites for electrochemical supercapacitors", Electrochim. Acta, **52**

(2007) 4411-4418.

[213] J. Gaudet, A.C. Tavares, S. Trasatti, D. Guay, "Physicochemical characterization of mixed RuO_2- SnO_2 solid solutions", **17** (2005) 1570-1579.

[214] X. Wu, J. Tayal, S. Basu, K. Scott, "Nano-crystalline $Ru_xSn_{1-x}O_2$ powder catalysts for oxygen evolution reaction in proton exchange membrane water electrolysers", Int. J. Hydrogen Energy, **36** (2011) 14796-14804.

[215] M. Ito, Y. Murakami, H. Kaji, K. Yahikozawa, Y. Takasu, "Surface characterization of RuO_2-SnO_2 coated titanium electrodes", J. Electrochem. Soc., **143** (1996) 32-36.

[216] L. Nanni, S. Polizzi, A. Benedetti, A. De Battisti, "Morphology, microstructure, and electrocatalytic properties of RuO_2-SnO_2 thin films", J. Electrochem. Soc., **146** (1999) 220-225.

[217] F. Ferrara, "New materials for eco-sustainable electrochemical processes: oxygen evolution reaction at different electrode materials", PhD thesis, University of Cagliari (2008).

[218] M. Vuković, D. Marijan1, D. Čukman, P. Pervan, M. Milun, "Electrocatalytic activity and anodic stability of electrodeposited ruthenium-rhodium coatings on titanium", J. Materials Science, **34** (1999) 869-874.

[219] F. Pico, J.Ibañez, T.A. Centeno, C. Pecharroman, R.M. Rojas, J.M. Amarilla, J.M. Rojo, "$RuO_2 \cdot xH_2O$/NiO composites as electrodes for electrochemical capacitors: Effect of the RuO_2 content and the thermal treatment on the specific capacitance", Electrochimica Acta, **51** (2006) 4693-4700.

[220] I.J. Godwin, R.L. Doyle, M.E.G. Lyons, "The mechanism of oxygen reactions at porous oxide electrodes III. Water Oxidation Catalysis at RuO_2/NiO Mixed Oxide Electrodes", J. Electrochem. Soc., **161** (2014) F906-F917.

[221] I.J. Godwin, M.E.G. Lyons, "Dimensionally Stable Anodes (DSA®) for Electrochemical Water Splitting: Redox Properties, OER Kinetics and Mechanism at RuO_2/NiO Modified Electrodes in Aqueous Base", ECS Trans., **53** (2013) 21-31.

[222] A. Colombo, "Preparation and performance evolution of materials for electrocatalytic applications", PhD thesis, University of Milan (2010).

[223] R. Bertoncello, S. Cattarin, I. Frateur, M. Musiani, "Preparation of anodes for oxygen evolution by electrodeposition of composite oxides of Pb and Ru on Ti", J. Electroanalytical Chemistry, **492** (2000) 145-149.

[224] T.A.F. Lassali, J.F.C. Boodts, S. Trasatti, "Electrocatalytic activity of the ternary oxide $Ru_{0.3}Pt_xTi_{(0.7-x)}O_2$ for chlorine evolution", Electrochimica Acta, **39** (1994) 1545-1549.

[225] S.M. Hoseinieh, F. Ashrafizadeh, M.H. Maddahi, "A Comparative investigation of the corrosion behavior of RuO_2-IrO_2-TiO_2 coated titanium anodes in chloride

solutions", J. Electrochem. Soc., **157** (2010) E50-E56.

[226] S. Barison, A. de Battisti M. Fabrizio, S. Daolio, C. Piccirillo, "Surface chemistry of $RuO_2/IrO_2/TiO_2$ mixed-oxide electrodes: secondary ion mass spectrometric study of the changes induced by electrochemical treatment", Rapid Communications in Mass Spectrometry, **14** (2000) 2165-2169.

[227] S. Barison, S. Daolio, M. Fabrizi, A. de Battisti, "Surface chemistry study of $RuO_2/IrO_2/TiO_2$ mixed-oxide electrodes", Rapid Communications in Mass Spectrometry, **18** (2004) 278-284.

[228] M.E. Makgae, C.C. Theron, W.J. Przybylowicz, A.M. Crouch, "Preparation and surface characterization of Ti/SnO_2-RuO_2-IrO_2 thin films as electrode material for the oxidation of phenol", Mater. Chem. Phys., **92** (2005) 559-564.

[229] L. Vazquez-Gomez, S. Ferro, A. de Battisti, "Preparation and characterization of RuO_2-IrO_2-SnO_2 ternary mixtures for advanced electrochemical technology", Applied Catalysis B: Environmental, **67** (2006) 34-40.

[230] R. Hutchings, K. Muller, R. Kotz, S. Stucki, "A structural investigation of stabilized oxygen evolution catalysts", J. Mater. Sci., **19** (1984) 3987-3994.

[231] J.F.C. Boodts, S. Trasatti, "Effect of composition on the electrocatalytic activity of the ternary oxide $Ru_{0.3}Ti_{(0.7-x)}Sn_xO_2$", J. Electrochem. Soc., **137** (1990) 3784-3789.

[232] A.I. Onuchukwu, S. Trasatti, "Effect of substitution of SnO_2 for TiO_2 on the surface and electrocatalytic properties of RuO_2+TiO_2 electrodes", J. Appl. Electrochem. **21** (1991) 858-862.

[233] D.T. Shieh, B. Hwang, "Morphology and electrochemical activity of Ru-Ti-Sn ternary-oxide electrodes in 1 M NaCl solution", J. Electrochim. Acta **38** (1993) 2239-2246.

[234] X. Chen, G. Chen, "Stable Ti/RuO_2-Sb_2O_5-SnO_2 electrodes for O_2 evolution", Electrochimica Acta, **50** (2005) 4155-4159.

[235] K.C. Fernandes, L.M. Da Silva, J.F.C. Boodts, L.A. de Faria, "Surface, kinetics and electrocatalytic properties of the $Ti/(Ti+Ru+Ce)O_2$-system for the oxygen evolution reaction in alkaline medium," Electrochim. Acta, **51** (2006) 2809-2818.

[236] H. Wu, Q. Ruan, L. Li, B. Wang, "Characterization and electrocatalytic properties of titanium-based $Ru_{0.3}Co_{0.7-x}Ce_x$ mixed oxide electrodes for oxygen evolution in alkaline solution", J. Nanomater., **2011** (2011) 1-7.

[237] J. Ribeiro, G. Tremiliosi-Filho, P. Olivi, A.R. de Andrade, "XAS characterization of the RuO_2-Ta_2O_5 system local (crystal) structure", Material Chemistry and Physics, **125** (2011) 449-460.

[238] T.Y. Chang, X. Wang, D.A. Evans, S.L. Robinson, J.P. Zheng, "Tantalum oxide–ruthenium oxide hybrid$^{(R)}$ capacitors", J. Power Sources, **110** (2002) 138-143.

[239] J. Kristóf, T. Szilágyi, E. Horváth, R.L. Frost, "Investigation of RuO_2/Ta_2O_5 thin film evolution by thermogravimetry combined with mass spectrometry", Thin Solid Films, **485** (2005) 90-94.

[240] Y. Chen, T. Zhang, X. Wang, Y. Shao, and D. Tang, "Phase structure and microstructure of a Nanoscale TiO_2-RuO_2-IrO_2-Ta_2O_5 anode coating on titanium", J. Am. Ceram. Soc., **91** (2008) 4154-4157.

[241] H. Nakata, K. Takahashi, Y. Kawashima, K. Ohnishi, "Electrolytic electrode and its production", JP patent application No. 1994-122988.

[242] T. Shimamune, Y. Nakashima, "Electrode for electrolysis", JP patent application No. 1993-059580.

[243] R.A.B. Devine, C. Chaneliere, J.L. Autran, B. Balland, P. Paillet, J.L. Leray, "Use of carbon-free Ta_2O_5 thin-films as a gate insulator", Microelectronic Engineering, **36** (1997) 61-64.

[244] K.A. McKinley, N.P. Sandler, Tantalum pentoxide for advanced DRAM applications, Thin Solid Films, **290-291** (1996) 440-446.

[245] S Jakobs, A Duparré, M Huter, H.K Pulker, "Surface roughness characterization of smooth optical films deposited by ion plating", Thin Solid Films, **351** (1999) 141-145.

[246] T. Ushikubo, "Recent topics of research and development of catalysis by niobium and tantalum oxides", Catalysis Today, **57** (2000) 331-338.

[247] B.L. Newalkar, S. Komarneni, H. Katsuki, "Synthesis and characterization of hexagonally packed mesoporous tantalum oxide thin film", Materials Letters, **57** (2002) 444-447.

Chapter 2

Experimental

2.1 Electrode preparation

RuO_2-Ta_2O_5 coated titanium electrodes and RuO_2 coated titanium electrodes were prepared by thermal decomposition of precursor solutions. The main steps in the preparation are shown in Figure 2.1. The precursor solutions were made by dissolving commercially available $RuCl_3 \cdot 3H_2O$ with and without $TaCl_5$ into 1-butanol containing 6 vol% HCl. The ratio of Ru:Ta was ranged from 30:70 mol% to 90:10 mol% for RuO_2-Ta_2O_5 coatings, and the total metal concentration was 50 g/L. Titanium substrates (10×50×1 mm) were degreased ultrasonically in acetone and etched in 10 wt.% oxalic acid solutions at 90 ^oC for 60 min, washed with distilled water, and dried. Then, the titanium substrate was dipped into the precursor solution at room temperature, dried at 120 ^oC for 10 min for solvent vaporization, and finally calcined at a temperature between 260 ^oC and 500 ^oC in air for 20 min. This dipping-drying-calcination process was repeated until the desired amount of coating was obtained enough for good reproducibility.

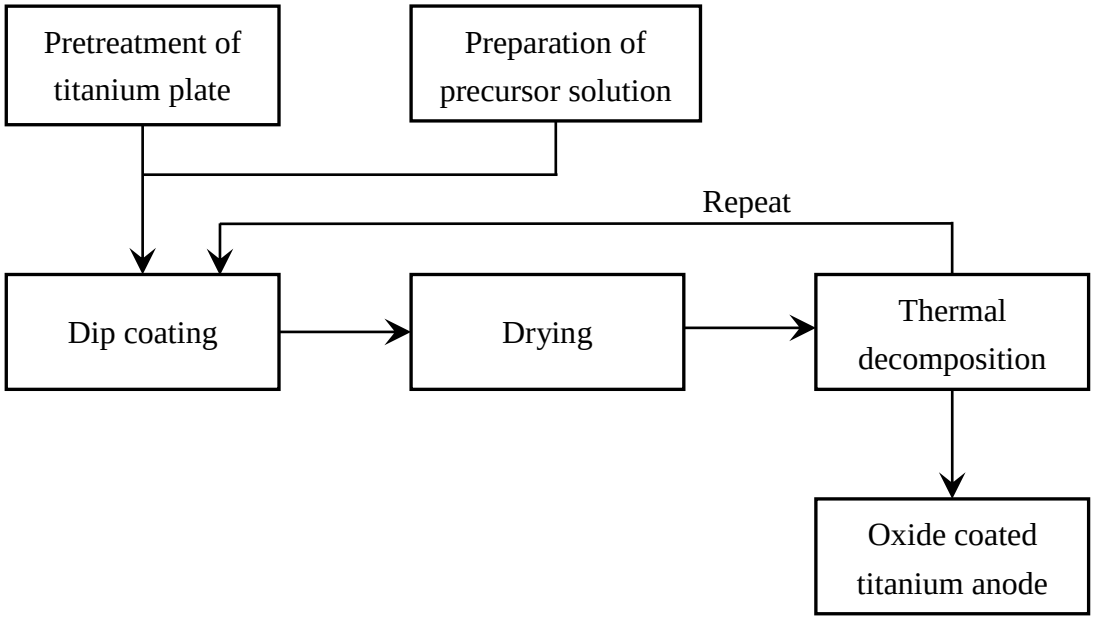

Figure 2.1 Preparation procedure of electrodes.

IrO_2-Ta_2O_5 coated titanium electrodes and RuO_2-TiO_2 coated titanium electrodes were also prepared by the similar preparation procedure for comparison. The precursor solutions were prepared by dissolving $H_2IrCl_6 \cdot 6H_2O$ and $TaCl_5$ into 1-butanol containing 6 vol% HCl or by dissolving $RuCl_3 \cdot 3H_2O$ and $Ti(C_4H_9O)_4$ into 1-butanol without HCl. The metal compositions in those solutions were Ir:Ta = 80:20 mol% and Ru:Ti = 30:70 mol%, and the total metal concentrations were 70 g/L for Ir + Ta and 100 g/L for Ru + Ti. The thermal decomposition was carried out at 360 ^oC or 470 ^oC for IrO_2-Ta_2O_5 coatings and at 280 ^oC for RuO_2-TiO_2 coatings.

2.2 Characterization of the oxide coatings

The crystallographic structure of the obtained oxide coatings was characterized by X-ray diffraction method (XRD) using Rigaku Model Ultima IV (CuKα radiation (λ=1.541Å), 40 kV at 40 mA current). The surface morphology was observed by scanning electron microscopy (SEM) using a ZEISS Model ULTRA55 with in-lens SE detector and 5 keV acceleration voltage. The elemental distribution was analyzed using AMETEK Model Genesis APEX2 energy dispersive X-ray spectrometer (EDX) with acceleration voltage of 5 keV.

2.3 Electrochemical measurements

Electrochemical measurements were conducted using a conventional three-electrode cell equipped with a KCl-saturated Ag/AgCl reference electrode and a platinum plate counter electrode as shown in Figure 2.2, in which the reference electrode's compartment was connected to the working electrode's one with a salt bridge and a Luggin capillary tip within 1 cm gap to suppress a large *iR* drop. The exposed surface area of the working electrode was limited to 1 cm^2 by using PTFE holder, and the solutions were used without stirring.

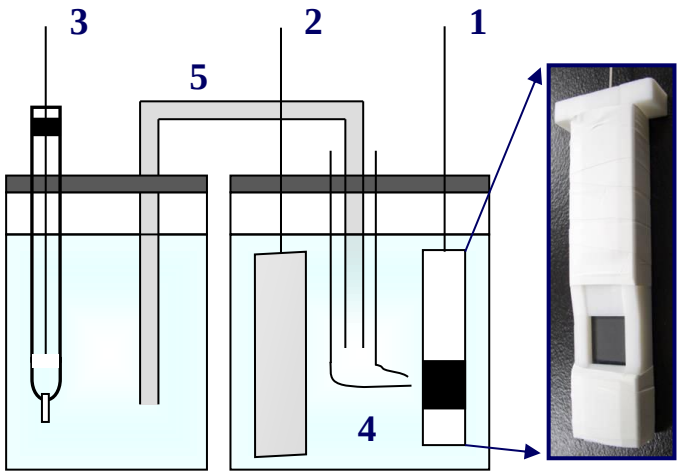

1. Working electrode (1 cm×1 cm) 2. Counter electrode (5 cm×5 cm)
3. Reference electrode 4. Electrolyte 5. Salt bridge

Figure 2.2 Schematic drawing of a three-electrode cell for electrochemical measurements.

Reagent grade H_2SO_4 and distilled water were used to prepare 2.0 mol dm^{-3} H_2SO_4 solution (pH = -0.38). HNO_3 solutions with and without $Pb(NO_3)_2$ were also used to investigated the suppression effects on anodic PbO_2 deposition. The pH of HNO_3 solutions was adjusted to 0.7. The reason why HNO_3 solutions were used is Pb(II) ions has a high solubility in HNO_3. The bath temperature was held at 40 ^oC for H_2SO_4 solution and at 30 ^oC for HNO_3 solutions.

All measurements were done with a potentio/galvanostat (EG&G, Model 263A) controlled by electrochemical analysis software (EG&G, Model 270). The data were not corrected for IR drop because it was almost zero in H_2SO_4 and HNO_3 solutions.

Double layer charging current and polarization curve were measured by cyclic

voltammetry in the H_2SO_4 solution at a scan rate of 5 mV s^{-1}. Tafel slope was obtained from the results of linear sweep voltammetry at 0.5 mV s^{-1}. Oxygen evolution potential was evaluated by constant current electrolysis at various current densities. Constant current electrolysis was also employed to determine the amount of the deposited PbO_2 deposition.

2.4 Cell voltage measurements

The cell voltages of zinc, copper, nickel or cobalt EW were measured by constant current electrolysis using a two-electrode cell as shown in Figure 2.3. In the measurements, the RuO_2-Ta_2O_5/Ti electrode, the amorphous IrO_2-Ta_2O_5/Ti electrode, and the commercially available Pb-5%Sb alloy electrode were used as the anode. The cathode was zinc, copper, nickel or cobalt plate, of which the size was 4 cm^2. The current density was based on the geometric surface area of the anode. The electrolyte composition and pH are shown in Table 2.1. All electrolytes comprised sulfates, and sodium hydroxide solution was used to adjust pH for nickel EW solutions.

2.5 Accelerated life tests

The durability of RuO_2-Ta_2O_5/Ti anodes was investigated by constant current electrolysis at high current density of 5,000 A m^{-2} based on the geometric surface area of the anode. A two-electrode cell used in this measurement is also shown in Figure 2.3, in which the anode was RuO_2-Ta_2O_5/Ti and the cathode was platinum plate (5×5 cm). The lifetime of the anode was defined as the time at which the cell voltage reached 4 V.

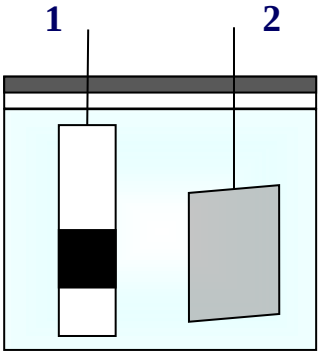

1. Anode (1 cm×1 cm)

2. Cathode (2 cm×2 cm in cell voltage measurements, 5 cm×5 cm in accelerated life tests)

Figure 2.3 Schematic drawing of a two-electrode cell used in cell voltage measurements and accelerated life tests.

Table 2.1 Electrolyte compositions for cell voltage measurements.

	Composition	pH	Temp.
Zinc	H_2SO_4 2.0 mol dm^{-3}, $ZnSO_4$ 0.80 mol dm^{-3}	-0.57	40 ^oC
Copper	H_2SO_4 0.90 mol dm^{-3}, $CuSO_4$ 0.60 mol dm^{-3}	0.0	
Nickel	$NiSO_4$ 1.3 mol dm^{-3}, Na_2SO_4 0.70 mol dm^{-3}	3.5	
Cobalt	H_2SO_4 2.0×10^{-3} mol dm^{-3}, $CoSO_4$ 0.30 mol dm^{-3}	2.8	

Chapter 3

Effects of thermal decomposition temperature

3.1 Introduction

In this Chapter, RuO_2-Ta_2O_5/Ti anodes were prepared at different thermal decomposition temperatures and investigated the relationship between the electrochemical properties of the coatings and their crystallographic structure or surface morphology. The cell voltage data of RuO_2-Ta_2O_5/Ti, IrO_2-Ta_2O_5/Ti and lead alloy anodes for zinc, copper, nickel or cobalt EW are reported.

3.2 Results and discussion

3.2.1 Crystallographic structure

Figure 3.1 (A) shows XRD patterns of RuO_2-Ta_2O_5/Ti which were prepared at 30 mol% Ru and calcined at different decomposition temperatures. First, three peaks at $2\theta = 38.4^o$, 40.2^o and 53.0^o were identified as titanium because the oxide coatings were thin so that X-ray diffraction from titanium was detected. Besides, clear diffraction peaks at $2\theta = 28.0^o$ and 35.0^o, corresponding to (110) and (101) of rutile RuO_2, together with a small peak at $2\theta = 54.2^o$ caused from (211) of RuO_2 were observed when the decomposition temperature was 500 ^{o}C or 360 ^{o}C. Such diffraction peaks of RuO_2 were weakened with decreasing decomposition temperature and finally disappeared at 280 ^{o}C or less. The results indicated that RuO_2 became less crystalline at lowering temperature and amorphization of RuO_2 occurred at 280 ^{o}C.

Figure 3.1 (B) shows XRD patterns of RuO_2-Ta_2O_5/Ti with 80 mol% Ru and obtained at different decomposition temperatures, which shows similar dependence on thermal decomposition temperature to those in Figure 3.1 (A). However, some weak diffraction peaks of RuO_2 were observed at 280 ^{o}C in Figure 3.1 (B), which are not seen in Figure 3.1 (A) at the same temperature, suggesting that Ta_2O_5 co-existing with RuO_2 promotes amorphization of RuO_2. Because RuO_2 and Ta_2O_5 have different crystallographic structures and these two metal oxides are immiscible, it is reasonable

that Ta_2O_5 suppresses the growth of RuO_2 crystallites, and it has been also observed for IrO_2-Ta_2O_5 system [1-7]. Comparing two binary oxide systems, the amorphization of IrO_2 occurred at 400 ^oC or less, so that the amorphous RuO_2 is produced at a temperature which is about 100 ^oC lower than that of amorphous IrO_2. This is a great advantage for anode production on industrial scale.

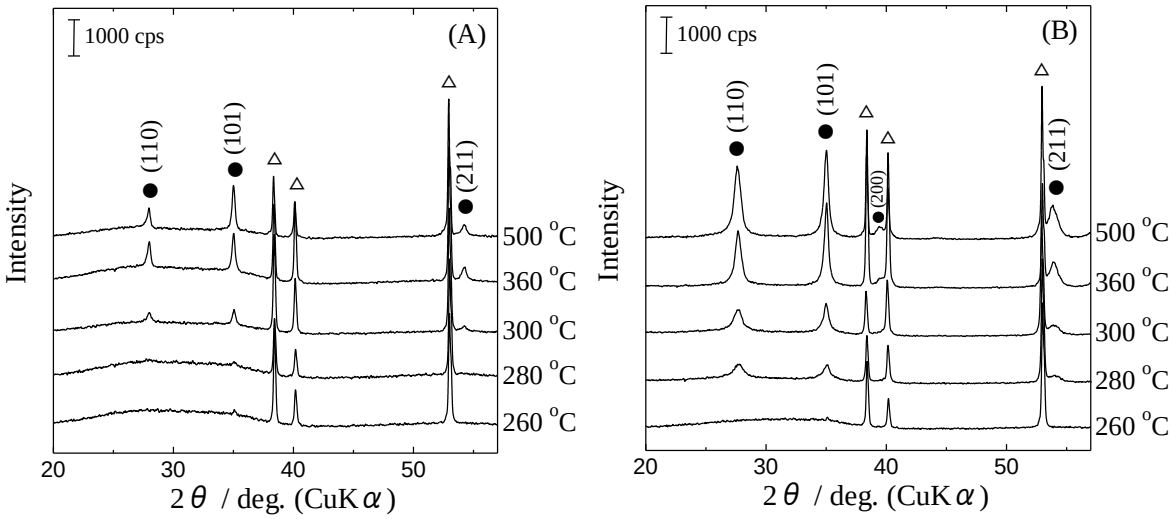

Figure 3.1 XRD patterns of RuO_2-Ta_2O_5/Ti electrodes prepared at different thermal decomposition temperature. Ru ratio: 30 mol% (A) and 80 mol% (B). ●: RuO_2, △: Ti.

Figures 3.1 (A) and (B) presents no diffraction peaks of Ta_2O_5 because crystalline Ta_2O_5 needs high temperature calcination above 600 ^oC, which means that Ta_2O_5 is amorphous in all oxide coatings prepared in this study. Therefore, the oxide coatings prepared at 500 ^oC or 360 ^oC consists of crystalline RuO_2 and amorphous Ta_2O_5, while amorphous RuO_2 and amorphous Ta_2O_5 are mixed in the coatings obtained at lower temperatures.

3.2.2 Surface morphology

Figure 3.2 depicts low magnification SEM images of RuO_2-Ta_2O_5 coatings (30 mol% Ru) prepared at different temperatures. It is well known that RuO_2-Ta_2O_5 and IrO_2-Ta_2O_5 coatings produced by thermal decomposition show a heterogeneous surface which is usually described as "mud-cracked" structure [5-11]. Such a heterogeneous feature was observed for the RuO_2-Ta_2O_5 coatings prepared at 500 ^oC, 360 ^oC or 300 ^oC, as shown in Figure 3.2, which comprises RuO_2 aggregates, flat areas, and cracks, while the coatings obtained at 280 ^oC or 260 ^oC showed no aggregates and consisted of flat areas and cracks. The results coincide with the XRD results; well-developed RuO_2 particles completely disappeared by amorphization of RuO_2. In addition, the number and width of cracks of RuO_2-Ta_2O_5 coatings increased with decreasing decomposition temperature. These surface morphologies of RuO_2-Ta_2O_5 coatings are quite similar to those of amorphous IrO_2-Ta_2O_5 coatings found in the previous studies by our group [2,3,5-7,12-14].

Figure 3.3 depicts magnified SEM images of the aggregated RuO_2 particles at 30 mol% Ru. The aggregate obtained at 500 ^oC is like a cuboid with a pyramid top, and the length was 100 nm to 150 and the height was 150 nm to 250 nm. Such aggregates were also observed on the coating calcined at 360 ^oC, while needle-like particles of 200-250 nm length co-existed in this case. As the temperature was reduced from 360 ^oC to 300 ^oC, RuO_2 became smaller and changed from cuboid to needle-like form. Furthermore, the coatings calcined at 280 ^oC or less presented nano RuO_2 particles with no cuboid and needle-like ones as observed on the coatings at 300 ^oC or more. Figure 3.3 (E-2) shows such nano RuO_2 particles on the coating calcined at 260 ^oC (magnification: 200,000), revealing the particle size is *ca.* 20 nm. These are in good agreement with the XRD results, and the amorphous RuO_2-Ta_2O_5 coatings developed in this work contained nano RuO_2 dispersed in amorphous Ta_2O_5.

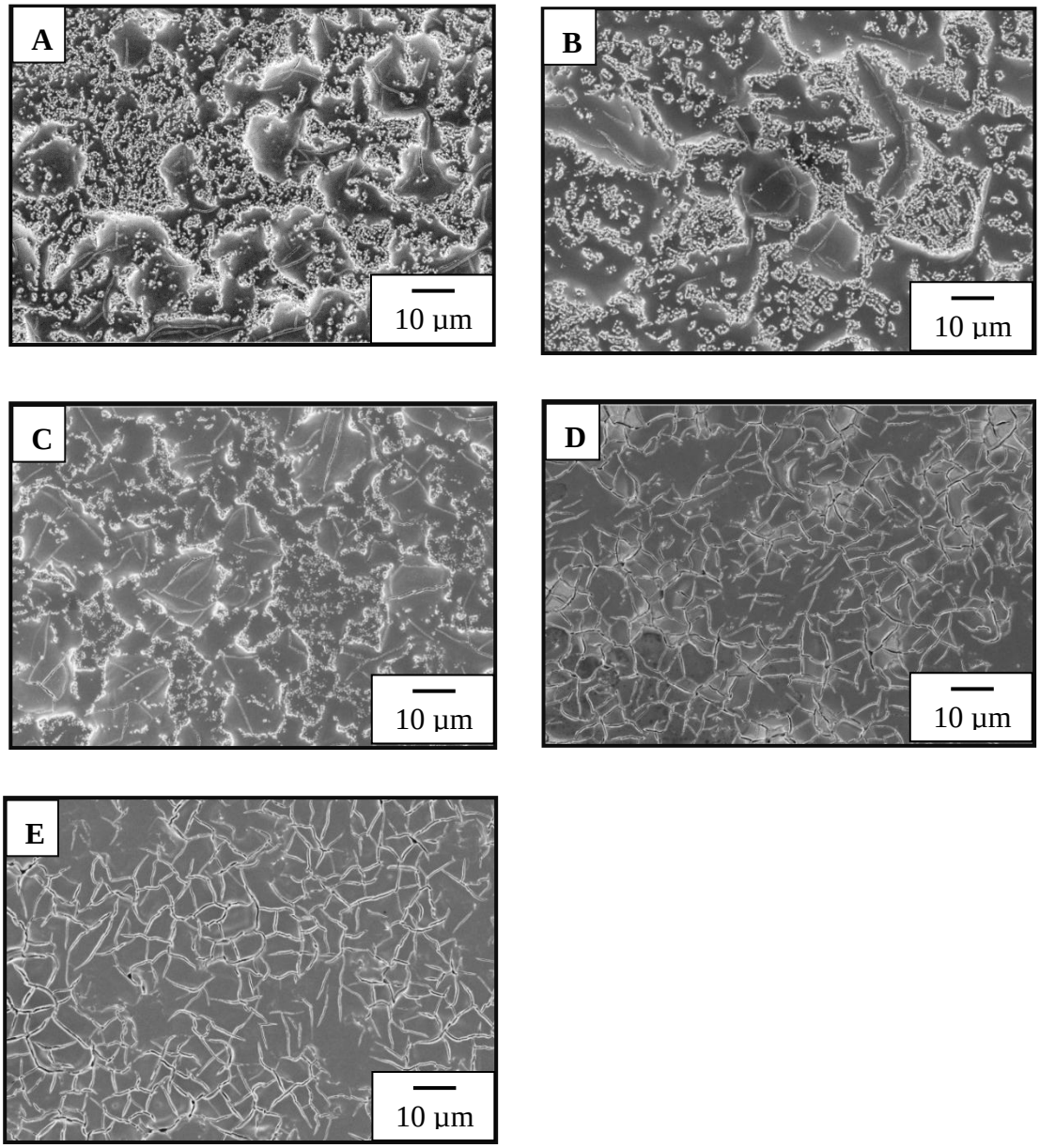

Figure 3.2 Surface morphologies of RuO_2-Ta_2O_5 coatings prepared at 500 ^oC (A), 360 ^oC (B), 300 ^oC (C), 280 ^oC (D) and 260 ^oC (E). Ru ratio: 30 mol%. Magnification: ×1,000.

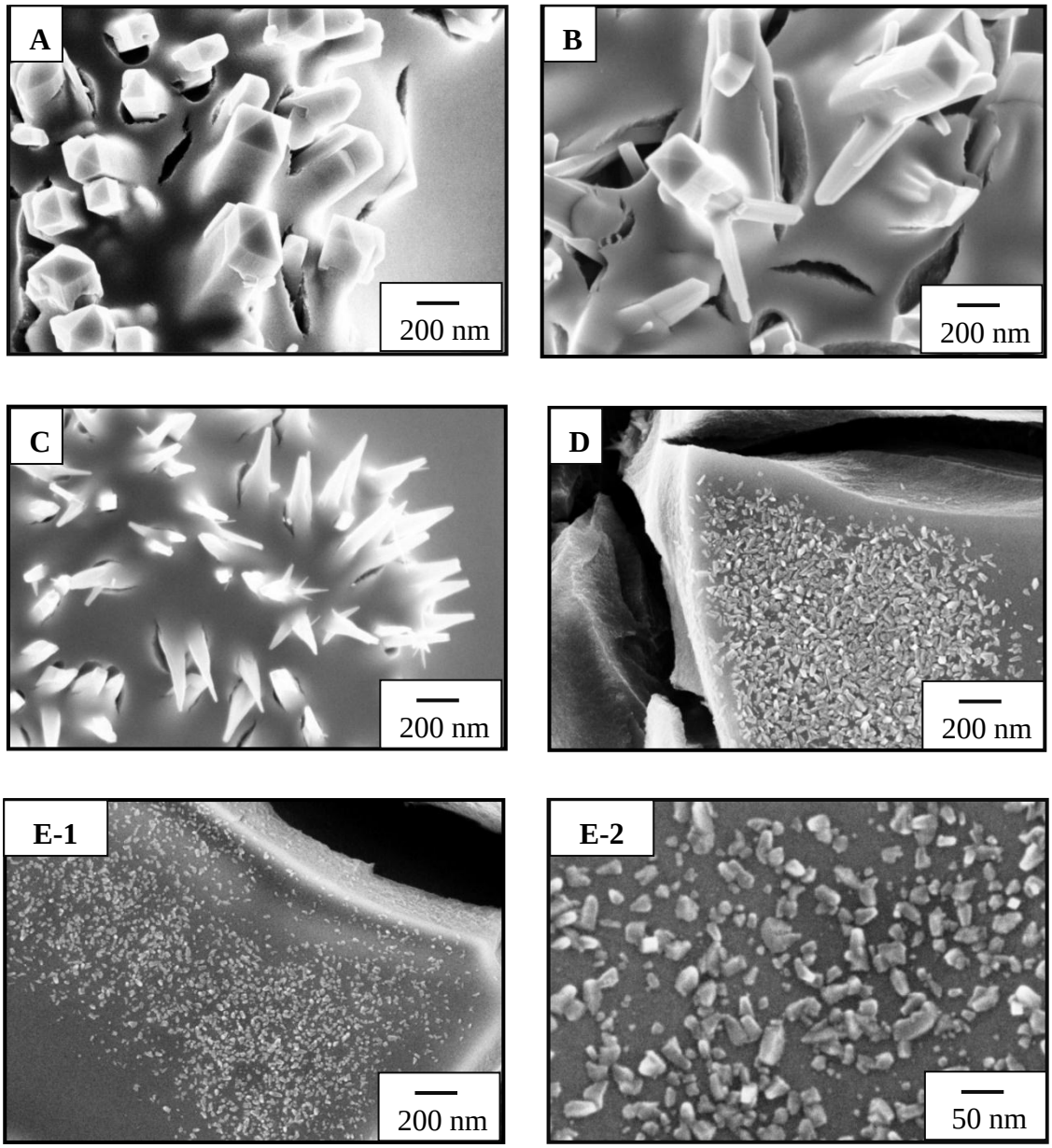

Figure 3.3 Surface morphologies of RuO_2-Ta_2O_5 coatings prepared at 500 ^oC (A), 360 ^oC (B), 300 ^oC (C), 280 ^oC (D) and 260 ^oC (E). Ru ratio: 30 mol%. Magnification: ×50,000 (A, B, C, D, E-1), ×200,000 (E-2).

Most of the surface of the coatings of 30 mol% Ru was covered with flat areas, as shown in Figure 3.4, and no RuO_2 particle was seen on the areas even at high magnification and it was independent of decomposition temperature. It seems that the main component of the flat area is Ta_2O_5 in the case, and this was supported from EDX elemental analysis; the flat area of the coating prepared at 500 ^oC contained only 10 mol% Ru.

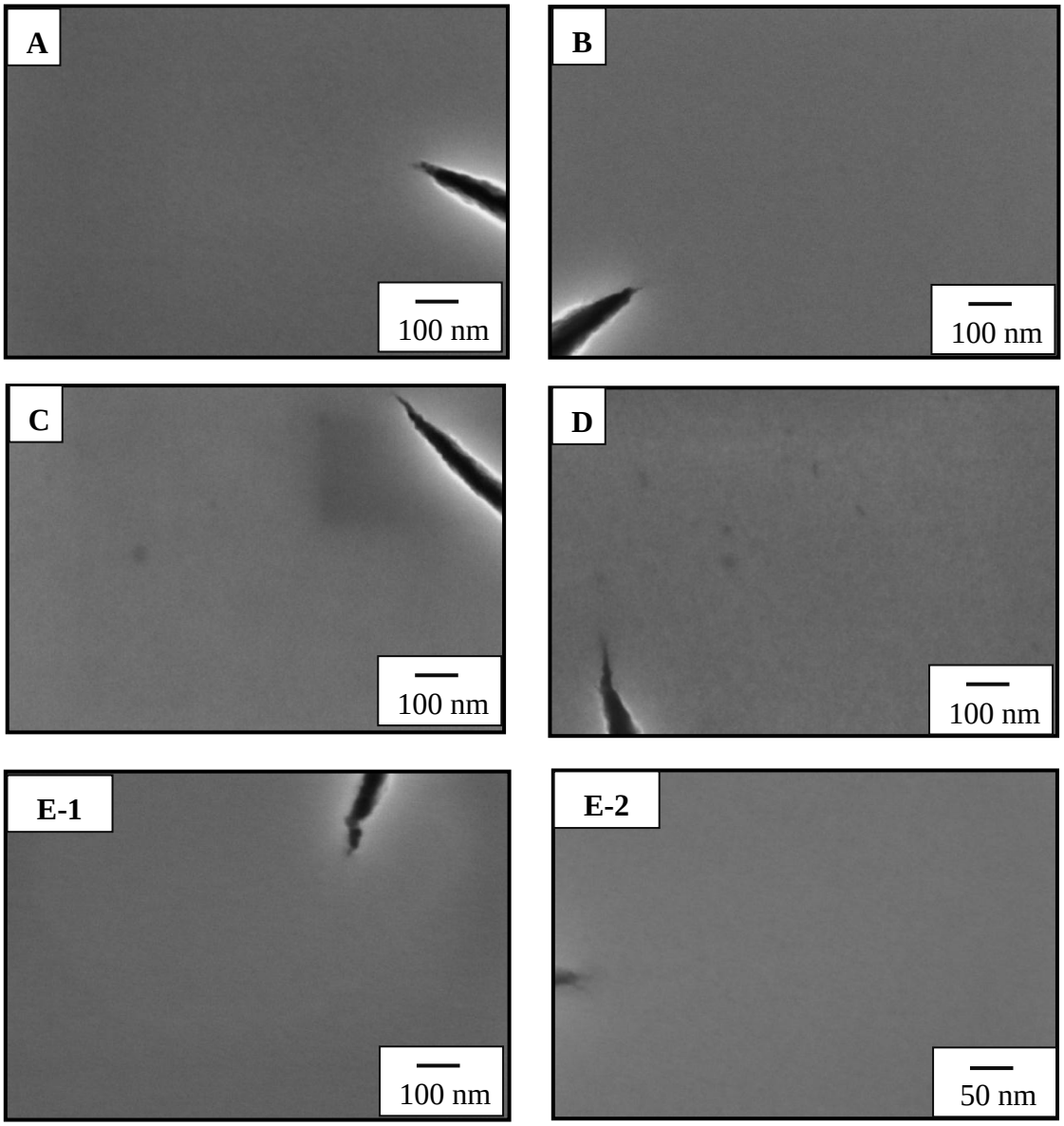

Figure 3.4 Surface morphologies of RuO_2-Ta_2O_5 coatings prepared at 500 ^oC (A), 360 ^oC (B), 300 ^oC (C), 280 ^oC (D) and 260 ^oC (E). Ru ratio: 30 mol%. Magnification: ×100,000 (A, B, C, D, E-1), ×200,000 (E-2).

The cracks of the 30 mol% Ru coatings are shown in Figure 3.5. The width of the cracks at 500 ^{o}C, 360 ^{o}C and 300 ^{o}C was *ca.* 200 nm and increased with lowering decomposition temperature; the width at 280 ^{o}C and 260 ^{o}C was almost double at 300 ^{o}C or more. Therefore, the number and width of cracks tends to increase with amorphization of RuO_2.

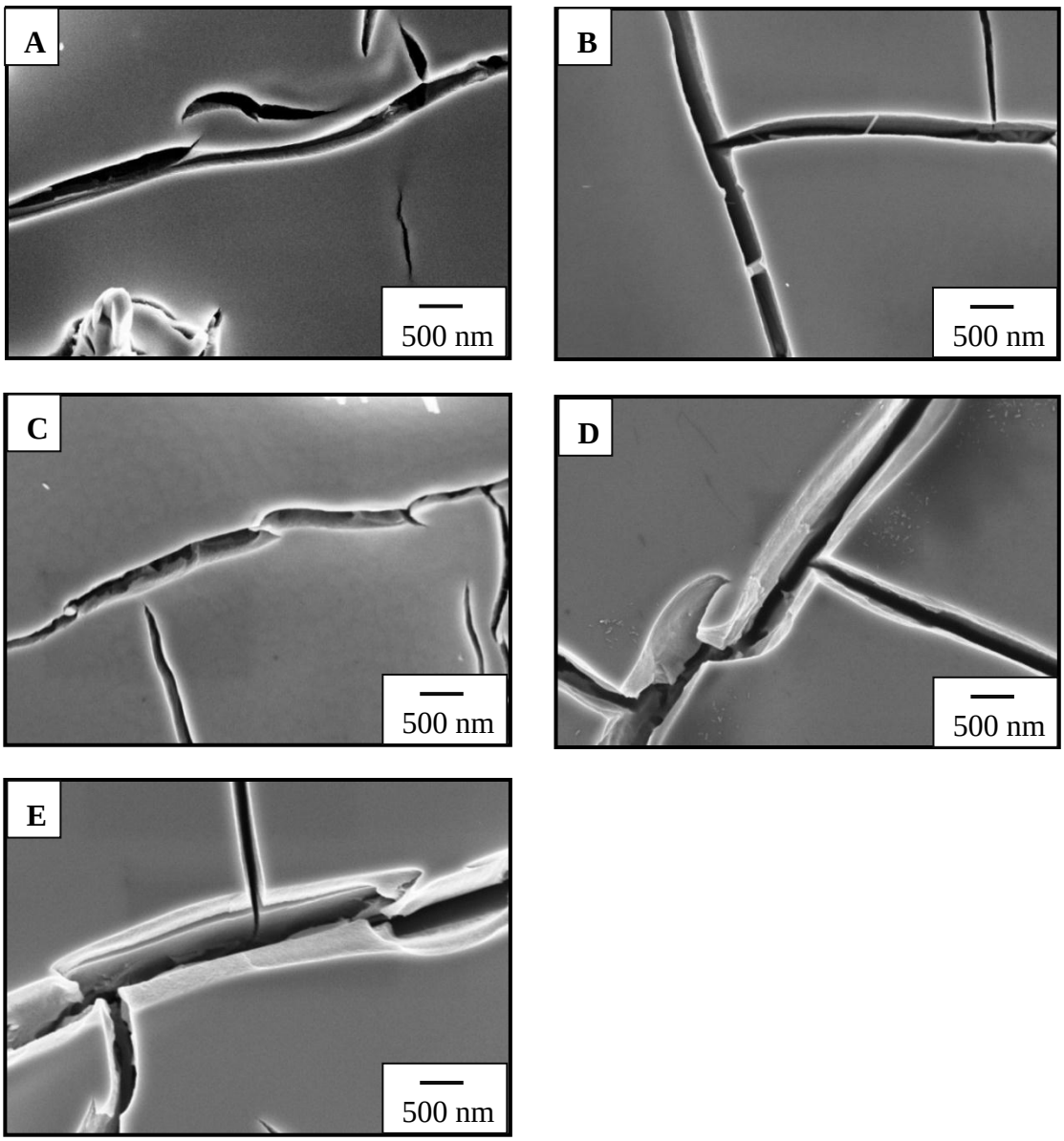

Figure 3.5 Surface morphologies of RuO_2-Ta_2O_5 coatings prepared at 500 ^{o}C (A), 360 ^{o}C (B), 300 ^{o}C (C), 280 ^{o}C (D) and 260 ^{o}C (E). Ru ratio: 30 mol%. Magnification: ×20,000.

Figure 3.6 depicts low magnification SEM images of RuO_2-Ta_2O_5 coatings (80 mol% Ru) calcined at different decomposition temperatures. The coatings calcined at 300 ^oC or more consisted of RuO_2 aggregates, flat areas and cracks, which is similar to the results mentioned above. One of the major differences between the coatings of 80 mol% Ru and 30 mol% Ru was found for the decomposition temperature at 280 ^oC; large RuO_2 aggregates existed on the coating at 80 mol% Ru, while they were not observed at 30 mol% Ru. As for 260 ^oC, the coating consisted of flat areas and cracks with no RuO_2 aggregates even at 80 mol% Ru. These results are in accordance with the XRD data, and the SEM images revealed that the number and width of cracks significantly increased when decomposition temperature was reduced from 280 ^oC to 260 ^oC as similar to 30 mol% Ru coatings. However, the number of cracks at 80 mol% Ru was lower than that at 30 mol% Ru at the same temperature, suggesting that more Ta_2O_5 induces more cracks.

Figure 3.7 depicts magnified SEM images of aggregated RuO_2 particles at 80 mol% Ru. The coatings calcined at 500 ^oC and 360 ^oC showed large cubic RuO_2 particles of *ca.* 150 nm in width and *ca.* 200 nm in height, of which the shape is similar to that at 30 mol% Ru at 500 ^oC, while the particles more agglomerated at 80 mol% Ru. The particle size became small when thermal decomposition temperature decreased from 360 ^oC to 280 ^oC; cube-like particles of 50-80 nm were seen at 300 ^oC and the size was down to 50 nm or less at 280 ^oC. The coating prepared at 260 ^oC shown in Figure 3.7 (E) is distinctive from the others, because the surface looks like very smooth with no particle. It is still different from the surface of the amorphous coating at 30 mol% Ru obtained at 260 ^oC.

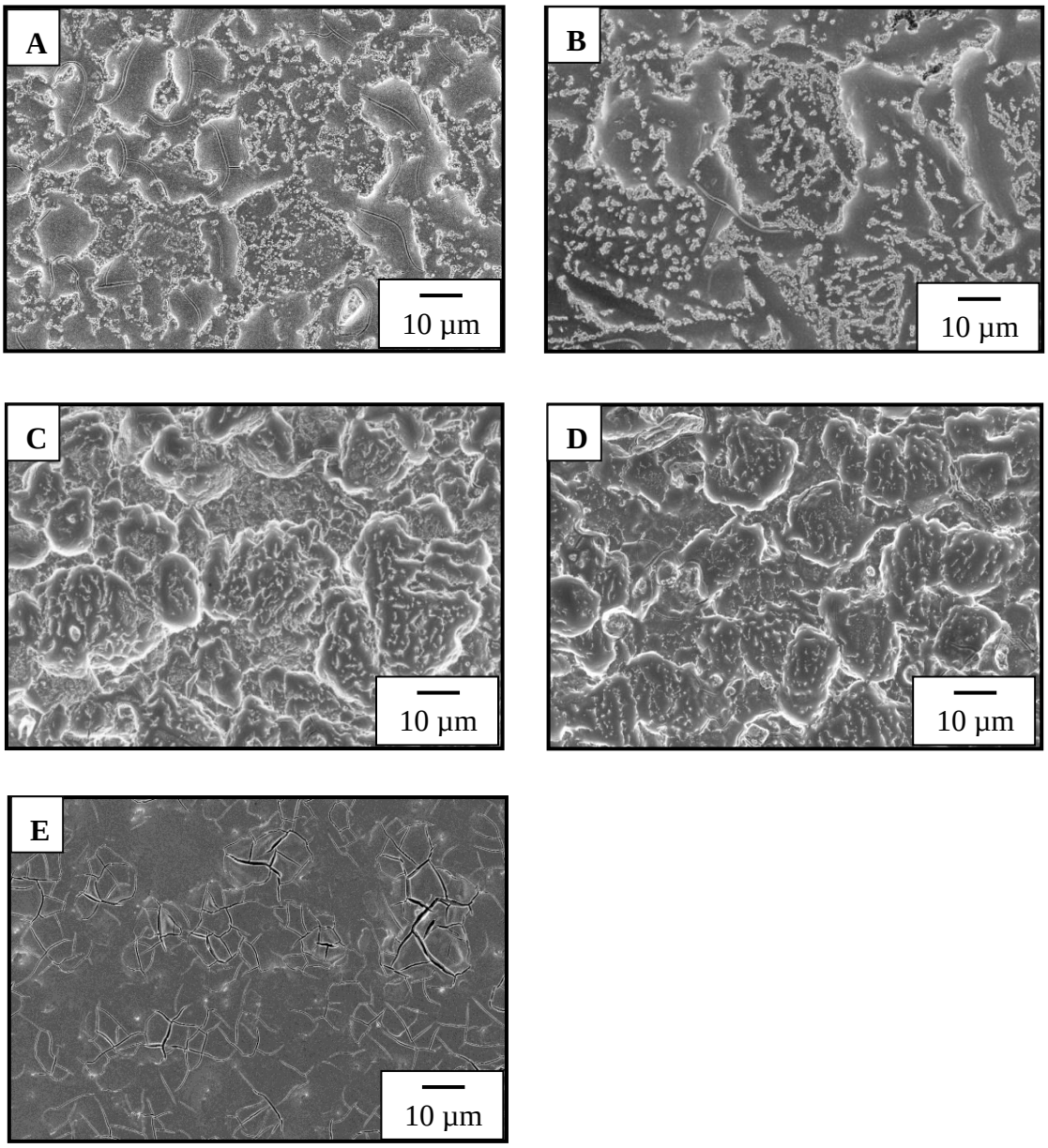

Figure 3.6 Surface morphologies of RuO_2-Ta_2O_5 coatings prepared at 500 ^oC (A), 360 ^oC (B), 300 ^oC (C), 280 ^oC (D) and 260 ^oC (E). Ru ratio: 80 mol%. Magnification: ×1,000.

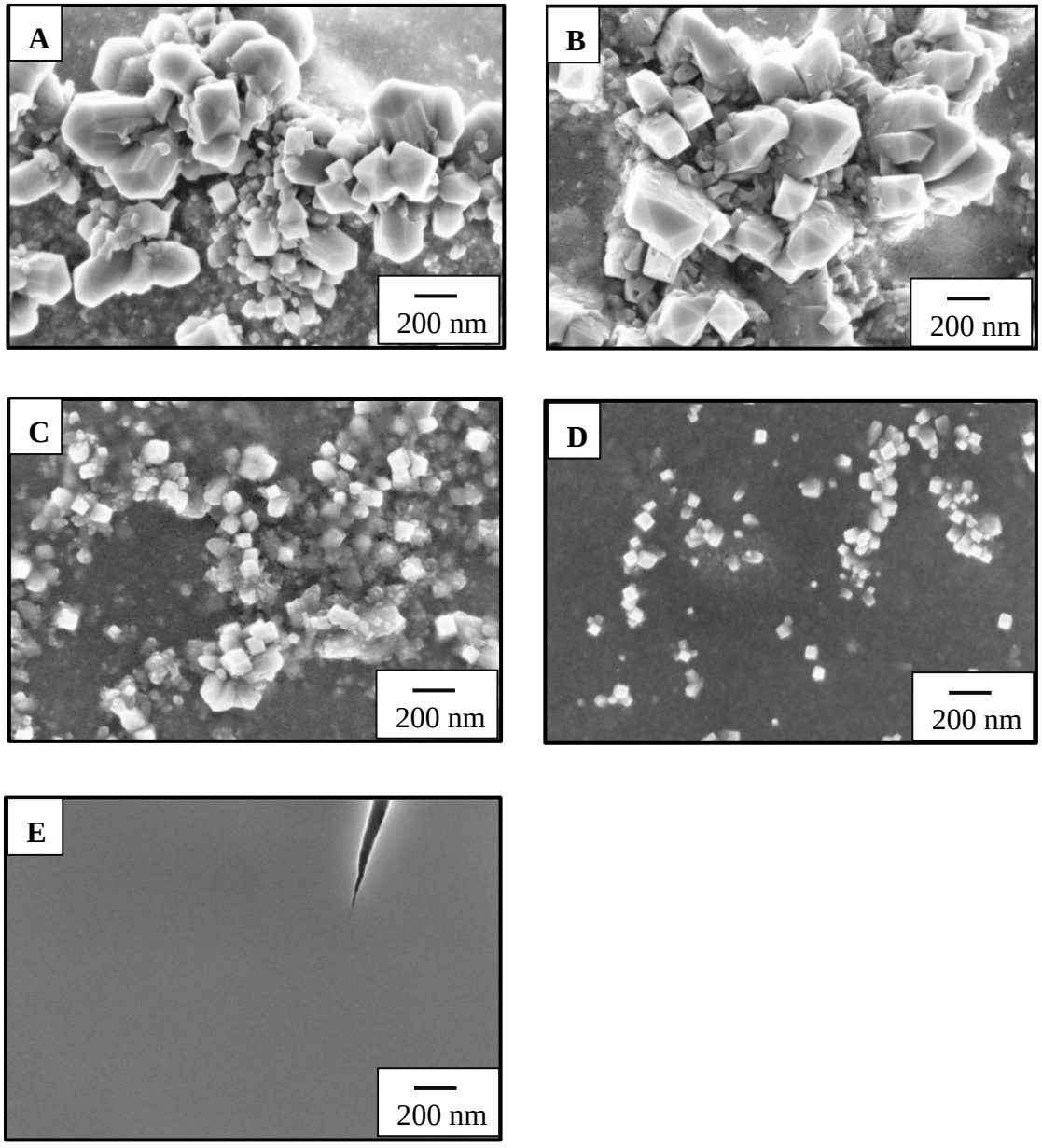

Figure 3.7 Surface morphologies of RuO_2-Ta_2O_5 coatings prepared at 500 ^oC (A), 360 ^oC (B), 300 ^oC (C), 280 ^oC (D) and 260 ^oC (E). Ru ratio: 80 mol%. Magnification: ×50,000.

The coatings of 80 mol% Ru gave more interesting features on flat areas at high magnification (100,000 or more), as shown in Figure 3.8. The flat areas were completely covered with nano RuO_2 particles of 20-30 nm for the coating at 500 ^oC, and the number of particles remarkably decreased as the decomposition temperature changed to 360 ^oC. Then the oxide coating calcined at 280 ^oC or less was seen with smooth surfaces and no RuO_2 particles of 20-30 nm as observed with the coating of 30 mol% Ru. Figure 3.8 (E-2) focuses on this smooth area of the coating prepared at 260 ^oC (magnification: 200,000). There is no RuO_2 particle even at such a high magnification, while the EDX data of this region clearly indicated a high ratio of Ru. Therefore, it is reasonable to consider that nano RuO_2 particles of 10 nm size or less, which is difficult to visualize at ×200,000 are contained in the flat area. This implies that the amorphous coating of 80 mol% Ru is expected to show more active surface area than that of 30 mol% Ru. In my best knowledge, no report on the nano structure of the amorphous RuO_2-Ta_2O_5 coatings described above has been published before this work.

The cracks formed on the coatings of 80 mol% Ru are shown in Figure 3.9. The cracks on the coatings at 280 ^oC to 500 ^oC indicated 150-200 nm width, while the width of cracks increased when decomposition temperature was 260 ^oC (300-400 nm). The number and width of cracks are strongly related to durability of the anode, because the major reason for degradation is titanium corrosion by acidic sulfate solution penetrated through the cracks to titanium surface. It should be noted that the number and width of cracks can be controlled by the method and condition of the anode preparation, as described in Chapter 6.

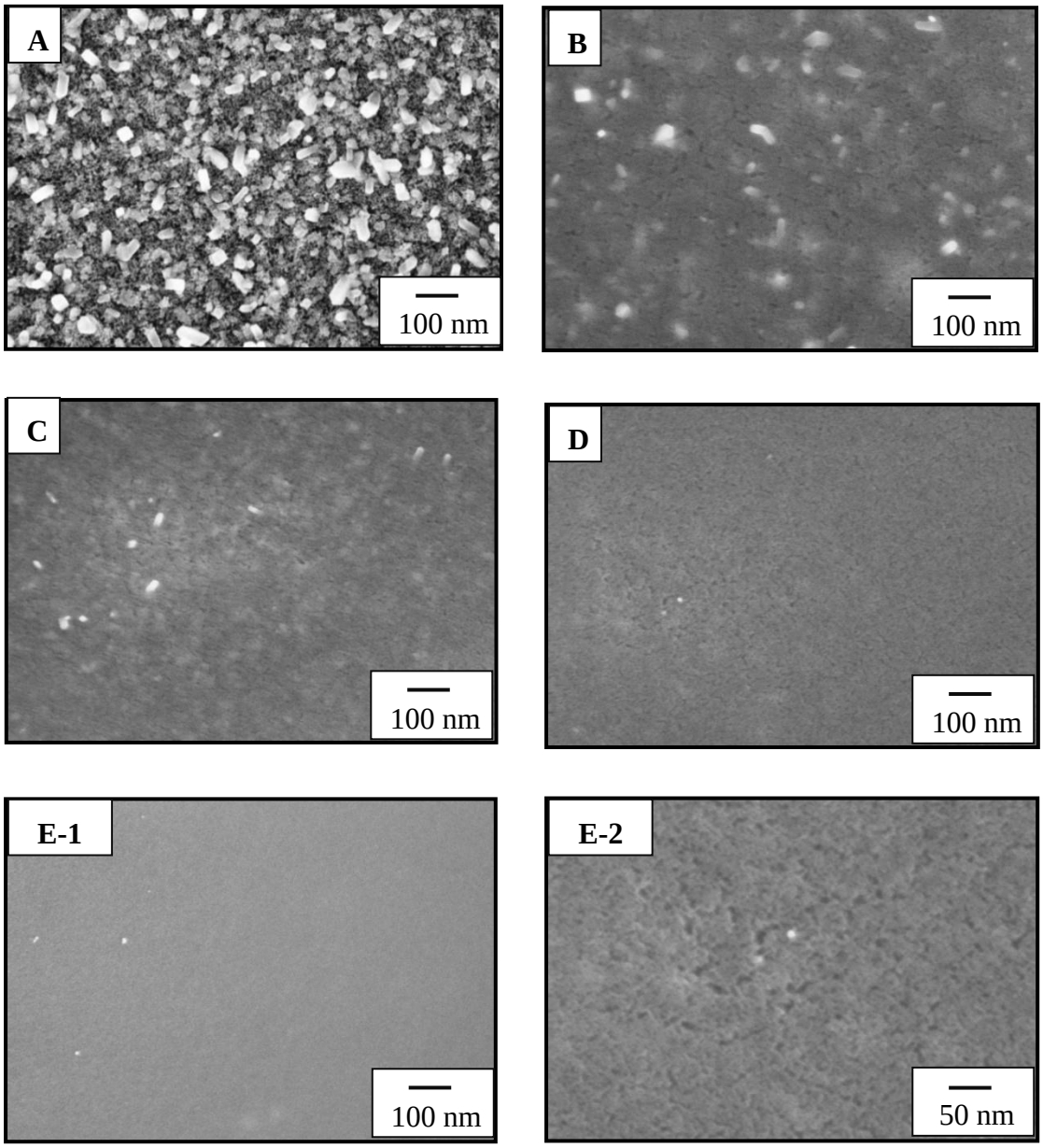

Figure 3.8 Surface morphologies of RuO_2-Ta_2O_5 coatings prepared at 500 ^oC (A), 360 ^oC (B), 300 ^oC (C), 280 ^oC (D) and 260 ^oC (E). Ru ratio: 80 mol%. Magnification: ×100,000 (A, B, C, D, E-1), ×200,000 (E-2).

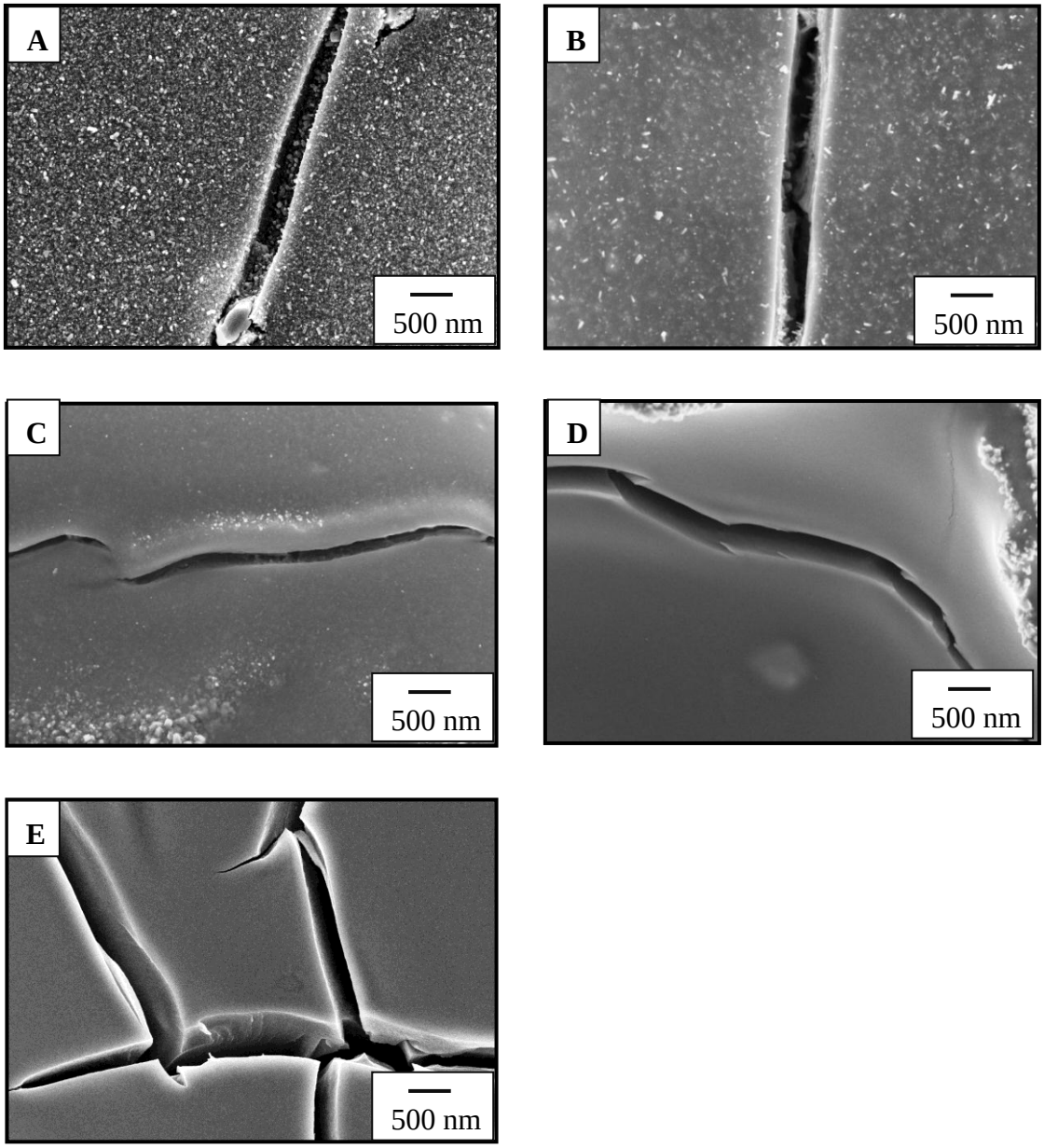

Figure 3.9 Surface morphologies of RuO_2-Ta_2O_5 coatings prepared at 500 ^oC (A), 360 ^oC (B), 300 ^oC (C), 280 ^oC (D) and 260 ^oC (E). Ru ratio: 80 mol%. Magnification: ×20,000.

3.2.3 Double layer charge

To evaluate the catalytic activity for oxygen evolution, cyclic voltammetry was first performed to know double layer charge in 2.0 mol dm^{-3} H_2SO_4 solution. Figure 3.10 shows the typical cyclic voltammograms of RuO_2-Ta_2O_5/Ti anodes at 30 mol% Ru (A) and 80 mol% Ru (B) at scan rate of 5 mV s^{-1}.

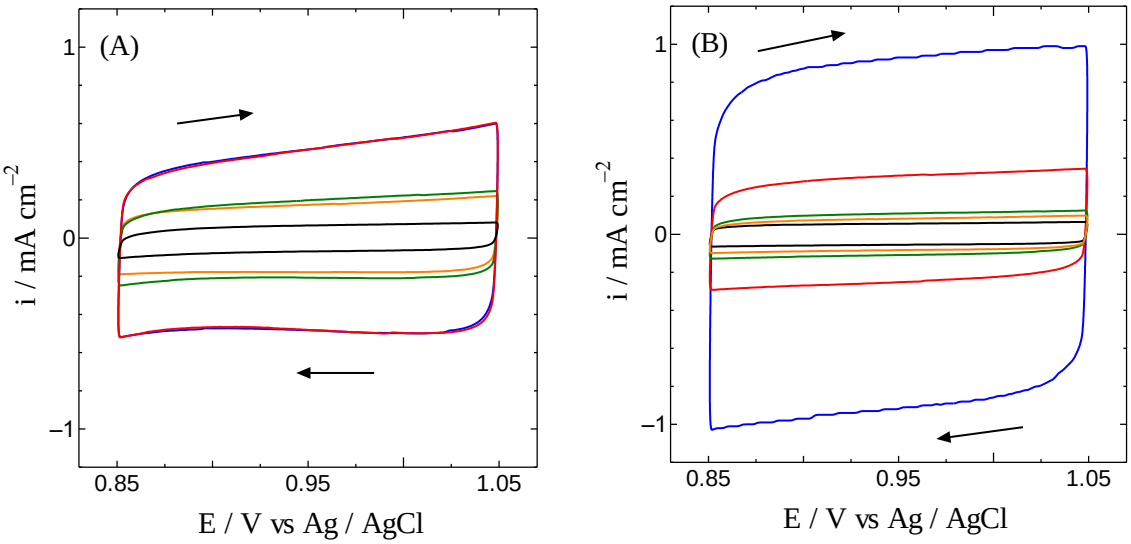

Figure 3.10 Cyclic voltammograms of RuO_2-Ta_2O_5/Ti anodes prepared at 500 ^oC (black), 360 ^oC (orange), 300 ^oC (green), 280 ^oC (red) and 260 ^oC (blue) in 2.0 mol dm^{-3} H_2SO_4 solution at 40 ^oC. Ru ratio: 30 mol% (A) and 80 mol% (B). Scan rate: 5 mV s^{-1}.

The voltammograms recorded in the potential range from 0.85 V to 1.05 V showed neither oxidation wave nor reduction wave, indicating no Faradic reaction occurs during the potential scan. Voltammetric charge calculated for a certain potential range can be used to estimate electrochemically effective surface area [15-22]. In this work, the double layer charge between 0.85 V and 1.05 V per unit geometric surface area (1 cm^2), Q_{dl}, was calculated by the following equation,

$$Q_{dl} = \int |\, i \,|\, dt \qquad (3\text{-}1)$$

where *i* is the current density based on the geometric surface area and *t* is time. The results are summarized with thermal decomposition temperature and shown in Figure 3.11. For the anodes at 30 mol% Ru, the double layer charge became larger with decreasing decomposition temperature from 500 ^{o}C to 280 ^{o}C; the double layer charge of 280 ^{o}C was 7.1 times larger than that at 500 ^{o}C, while the double layer charge is almost the same for 260 ^{o}C and 280 ^{o}C. This indicates that the effective surface area was significantly changed with phase transition of RuO_2 from crystalline to amorphous, and drastically increased with generation of nano RuO_2 particles.

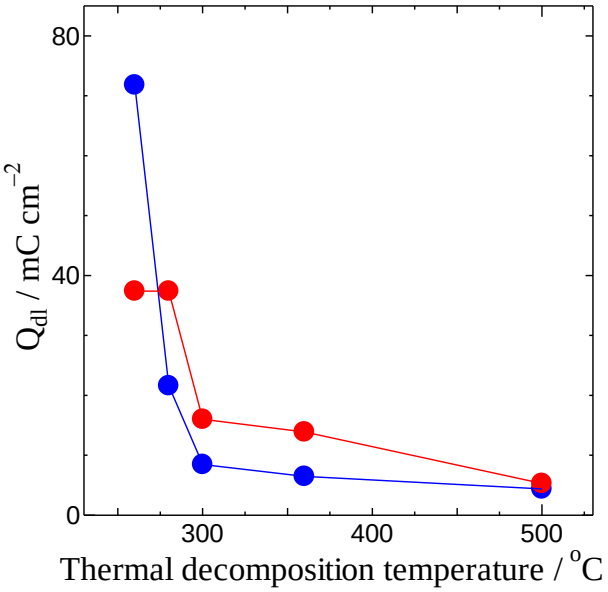

Figure 3.11 Dependence of the double layer charge of RuO_2-Ta_2O_5/Ti anodes in 2.0 mol dm^{-3} H_2SO_4 solution at 40 ^{o}C on thermal decomposition temperature. Ru ratio: 30 mol% (red) and 80 mol% (blue).

The double layer charge measured with the anode of 80 mol% Ru showed a similar relationship with decomposition temperature to that at 30 mol%, except that the double layer charge increased significantly from 280 ^{o}C to 260 ^{o}C; the double layer charge at 260 ^{o}C was 16.4 times larger than that at 500 ^{o}C and still 3.3 times larger than that at 280 ^{o}C. This is because the phase transition of RuO_2 from crystalline to amorphous occurred within 280 ^{o}C and 260 ^{o}C at 80 mol% Ru. The results also suggest

that disappearance of cube-like RuO_2 particles and distinctive nano structure of the flat area of the coating at 80 mol% Ru induces a large difference in double layer charge.

From the comparison between 30 mol% Ru and 80 mol% Ru on double layer charge, 30 mol % Ru is larger than 80 mol% in the temperature range from 280 ^oC to 500 ^oC contrary to Ru ratio. However, this is not the case at 260 ^oC. At the temperatures more than 280 ^oC, the crystallinity of RuO_2 in the coating at 30 mol% Ru was lower than that at 80 mol% Ru because more Ta_2O_5 promotes amorphization of RuO_2, which means that the size down of RuO_2 particles is more dominant to the effective surface area than the Ru ratio. Both the coatings of 30 mol% Ru and 80 mol% Ru have nano particles of 20 nm or less, especially 10 nm or less for 80 mol% Ru, so that the Ru ratio is the dominant factor at a thermal decomposition temperature of 260 ^oC.

3.2.4 Polarization curve

Polarization curves for oxygen evolution of RuO_2-Ta_2O_5/Ti anodes at 30 mol% Ru and 80 mol% Ru were measured by cyclic voltammetry in 2.0 mol dm^{-3} H_2SO_4 solution at 5.0 mV s^{-1}, and the results are shown in Figure 3.12. In this figure, oxygen evolution current is seen at 1.2 V or more, and there are two trends of polarization curves; as thermal decomposition temperature decreases, the oxygen evolution current increases and the onset potential shifts negatively. These are consistent with the results on the double layer charge; *i.e.*, the double layer charge increases and simultaneously oxygen evolution is more enhanced, suggesting the increase in effective surface area for oxygen evolution.

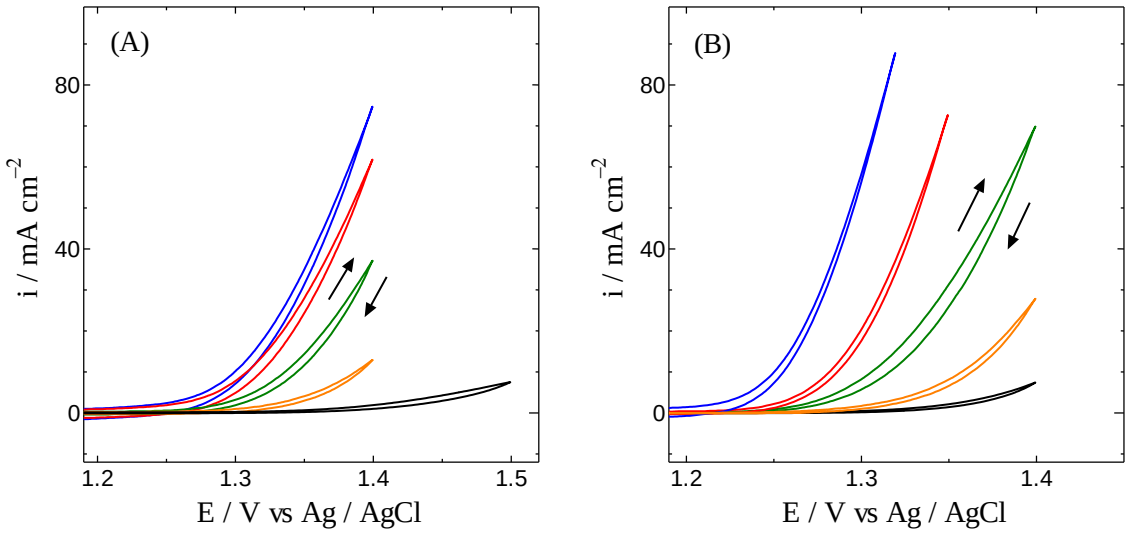

Figure 3.12 Cyclic voltammograms of RuO_2-Ta_2O_5/Ti anodes prepared at 500 ^oC (black), 360 ^oC (orange), 300 ^oC (green), 280 ^oC (red) and 260 ^oC (blue) in 2.0 mol dm^{-3} H_2SO_4 solution at 40 ^oC. Ru ratio: 30 mol% (A) and 80 mol% (B). Scan rate: 5 mV s^{-1}.

If the effective surface area for oxygen evolution is simply proportional to the double layer charge, the normalized current density by double layer change gives the same polarization curve, irrespective of thermal decomposition temperature and Ru ratio. Here, Figure 3.13 shows the polarization curves of crystalline and amorphous IrO_2-Ta_2O_5/Ti anodes at 80 mol% Ir. The maximum current density of the amorphous anode in this figure was 47 mA cm^{-2} at 1.4 V, while that is 2 mA cm^{-2} for the crystalline anode. Figure 3.14 shows the normalized current density data originated from Figure 3.13. The result demonstrates that the 'normalized' polarization with i/Q_{dl} of the amorphous IrO_2-Ta_2O_5/Ti anode was close to that of the crystalline anode. This means that as for IrO_2-Ta_2O_5/Ti anodes, the double layer charge reflects the effective surface area for oxygen evolution, and the oxygen evolution current increases linearly to the effective surface area, suggesting that enhancement of the mass transfer process is more important rather than the charge transfer process. It is also noted that the amorphous RuO_2-Ta_2O_5/Ti anode at 80 mol% Ru (Figure 3.12 (B)) has higher catalytic activity than the amorphous IrO_2-Ta_2O_5/Ti anode at 80 mol% Ir (Figure 3.13) from the difference in current density at the same potential.

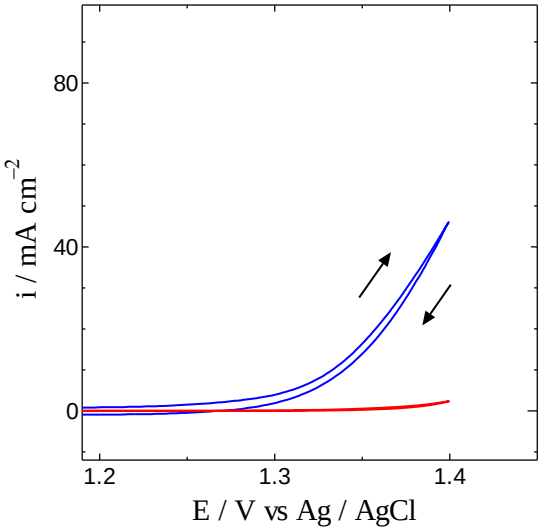

Figure 3.13 Cyclic voltammograms of crystalline (red) and amorphous (blue) IrO_2-Ta_2O_5/Ti anodes in 2.0 mol dm^{-3} H_2SO_4 solution at 40 ^oC. Ir ratio: 80 mol%. Scan rate: 5 mV s^{-1}.

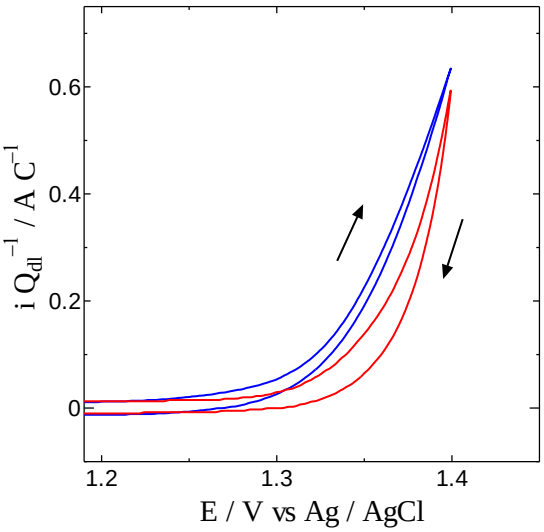

Figure 3.14 Cyclic voltammograms of crystalline (red) and amorphous (blue) IrO_2-Ta_2O_5/Ti anodes constructed from those shown in Figure 3.13 by dividing the current density by corresponding double layer charge.

The same treatment of normalization mentioned above was applied to the results of RuO_2-Ta_2O_5/Ti anodes in Figure 3.12, of which the results are shown in Figure 3.15. The normalized curves of the anodes at 260 ^oC, 280 ^oC and 300 ^oC were overlapped, and the two curves of 360 ^oC and 500 ^oC are not included in the group and

showed lower normalized current density, in which the anode at 360 °C shows higher normalized current density than that at 500 °C. It is interesting that the results of RuO_2-Ta_2O_5/Ti anodes are independent of Ru ratio and quite different from those of IrO_2-Ta_2O_5/Ti anodes. There seems to be two important points to understand the above analysis on normalized polarization curves for RuO_2-Ta_2O_5/Ti anodes; in the temperature range of 260 °C and 300 °C, at which amorphization of RuO_2 occurs partly or completely and large RuO_2 aggregates are little or not seen on the surface, the oxygen evolution current simply increases with the effective surface area which can be estimated by double layer charge, while the difference between the group and the other two (360 °C and 500 °C) implies the catalytic activity of RuO_2-Ta_2O_5 further depends on the charge transfer process; *i.e.*, the intrinsic activity of RuO_2 affecting the charge transfer rate would be varied with the particle size of RuO_2 obtained at 360 °C or more. This would be also possible to be the reason why the amorphous RuO_2-Ta_2O_5/Ti anode is superior to that of the amorphous IrO_2-Ta_2O_5/Ti anode on oxygen evolution even at the same ratio of the active component (Ru and Ir).

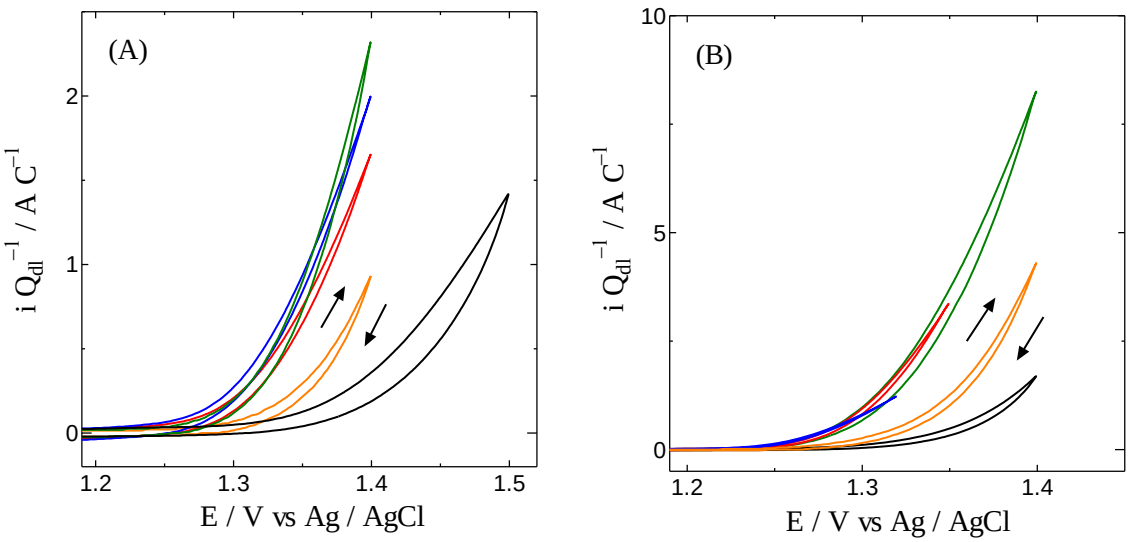

Figure 3.15 Cyclic voltammograms constructed from those shown in Figure 3.12 (A) and (B) by dividing the current density by corresponding double layer charge. Thermal decomposition temperature: 500 °C (black), 360 °C (orange), 300 °C (green), 280 °C (red) and 260 °C (blue).

3.2.5 Oxygen overpotential

From the result shown in Figure 3.12, the onset potential for oxygen evolution was obtained and the oxygen overpotential was also calculated by subtracting the equilibrium potential from the onset potential, of which the results are presented in Figure 3.16 and Table 3.1. Here, the onset potential was defined as the potential where the anodic current reached 3.0 mA cm^{-2}. The standard potential for oxygen evolution referred to the reference electrode used in this work is,

$$2H_2O \rightarrow 4H^+ + 4e + O_2 \qquad E^o = 1.030 \text{ V } \textit{vs.} \text{ Ag/AgCl sat. KCl} \qquad (3\text{-}2)$$

and the equilibrium potential (E_{eq}) of Equation (3-2) is expressed as follows;

$$E_{eq} = 1.030 + \frac{RT}{4F} \ln \frac{a_{O_2} \cdot a_{H^+}{}^4}{a_{H_2O}{}^2} \qquad (3\text{-}3)$$

where R is gas constant (8.314 J K^{-1} mol^{-1}), T is absolute temperature (313 K in this work), F is Faraday constant (96,485 C mol^{-1}), the number of electrons involved in oxygen evolution is 4, and a_{O_2}, a_{H^+}, and a_{H_2O} are the activity of O_2, H^+, and H_2O, respectively. In the calculation, a_{O_2} was oxygen partial pressure, $p_{O_2} = 0.2$, $a_{H_2O} = 1$, and a_{H^+} is calculated from pH of sulfuric acid solution using the following equation;

$$a_{H^+} = 10^{(-pH)} \qquad (3\text{-}4)$$

As shown in Figure 3.16 and Table 3.1, the onset potential shifted negatively with decreasing decomposition temperature at 30 mol% Ru and 80 mol% Ru, in which the onset potential at 260 ^oC is *ca*. 0.16 V and 0.14 V lower than that at 500 ^oC for the Ru ratio of 30 mol% and 80 mol%, respectively. The amorphous anode (80 mol% Ru)

obtained at 260 °C showed the lowest onset potential, 1.225 V (*vs.* Ag/AgCl sat. KCl), and the lowest overpotential, *ca.* 0.18 V, which is much smaller than the overpotential (0.6 to 0.8 V) on the lead alloy anode mentioned in Chapter 1.

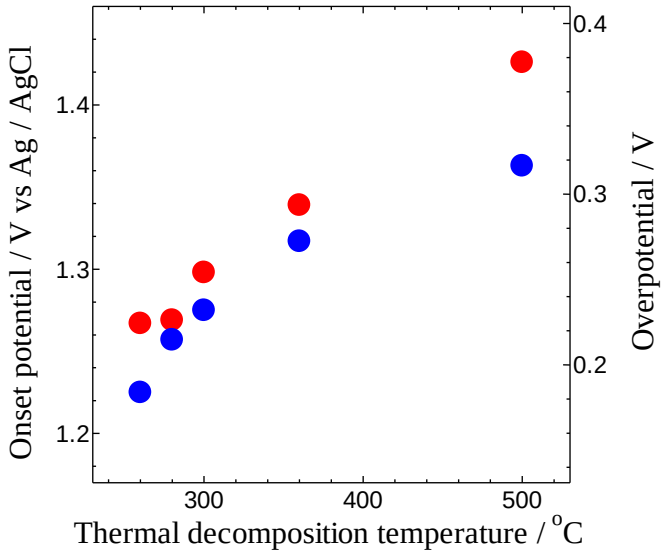

Figure 3.16 Dependence of the onset potential and overpotential of oxygen evolution on RuO_2-Ta_2O_5/Ti anodes in 2.0 mol dm^{-3} H_2SO_4 solution at 40 °C on thermal decomposition temperature. Ru ratio: 30 mol% (red) and 80 mol% (blue).

Table 3.1 Onset potential and overpotential of oxygen evolution on RuO_2-Ta_2O_5/Ti anodes in 2.0 mol dm^{-3} H_2SO_4 solution at 40 °C.

	Onset potential		Overpotential	
	Ru = 30 mol%	Ru = 80 mol%	Ru = 30 mol%	Ru = 80 mol%
500 °C	1.426 V	1.363 V	0.383 V	0.320 V
360 °C	1.339 V	1.317 V	0.296 V	0.274 V
300 °C	1.298 V	1.275 V	0.255 V	0.232 V
280 °C	1.269 V	1.257 V	0.226 V	0.214 V
260 °C	1.267 V	1.225 V	0.224 V	0.182 V

3.2.6 Tafel slope

The results in Section 3.2.4 suggested a possible change in electron transfer process for oxygen evolution on RuO_2-Ta_2O_5/Ti anodes, depending on thermal decomposition temperature and the size of RuO_2 particles. One of the indicators for this is Tafel slope from the basic theory of electrochemistry. Tafel slopes for oxygen evolution on RuO_2-based anodes in acid aqueous solutions have been extensively investigated as shown in Table 3.2, in which the data were obtained different conditions on thermal decomposition temperature, electrolyte, electrolyte temperature, current density range for analysis of Tafel slope.

Table 3.2 Tafel slopes on various RuO_2-based catalytic coatings in acid aqueous solutions.

Ref.	Oxide	Thermal decom. Temp.	Electrolyte	Temp.	Log (i / A cm^{-2})	Tafel slope
22	$RuO_2(0.2)$-$Co_3O_4(0.8)$	470 °C	0.5 mol dm^{-3} H_2SO_4	25 °C	-3.5 ~ -2.5	40
	$RuO_2(0.5)$-$Co_3O_4(0.5)$				-3.5 ~ -1	30
	$Co_3O_4(1)$				-4 ~ -3	60
23	RuO_2	425 °C	1.0 mol dm^{-3} H_2SO_4	20 °C	-6 ~ -3	41
	$RuO_2(0.8)$-$IrO_2(0.2)$				-5.5 ~ -2.5	48
	$RuO_2(0.5)$-$IrO_2(0.5)$				-5 ~ -3	55
	$RuO_2(0.2)$-$IrO_2(0.8)$				-5 ~ -3.5	61
	IrO_2				-5.5 ~ -3.5	58

Table 3.2 (*Continued*)

Ref.	Oxide	Thermal decom. Temp.	Electrolyte	Temp.	Log (i / A cm^{-2})	Tafel slope
24	RuO_2	350 °C	1.0 mol dm^{-3} H_2SO_4	25 °C	-7 ~ -5	42
	RuO_2-Ta_2O_5				-6.5 ~ -5	40
	RuO_2-IrO_2				-7 ~ -5	40
	RuO_2-IrO_2-Ta_2O_5				-7 ~ -5	40
	IrO_2				-7 ~ -5	55
25	RuO_2	600 °C	0.5 mol dm^{-3} H_2SO_4	Unknown	-5 ~ -3	35-40
	RuO_2(0.6)-IrO_2(0.4)					39-41
	RuO_2(0.35)-IrO_2(0.45)					39
	IrO_2					38-39
26	RuO_2(0.8)-Ta_2O_5(0.2)	450 °C	0.5 mol dm^{-3} H_2SO_4	R.T.	-5 ~ -3	35
	RuO_2(0.5)-Ta_2O_5(0.5)				-5 ~ -3.5	44
	RuO_2(0.3)-Ta_2O_5(0.7)				-5 ~ -3.5	56
27	RuO_2(0.7)-Ta_2O_5(0.3)	300 °C	0.5 mol dm^{-3} H_2SO_4	26±1 °C	-4 ~ -3	46
28	RuO_2	450 ~ 500 °C	0.5 mol dm^{-3} H_2SO_4	25 °C	-3.75 ~ -2.75	41.98 ±0.39
	RuO_2(0.8)-SnO_2(0.2)					37.06 ±0.29
	RuO_2(0.6)-SnO_2(0.4)					34.16 ±1.06

Table 3.2 (*Continued*)

Ref.	Oxide	Thermal decom. Temp.	Electrolyte	Temp.	Log (i / A cm^{-2})	Tafel slope
28	RuO_2(0.4)-SnO_2(0.6)	450 ~ 500 °C	0.5 mol dm^{-3} H_2SO_4	25 °C	-3.75 ~ -2.75	61.22 ±0.41
	RuO_2(0.2)-SnO_2(0.8)					81.33 ±0.66
29	RuO_2(0.3)-TiO_2(0.7)	400 °C	1.0 mol dm^{-3} $HClO_4$	25 ± 0.1 °C	Unknown	42.5
	RuO_2(0.3)-TiO_2(0.6)-SnO_2(0.1)					41.5
	RuO_2(0.3)-TiO_2(0.5)-SnO_2(0.2)					38.0
	RuO_2(0.3)-TiO_2(0.4)-SnO_2(0.3)					38.5
	RuO_2(0.3)-TiO_2(0.3)-SnO_2(0.4)					37.0
	RuO_2(0.3)-TiO_2(0.2)-SnO_2(0.5)					38.0
	RuO_2(0.3)-TiO_2(0.1)-SnO_2(0.6)					41.0
	RuO_2(0.3)-SnO_2(0.7)					44.0
30	RuO_2	400 °C	0.5 mol dm^{-3} H_2SO_4	25 °C	Unknown	39
	RuO_2(0.9)-IrO_2(0.1)					42

Table 3.2 (*Continued*)

Ref.	Oxide	Thermal decom. Temp.	Electrolyte	Temp.	Log (i / A cm^{-2})	Tafel slope
30	RuO_2(0.7)-IrO_2(0.3)	400 °C	0.5 mol dm^{-3} H_2SO_4	25 °C	Unknown	45
	RuO_2(0.5)-IrO_2(0.5)					46
	RuO_2(0.3)-IrO_2(0.7)					49
	RuO_2(0.1)-IrO_2(0.9)					57
	IrO_2					61
31	RuO_2(0.5)-TiO_2(0.5)	450 °C	1.0 mol dm^{-3} H_2SO_4	Unknown	-3.5 ~ -2	50
32	RuO_2	300 °C (1 hour)	0.1 mol dm^{-3} H_2SO_4	80 °C	-2 ~ -1.5	65
		300 °C (3 hours)			-2 ~ -0.5	75
33	RuO_2	500 °C	0.5 mol dm^{-3} H_2SO_4	Unknown	-1.5 ~ 0.5	40
		450 °C			Unknown	39
		400 °C				40
		360 °C				37~38
		330 °C				36
		300 °C				34~36
		270 °C			-1 ~ 0.5	33~35

Table 3.2 (*Continued*)

Ref.	Oxide	Thermal decom. Temp.	Electrolyte	Temp.	Log (i / A cm^{-2})	Tafel slope
34	RuO_2	500 °C	1.0 mol dm^{-3} H_2SO_4	Unknown	Unknown	40.8
		475 °C				39.8
		450 °C				34.5
		425 °C				35.0
		400 °C				34.8
		375 °C				34.0
		350 °C				33.9
		375 °C				33.1
		350 °C				30.5
35	RuO_2	400 °C	1.0 mol dm^{-3} $HClO_4$	25 ± 0.1 °C	-4.5 ~ -3.5	39
		300 °C			-5 ~ -3.5	40
		200 °C			-5 ~ -4	33

Tafel slopes of metals and metal oxides in acidic and alkaline solutions are also summarized by Kinoshita [36], while most of the works has been done focusing on the effect of Ru ratio on Tafel slope; in case of RuO_2-Ta_2O_5 coatings, Ribeiro [26] found that Tafel slope decreased with increasing Ru ratio when decomposition temperature was 450 °C, although there are few report focusing on the effect of thermal decomposition temperature. There are only a few literatures by Ardizzone [33],

Melsheimer [34] and Tsuji [35] discussing the effect of decomposition temperature of pure RuO_2 coatings on the Tafel slope, in which Tafel slope decreases with a decrease in decomposition temperature [33,34] and Tafel slope decreases when the phase transition of RuO_2 from crystalline to amorphous occurs [35]. Tafel slope of RuO_2-Ta_2O_5/Ti anodes prepared at different thermal decomposition temperatures has not been measured or reported.

Tafel plots constructed from the polarization curves recorded in 2.0 mol dm^{-3} H_2SO_4 solution at 40 ^oC at 0.5 mV s^{-1} are shown in Figure 3.17, and Tafel slopes were obtained from the linear region. Figure 3.18 shows a summary of Tafel slope and thermal decomposition temperature.

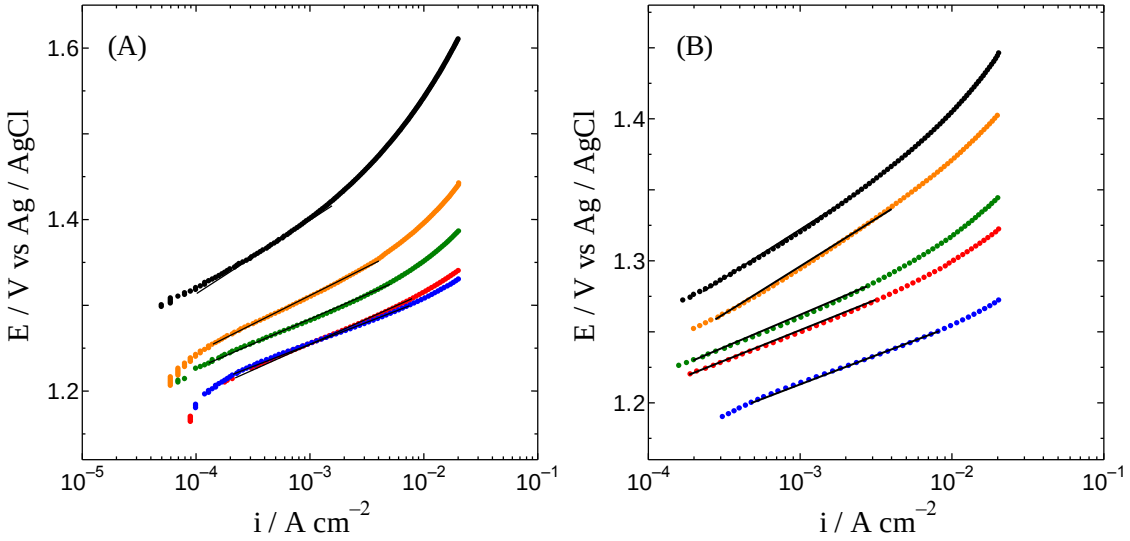

Figure 3.17 Polarization curves of RuO_2-Ta_2O_5/Ti anodes prepared at 500 ^oC (black), 360 ^oC (orange), 300 ^oC (green), 280 ^oC (red) and 260 ^oC (blue) in 2.0 mol dm^{-3} H_2SO_4 solution at 40 ^oC. Ru ratio: 30 mol% (A) and 80 mol% (B). Scan rate: 0.5 mV s^{-1}.

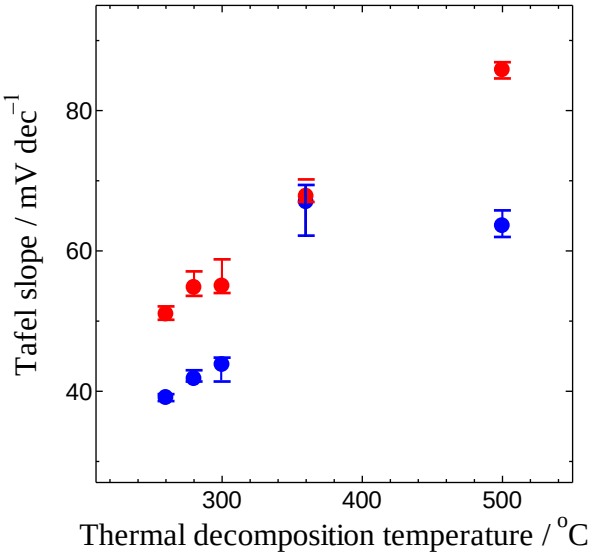

Figure 3.18 Dependence of the Tafel slope on RuO_2-Ta_2O_5/Ti anodes in 2.0 mol dm^{-3} H_2SO_4 solution at 40 ^{o}C on thermal decomposition temperature. Ru ratio: 30 mol% (red) and 80 mol% (blue).

The Tafel slope at 500 ^{o}C is close to that at 360 ^{o}C for the anodes at 80 mol% Ru, while a significant decrease in Tafel slope was observed as the decomposition temperature was changed from 360 ^{o}C to 300 ^{o}C and the lowest Tafel slope of *ca*. 39 mV dec^{-1} was obtained at 260 ^{o}C. The Tafel slope decreased with decreasing decomposition temperature for the anodes of 30 mol% Ru, in which the Tafel slope varied from *ca*. 85 mV dec^{-1} at 500 ^{o}C to *ca*. 51 mV dec^{-1} at 260 ^{o}C. The decrease in Tafel slope at lower thermal decomposition temperature is consistent with the results observed on pure RuO_2 coatings [33-35]. The Tafel slope at 80 mol% Ru was lower than that at 30 mol% Ru at the same decomposition temperature in Figure 3.18. A similar dependence of Tafel slope on Ru ratio in RuO_2-Co_3O_4, RuO_2-Ta_2O_5, RuO_2-SnO_2 and RuO_2-IrO_2 coatings were reported [22,26,28,30], for which the Tafel slopes of the RuO_2-Ta_2O_5/Ti anodes prepared in this study are higher than those reported by Ribeiro [26] as thermal decomposition temperature is same. In general, Tafel slope changes with the measurement conditions of polarization curve and the current range to set Tafel slope. Besides, the preparation method and condition of RuO_2-Ta_2O_5/Ti anodes have a large influence on Tafel slope. Ribeiro used isopropyl alcohol to prepare the precursor

solution and the other preparation procedures of their anodes including the pretreatment of titanium substrates were quite different with this study, which seems to be the reason for the difference in Tafel slope.

Various reaction pathways have been proposed for oxygen evolution, which depend on the electrode material and the measurement condition [36,37]. For oxygen evolution in acidic aqueous solutions, *i.e.*, oxygen evolution by water decomposition, the following reaction steps are proposed in general for metal oxides [37],

$$\text{(Step 1) } S + H_2O \rightleftarrows S\text{-}OH + H^+ + e^- \quad (3\text{-}5)$$

$$\text{(Step 2) } S\text{-}OH \rightleftarrows S\text{-}O^- + H^+ \quad (3\text{-}6)$$

$$\text{(Step 3) } S\text{-}O^- \rightleftarrows S\text{-}O + e^- \quad (3\text{-}7)$$

$$\text{(Step 4) } 2S\text{-}O \rightleftarrows 2S + O_2 \quad (3\text{-}8)$$

where S denotes the active site for oxygen evolution of the electrode and S-OH and S-O are the intermediates, OH or O, adsorbed on the active site. For the multi-step reaction as indicated above, Tafel slope, *b*, is expressed as [38],

$$b = \frac{2.303RT}{\alpha F} \quad (3\text{-}9)$$

where R is gas constant (8.314 J K^{-1} mol^{-1}), T is absolute temperature (K), F is Faraday constant (96,485 C mol^{-1}), α is transfer coefficient which changes with the rate determining step (rds). The transfer coefficient is 0.5 as Step 1 is rds, and the Tafel slope, 2.303RT/αF, is 124 mV dec^{-1} at 40 ^oC. Similarly, Tafel slopes are 2.303RT/F, 2.303RT/1.5F, and 2.303RT/2F for Step 2, Step 3 and Step 4 [39], which are calculated to be 62 mV dec^{-1}, 41 mV dec^{-1} and 32 mV dec^{-1}, respectively.

The RuO_2-Ta_2O_5/Ti anodes at 80 mol% Ru in this work gave Tafel slopes of 63 mV dec^{-1} and 67 mV dec^{-1} as thermal decomposition temperature were 500 ^oC and 360 ^oC, respectively, which suggests that the rds is Step 2. However, the anodes prepared at

260-300 ^{o}C showed the Tafel slopes of 39-43 mV dec^{-1}, which are in the range close to Tafel slope given for Step 3. Therefore, the Tafel slope obtained in this work clearly indicates that the rds for oxygen evolution on RuO_2-Ta_2O_5/Ti anode changes from 360 ^{o}C to 300 ^{o}C, at which the surface morphology also changes in the shape and size of RuO_2 (Section 3.2.2). Especially, the size of RuO_2 particles decreased with thermal decomposition temperature from 360 ^{o}C to 300 ^{o}C, which seems to strongly affect the rds.

On the other hand, the normalized current density (i/Q_{dl}) at 80 mol% Ru at 360 ^{o}C was higher than that at 500 ^{o}C as shown in Figure. 3.15 (B), and the Tafel slopes of these two anodes were almost the same. The number of nano RuO_2 particles of 20-30 nm completely covering the flat areas of the coating at 500 ^{o}C decreased significantly at 360 ^{o}C, at which the nano structured surface with RuO_2 particles of 10 nm or less were formed, as shown in Figure 3.8. Therefore, the ultrafine RuO_2 particles of 10 nm or less seem to give the active sites for oxygen evolution, which cannot be quantified by normalization with double layer charge and have little effect on the rds.

The change in the shape and size of RuO_2 particles at 30 mol% Ru, at which the flat area mostly consisted of amorphous Ta_2O_5 matrix, is discussed with Tafel slopes below. The Tafel slope was 86 mV dec^{-1} at 500 ^{o}C, which may correspond to the mixed rds of Step 1 and Step 2, while the Tafel slope decreased to 68 mV dec^{-1} or 55 mV dec^{-1} at 360 ^{o}C or 300 ^{o}C. In the same temperature range, RuO_2 changed from cuboid to needle-like, in which both of cuboid and needle-like particles were seen at 360 ^{o}C. At lower temperatures, the Tafel slopes were 55 mV dec^{-1} at 300 ^{o}C and 51 mV dec^{-1} at 260 ^{o}C, suggesting the change from needle-like particles of 200-250 nm to nano particles of *ca.* 20 nm has no significant effect on rds. These results are consistent with the normalized polarization curves, as explained in Figure 3.15 (A).

3.2.7 Oxygen evolution potential

Oxygen evolution potential was measured by chronopotentiometry in 2.0 mol dm^{-3} H_2SO_4 solution at 100 A m^{-2}, 250 A m^{-2} and 500 A m^{-2} (based on the geometrical surface area of the anode). Figures 3.19 and 3.20 show the chronopotentiograms of the anodes at 30 mol% Ru and 80 mol% Ru, in which the oxygen evolution potential is stable all anodes throughout the electrolysis. Table 3.3 is a summary of the results of oxygen evolution potential, which becomes lower with reducing decomposition temperature, which is in good agreement with the polarization curves shown in Figure 3.12.

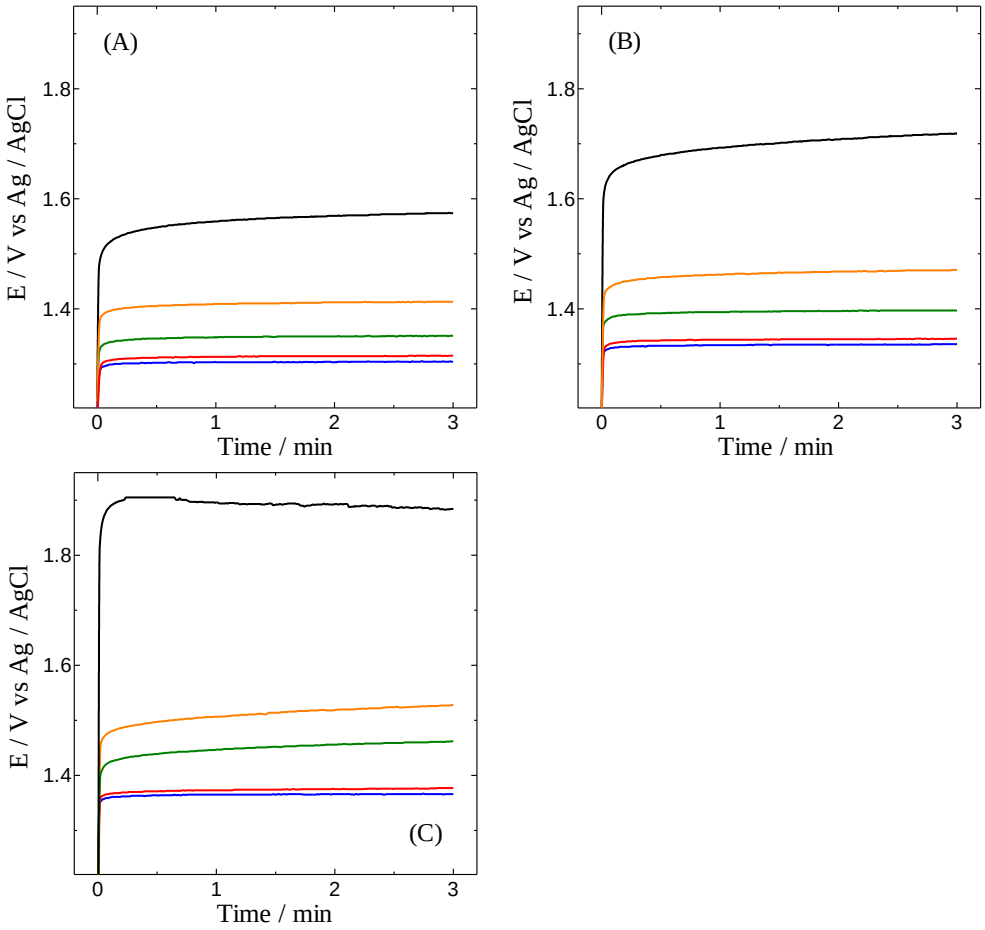

Figure 3.19 Potential variations of RuO_2-Ta_2O_5/Ti anodes prepared at 500 ^oC (black), 360 ^oC (orange), 300 ^oC (green), 280 ^oC (red) and 260 ^oC (blue) during in constant current electrolysis at 100 A m^{-2} (A), 250 A m^{-2} (B) and 500 A m^{-2} (C) in 2.0 mol dm^{-3} H_2SO_4 solution at 40 ^oC. Ru ratio: 30 mol%.

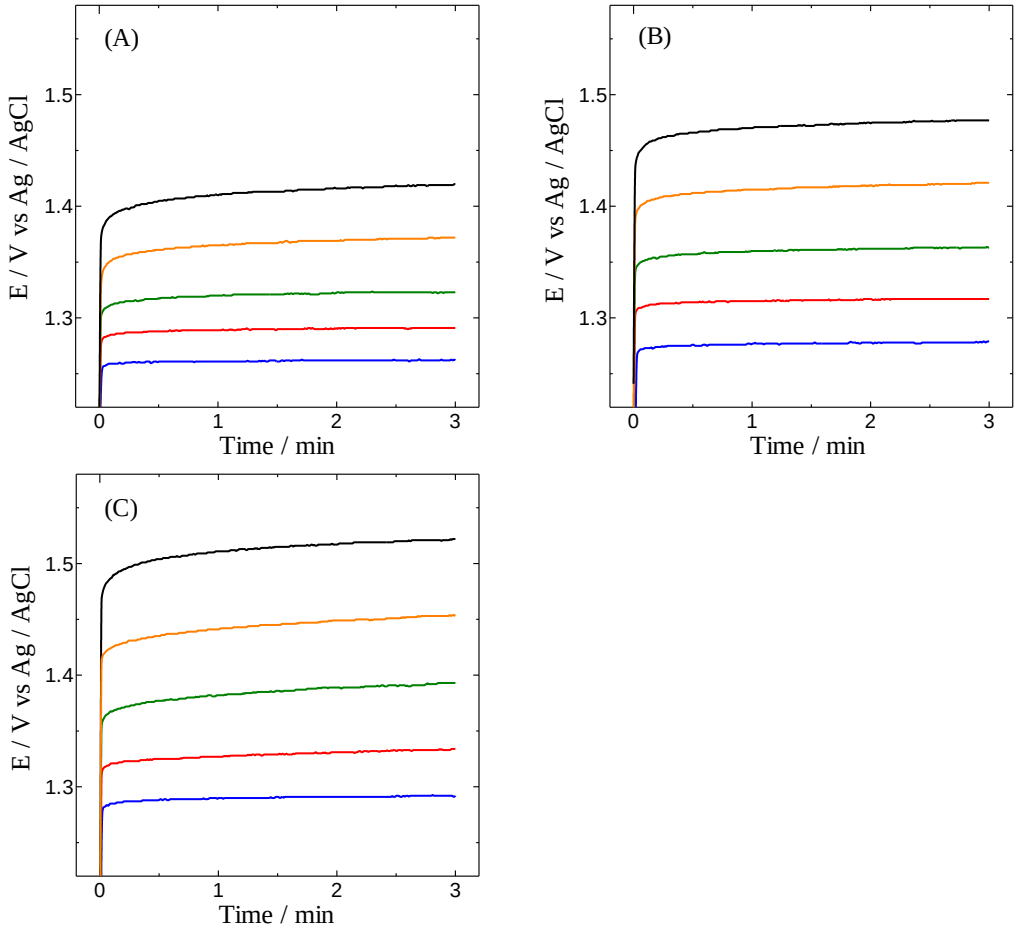

Figure 3.20 Potential variations of RuO_2-Ta_2O_5/Ti anodes prepared at 500 ^oC (black), 360 ^oC (orange), 300 ^oC (green), 280 ^oC (red) and 260 ^oC (blue) during in constant current electrolysis at 100 A m^{-2} (A), 250 A m^{-2} (B) and 500 A m^{-2} (C) in 2.0 mol dm^{-3} H_2SO_4 solution at 40 ^oC. Ru ratio: 80 mol%.

For the oxygen evolution potential at 500 A m^{-2}, the difference between 500 ^oC and 260 ^oC in Table 3.3 is 0.51 V at 30 mol% Ru and 0.23 V at 80 mol% Ru. It is interesting that the potential difference at 100 A m^{-2} and 500 A m^{-2} is smaller at low temperature than at high temperature; *e.g.*, they are 0.03 V at 260 ^oC and 0.10 V at 500 ^oC for the anode at 80 mol% Ru. This is reasonable, because the effective surface area of the amorphous anode is high so that the actual current density range is small compared to that examined in this study.

Table 3.3 Oxygen evolution potentials on RuO_2-Ta_2O_5/Ti anodes at various current densities. Ru ratio: 30 mol% (A) and 80 mol% (B).

(A)	100 A m^{-2}	250 A m^{-2}	500 A m^{-2}
500 ^{o}C	1.57 V	1.72 V	1.88 V
360 ^{o}C	1.41 V	1.47 V	1.53 V
300 ^{o}C	1.35 V	1.40 V	1.46 V
280 ^{o}C	1.32 V	1.35 V	1.38 V
260 ^{o}C	1.30 V	1.34 V	1.37 V

(B)	100 A m^{-2}	250 A m^{-2}	500 A m^{-2}
500 ^{o}C	1.42 V	1.48 V	1.52 V
360 ^{o}C	1.37 V	1.42 V	1.45 V
300 ^{o}C	1.32 V	1.36 V	1.39 V
280 ^{o}C	1.29 V	1.32 V	1.33 V
260 ^{o}C	1.26 V	1.28 V	1.29 V

3.2.8 Cell voltage

Constant current electrolysis using a two-electrode cell was performed to measure the cell voltage of zinc, copper, nickel and cobalt EW, for which the electrolytes used are listed in Table 2.1. Four kinds of anodes, amorphous RuO_2-Ta_2O_5/Ti anode (Ru = 80 mol%, 260 ^oC), crystalline RuO_2-Ta_2O_5/Ti anode (Ru = 80 mol%, 500 ^oC), amorphous IrO_2-Ta_2O_5/Ti anode (Ir = 80 mol%, 360 ^oC), and Pb-Sb(5%) alloy anode were used for comparison. The cathode was zinc, copper, nickel or cobalt plates (2×2 cm^2), and the cell voltage was measured at different current densities.

Table 3.4 shows the measured cell voltages, and the results indicates the order of the cell voltage for all EW is amorphous RuO_2-Ta_2O_5/Ti < amorphous IrO_2-Ta_2O_5/Ti < crystalline RuO_2-Ta_2O_5/Ti < Pb-Sb alloy. In case of zinc EW, the cell voltage with the amorphous RuO_2-Ta_2O_5/Ti anode was 0.14 V lower than that with the amorphous IrO_2-Ta_2O_5/Ti anode and 0.24 V lower than that with the crystalline RuO_2-Ta_2O_5/Ti anode when the current density was 500 A m^{-2} that is the typical one for zinc EW. Especially, the amorphous RuO_2-Ta_2O_5/Ti anode showed the cell voltage reduction of 0.70 V compared to the Pb-Sb alloy anode, which corresponds to 23 % voltage reduction. In case of copper EW, the voltage reduction was 0.11 V by replacing the amorphous IrO_2-Ta_2O_5/Ti anode and was 0.25 V by replacing the crystalline RuO_2-Ta_2O_5/Ti anode with the amorphous RuO_2-Ta_2O_5/Ti anode at 250 A m^{-2}, which is the typical operating current density for copper EW. The amorphous also exhibited 0.67 V lower cell voltage compared to the Pb-Sb alloy anode, which corresponds to 37 % reduction. Voltage reduction with the amorphous RuO_2-Ta_2O_5/Ti anode was also observed for nickel and cobalt EW; it is 0.46 V or 0.33 V compared to the Pb-Sb alloy anode in nickel and cobalt EW, respectively, at 250 A m^{-2}, which are 19 % or 13 % voltage reduction for each case. Consequently, large amounts of electric energy used in EW processes are expected to be decreased by replacing Pb alloy anodes with amorphous RuO_2-Ta_2O_5/Ti anodes developed in this study.

Table 3.4 Cell voltages during zinc, copper, nickel and cobalt EW with different anodes at various current densities.

[Zinc]	100 A m^{-2}	250 A m^{-2}	500 A m^{-2}
Pb-5%Sb	2.86 V	2.90 V	3.02 V
Crystalline RuO_2-Ta_2O_5	2.42 V	2.49 V	2.56 V
Amorphous IrO_2-Ta_2O_5	2.29 V	2.33 V	2.46 V
Amorphous RuO_2-Ta_2O_5	2.21 V	2.25 V	2.32 V

[Copper]	100 A m^{-2}	250 A m^{-2}	500 A m^{-2}
Pb-5%Sb	1.75 V	1.83 V	1.92 V
Crystalline RuO_2-Ta_2O_5	1.33 V	1.41 V	1.51 V
Amorphous IrO_2-Ta_2O_5	1.23 V	1.27 V	1.38 V
Amorphous RuO_2-Ta_2O_5	1.12 V	1.16 V	1.22 V

[Nickel]	100 A m^{-2}	250 A m^{-2}	500 A m^{-2}
Pb-5%Sb	2.15 V	2.48 V	2.71 V
Crystalline RuO_2-Ta_2O_5	2.07 V	2.25 V	2.51 V
Amorphous IrO_2-Ta_2O_5	1.95 V	2.11 V	2.32 V
Amorphous RuO_2-Ta_2O_5	1.86 V	2.02 V	2.20 V

[Cobalt]	100 A m^{-2}	250 A m^{-2}	500 A m^{-2}
Pb-5%Sb	2.28 V	2.59 V	3.34 V
Crystalline RuO_2-Ta_2O_5	2.12 V	2.47 V	2.97 V
Amorphous IrO_2-Ta_2O_5	2.06 V	2.37 V	2.93 V
Amorphous RuO_2-Ta_2O_5	1.94 V	2.26 V	2.73 V

As described in Chapter 1, the annual energy consumption by EW in the world are 45,500 GWh and 9,072 GWh in zinc and copper EW. These values correspond to 4,200,000 and 837,000 households of electricity consumption in U.S.A. A simple calculation gave us that the cell voltage reduction of 23 % in zinc EW and 37 % in copper EW worldwide may equal to 13,800 GWh which corresponds to 1,280,000 households of energy consumption per year in U.S.A. Therefore, a significant energy saving will be possible, when the anode is changed from Pb alloy to amorphous RuO_2-Ta_2O_5/Ti. Moreover, this anode should be useful in other important applications such as chlor-alkali industry, water treatment and oxygen production.

3.3 Conclusion

The crystallographic structure and surface morphology of RuO_2-Ta_2O_5/Ti anodes were strongly affected by thermal decomposition temperature; the crystallographic structure of RuO_2 changed from crystalline to amorphous, and the size of RuO_2 particles became smaller with decreasing thermal decomposition temperature. Such changes enhanced the catalytic activity for oxygen evolution in two ways. First, the effective surface area of the coating was significantly increased by the phase transition of RuO_2 from crystalline to amorphous, because nano RuO_2 particles were formed on the coating surface along with disappearance of large RuO_2 aggregates. Secondly, the rds for oxygen evolution changed with the variation in the size and shape of RuO_2 particles from cuboid with 150 nm or more to 80 nm or less on the coatings at 80 mol% Ru and from cuboid to needle-like at 30 mol% Ru. These features of the amorphous anode accelerated oxygen evolution and resulted in the decrease in the anode potential, which is superior to other anode materials including the amorphous IrO_2-Ta_2O_5/Ti anodes. As a result, the cell voltage for the zinc, copper, nickel and cobalt EW can be significantly reduced by replacing practically utilizing Pb alloy anodes with the amorphous RuO_2-Ta_2O_5/Ti anodes.

3.4 References

[1] M. Morimitsu, K. Uno, "A novel electrode for cobalt electrowinning to suppress CoOOH deposition", Proc. of Hydrometallurgy of Nickel and Cobalt 2009 (2009) 571-580.

[2] M. Morimitsu, T. Yamaguchi, N. Oshiumi, T. Zhang, "Energy-efficient electrowinning process with smart anode comprising nano-oxide catalyst", Proc. of European Metallurgical Conference 2011, **3** (2011) 975-984.

[3] M. Morimitsu, "Oxide coated titanium electrode for oxygen evolution", J. MMIJ, **130** (2014) 415-420. (in Japanese)

[4] K. Kawaguchi, G.M. Haarberg, M. Morimitsu, "Control of amorphization of IrO_2-Ta_2O_5/Ti electrodes to suppress unwanted side reactions", ECS Transactions, **16** (2009) 41-47.

[5] K. Kawaguchi, G.M. Haarberg, M. Morimitsu, "Ordered nano particles in amorphous IrO_2-Ta_2O_5 coatings detected by SEM detected by low accelerated incident electrons acidic solutions", Electrochemistry, **77** (2009) 879-881.

[6] K. Kawaguchi, G.M. Haarberg, M. Morimitsu, "Nano-architecture on the mud-cracked surface of IrO_2-Ta_2O_5 binary system", ECS Transactions, **25** (2010) 67-73.

[7] K. Kawaguchi, G.M. Haarberg, M. Morimitsu, "Suppression of PbO_2 deposition on nano-structure surface of IrO_2-Ta_2O_5/Ti anodes in acidic solutions", ECS Transactions, **50** (2013) 75-85.

[8] G.P. Vercesi, J. Rolewicz, Ch. Comninellis, J. Hinder, "Characterization of DSA-type oxygen evolving electrodes. Choice of base metal", Thermochim. Acta, **176** (1991) 31-47.

[9] G.P. Vercesi, J.Y. Salamin, Ch. Comninellis, "Morphological and microstructural study of the Ti/IrO_2-Ta_2O_5 electrode: effect of the preparation temperature", Electrochimica Acta, **36** (1991) 991-998.

[10] R. Otogawa, K. Soda, S. Yamauchi, Y. Nagatoishi, M. Morimitsu, M. Matsunaga, "Morphological deterioration of iridium oxide-tantalum oxide anode by oxygen

evolution", Denki Kagaku, **65** (1997) 987-991.

[11] R. Otogawa, M. Morimitsu, M. Matsunaga, "Effects of microstructure of IrO_2-based anodes on electrocatalytic properties", Electrochim. Acta, **44** (1998) 1509-1513.

[12] M. Morimitsu, "Development of a novel smart anode for environmentally friendly electrowinning process", Prof. ALTA 2011 Ni/Co/Cu Conference (2011) 260-265.

[13] M. Morimitsu, "New technology of oxygen evolution anodes for electrowinning", Proc. New Technology Implementation in Metallurgical Processes CIM (2011) 313-320.

[14] M. Morimitsu, "Performance and commercialization of the smart anode, MSA^{TM}, for environmentally friendly electrometallurgical process", Proc. Electrometallurgy 2012, TMS (2012) 49-54.

[15] M. Morimitsu, "Polarization curve・Cyclic voltammetry", Electrochemistry, **77** (2009) 838-843.

[16] J. Gaudet, A.C. Tavares, S. Trasatti, D. Guay, "Physicochemical characterization of mixed RuO_2- SnO_2 solid solutions", **17** (2005) 1570-1579.

[17] S. Ardizzone, G. Fregonara, S. Trasatti, "Inner" and "outer" active surface of RuO_2 electrodes, Electrochimica Acta, **35** (1990) 263-267.

[18] O.R. Camara, S. Trasatti, "Surface electrochemical properties of Ti/(RuO_2+ZrO_2) electrodes", Electrochim. Acta, **41** (1996) 419-427.

[19] C.P. de Pauli, S. Trasatti, "Composite materials for electrocatalysis of O_2 evolution: IrO_2+SnO_2 in acid solution", J. Electroanal. Chem., **538-539** (2002) 145-151.

[20] A.J. Terezo, E.C. Pereira, "Preparation and characterization of Ti/RuO_2-Nb_2O_5 electrodes obtained by polymeric precursor method", Electrochim. Acta, **44** (1999) 4507-4513.

[21] J.F.C. Boodts, S. Trasatti, "Effect of composition on the electrocatalytic activity of the ternary oxide $Ru_{0.3}Ti_{(0.7-x)}Sn_xO_2$", J. Electrochem. Soc., **137** (1990) 3784-3789.

[22] L.M. Da Silva, J.F.C. Boodts, L.A. De Faria, "Oxygen evolution at

$RuO_2(x)+Co_3O_4(1-x)$ electrodes from acid solution," Electrochim. Acta, **46** (2001) 1369-1375.

[23] M.E.G. Lyons, S. Floquet, "Mechanism of oxygen reactions at porous oxide electrodes. Part 2-Oxygen evolution at RuO_2, IrO_2 and $Ir_xRu_{1-x}O_2$ electrodes in aqueous acid and alkaline solution", Phys. Chem. Chem. Phys., **13** (2011) 5314-5335.

[24] R.S. Yeo, J. Orehotsky, W. Visscher, S. Srinivasan, "Ruthenium-based mixed oxides as electrocatalysts for oxygen evolution in acid electrolytes", J. Electrochem. Soc., **128** (1981) 1900-1904.

[25] L.E. Owe, M. Tsypkin, K.S. Wallwork, R.G. Haverkamp, S. Sunde, "Iridium-ruthenium single phase mixed oxides for oxygen evolution: Composition dependence of electrocatalytic activity", Electrochim. Acta, **70** (2012) 158-164.

[26] J. Ribeiro, A.R. de Andrade, "Characterization of RuO_2-Ta_2O_5 coated titanium electrode microstructure, morphology, and electrochemical investigation", J. Electrochem. Soc., **151** (2004) D106-D112.

[27] J.J. Jow, H.H. Lai, H.R. Chen, C.C. Wang, M.S. Wu, T.R. Ling, "Effect of hydrothermal treatment on the performance of RuO_2-Ta_2O_5/Ti electrodes for use in supercapacitors", Electrochimica Acta, **55** (2010) 2793-2798.

[28] X. Wu, J. Tayal, S. Basu, K. Scott, "Nano-crystalline $Ru_xSn_{1-x}O_2$ powder catalysts for oxygen evolution reaction in proton exchange membrane water electrolysers", Int. J. Hydrogen Energy, **36** (2011) 14796-14804.

[29] A.I. Onuchukwu, S. Trasatti, "Effect of substitution of SnO_2 for TiO_2 on the surface and electrocatalytic properties of RuO_2+TiO_2 electrodes", J. Appl. Electrochem. **21** (1991) 858-862.

[30] F.I. Mattos-Costa, P. de Lima-Neto, S.A.S. Machado, L.A. Avaca, "Characterisation of surfaces modified by sol-gel derived $Ru_xIr_{1-x}O_2$ coatings for oxygen evolution in acid medium", Electrochim. Acta, **44** (1998) 1515-1523.

[31] V.V. Panić, V.M. Jovanović, S.I. Terzić, M.W. Barsoum, V.D. Jović, A.B. Dekanski, "The properties of electroactive ruthenium oxide coatings supported by titanium-based ternary carbides", Surface and Coating Technology, **202** (2007)

319-324.

[32] J.C. Cruz, S. Siracusano, V. Antonucci, A.S. Aricò, R. Ornelas, L. Ortiz-Frade, G. Osorio-Monreal, S. M. Durón-Torres, L.G. Arriaga, "Preparation and characterization of RuO_2 catalysts for oxygen evolution in a solid polymer electrolyte", Int. J. Electrochem. Sci., **6** (2011) 6607-6619.

[33] S. Ardizzone, M. Falciola, S. Trasatti, "Effect of the Nature of the Precursor on the Electrocatalytic Properties of Thermally Prepared Ruthenium Oxide", J. Electrochem. Soc., **136** (1989) 1545-1550.

[34] J. Melsheimer, D. Ziegler, "The oxygen electrode reaction in acid solutions on RuO_2 electrodes prepared by the thermal decomposition method", Thin Solid Films, **163** (1988) 301-308.

[35] E. Tsuji, A. Imanishi, K. Fukui, Y. Nakato, "Electrocatalytic activity of amorphous RuO_2 electrode for oxygen evolution in an aqueous solution", Electrochim. Acta, **56** (2011) 2009-2016.

[36] K. Kinoshita, "Oxygen evolution", Electrochemical Oxygen Technology, The Electrochemical Society Series (1992) 78-94.

[37] A. Damjanovic, Modern Aspects of Electrochemistry, Vol. 5, J.O'M. Bockris and B.E. Conway, eds, (Plenum Press, New York, 1969) p. 369.

[38] C.H. Hamann, A. Hamnett, W. Vielstich, Electrochemistry, (Wiley, 2007) p. 531.

[39] A. Colombo, "Preparation and performance evolution of materials for electrocatalytic applications", PhD thesis, University of Milan (2010).

Chapter 4

Effect of catalytic coating composition

4.1 Introduction

As mentioned in Chapter 3, the catalytic activity of RuO_2-Ta_2O_5/Ti anodes for oxygen evolution is improved by low temperature thermal decomposition due to the amorphization of the oxide coating which occurs at 280 ^oC or less. The objective of this Chapter is to determine the most appropriate Ru:Ta mole ratio of the amorphous coatings for oxygen evolution, for which the anodes were prepared at different Ru:Ta mole ratios at 260 ^oC. The crystallographic structure and surface morphology of the anodes were examined and the oxygen evolution behaviors were investigated with a comparison to pure RuO_2/Ti anodes.

4.2 Results and discussion

4.2.1 Crystallographic structure

Figure 4.1 shows XRD patterns of RuO_2/Ti and RuO_2-Ta_2O_5/Ti anodes prepared at 260 ^oC, in which no diffraction peaks of RuO_2 were observed on the RuO_2-Ta_2O_5 coatings at 30 mol% to 80 mol% Ru, indicating that the amorphous RuO_2-Ta_2O_5 coating was obtained for the wide range of Ru:Ta ratio. It is noted that the diffraction peak corresponding to (100) of Ti located at $2\theta = 35.1^o$ so that a small peak for this was seen in Figure 4.1. The diffraction peaks corresponding to (110), (101) and (211) of crystalline RuO_2 were observed on pure RuO_2 coating, so that the amorphization of RuO_2 is promoted in a mixture with Ta_2O_5, as mentioned in Chapter 3. The peak intensity of RuO_2 in pure RuO_2 coating at 260 ^oC was comparable to that in RuO_2-Ta_2O_5 coating at 80 mol% Ru calcined at 280 ^oC, suggesting that both the coatings have a similar crystallinity of RuO_2.

Figure 4.2 shows the XRD results constructed from those in Figure 4.1, and results of RuO_2-Ta_2O_5 coatings at 30 mol%, 50 mol% and 80 mol% Ru are enlarged and overlapped each other, in which the broad diffraction peak observed at $2\theta = 20\text{-}30^o$

becomes larger when the Ta ratio increases from 20 mol% to 70 mol%. This is reasonable, because crystalline Ta_2O_5 has diffraction peaks corresponding to (001) and (110) at $2\theta = 22.4^o$ and 29.3^o, respectively.

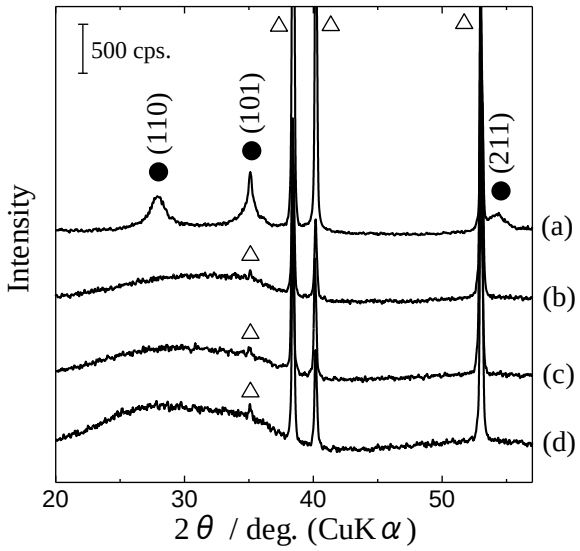

Figure 4.1 XRD patterns of RuO_2/Ti (a) and RuO_2-Ta_2O_5/Ti electrodes prepared at various Ru ratio: 80 mol% (b), 50 mol% (c) and 30 mol% (d). Thermal decomposition temperature: 260 ^oC. ●: RuO_2, △: Ti

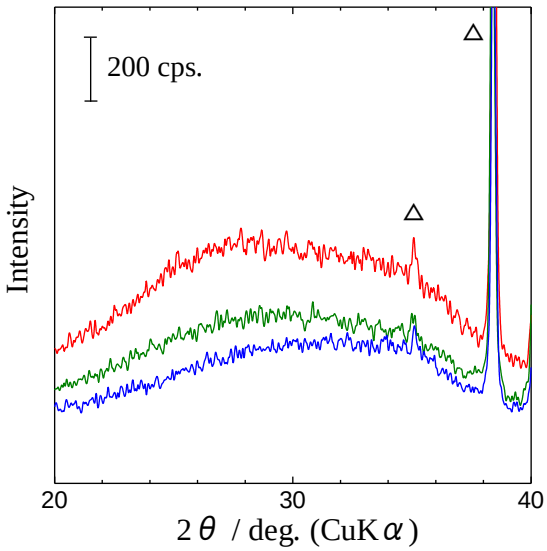

Figure 4.2 XRD patterns of RuO_2-Ta_2O_5/Ti electrodes prepared at various Ru ratio: 80 mol% (blue), 50 mol% (green) and 30 mol% (red). Thermal decomposition temperature: 260 ^oC. △: Ti

4.2.2 Surface morphology

Figure 4.3 depicts low magnification (×1,000) SEM images of RuO_2-Ta_2O_5 and pure RuO_2 coatings prepared at 260 ^oC. For all coatings, flat areas and cracks are seen without aggregated large RuO_2 particles and the number of cracks decreases as the Ru ratio increases.

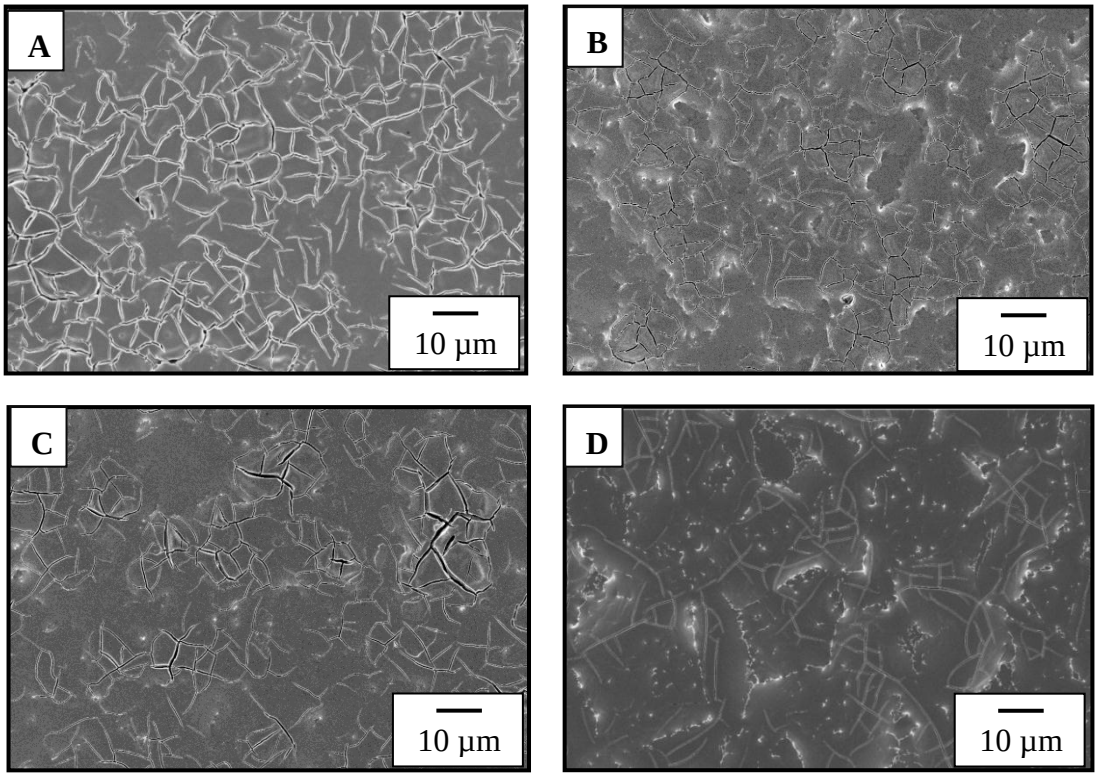

Figure 4.3 Surface morphologies of RuO_2-based coatings prepared at various Ru ratio: 30 mol% (A), 50 mol% (B), 80 mol% (C) and 100 mol%, *i.e*. pure RuO_2 (D). Thermal decomposition temperature: 260 ^oC. Magnification: ×1,000.

Figure 4.4 focuses on the surface morphologies at high magnification (×200,000). As shown in Figure 4.4 (A), nano RuO_2 particles of 20-30 nm were formed partly on the coating at 30 mol% Ru. Such particles became smaller and more uniformly dispersed in amorphous Ta_2O_5 matrix when the Ru ratio increased from 30 mol% to 80

mol%. In particular, the coating at 80 mol% Ru showed nano structured surface containing RuO_2 particles of 10 nm size or less, and the RuO_2 coating presented such a nano structure, too. The results indicate that the Ru:Ta mole ratio has a significant influence on nano structure of the coatings, and it is expected that a higher effective surface area can be obtained with increasing the Ru ratio from 30 mol% to 80 mol%.

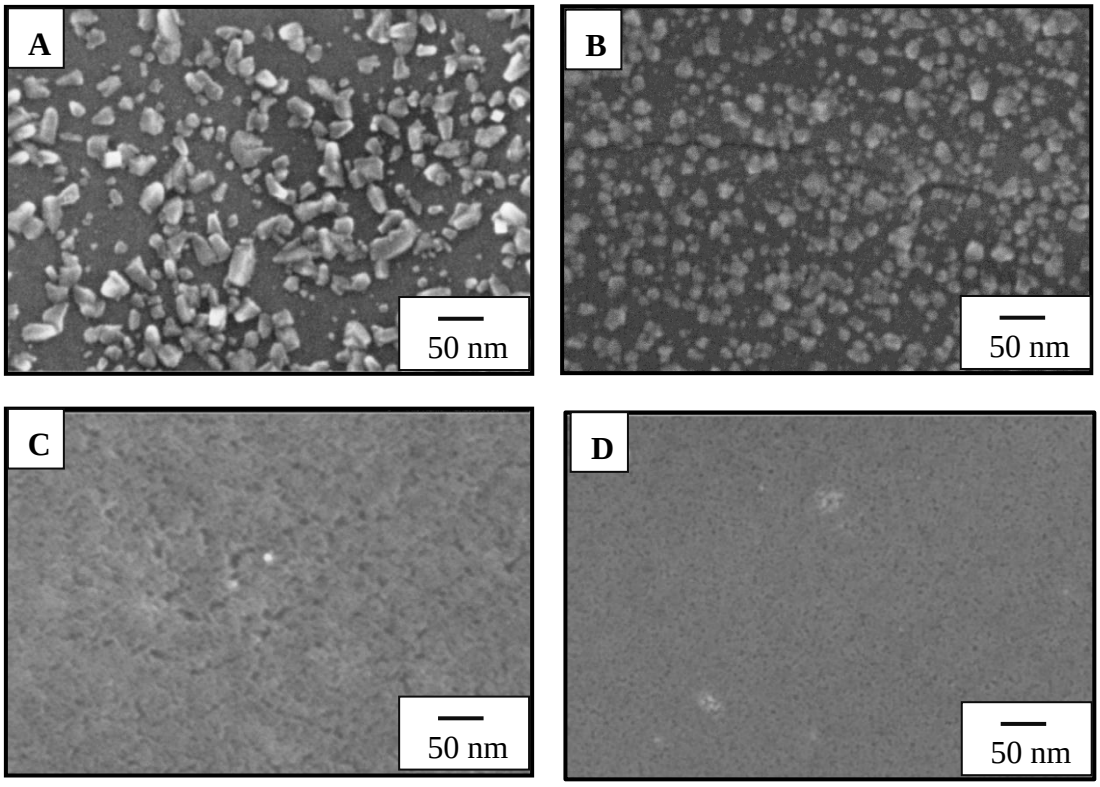

Figure 4.4 Surface morphologies of RuO_2-based coatings prepared at various Ru ratio: 30 mol% (A), 50 mol% (B), 80 mol% (C) and 100 mol% (D). Thermal decomposition temperature: 260 ^{o}C. Magnification: ×200,000.

A significant difference between RuO_2-Ta_2O_5 and RuO_2 coatings was observed from the SEM images at ×20,000, as shown in Figure 4.5. Figure 4.5 (D) demonstrates that aggregated RuO_2 particles of 50-80 nm are formed on the RuO_2 coating, while the RuO_2-Ta_2O_5 coatings at 30 mol% Ru to 80 mol% Ru have no such aggregated particles

even at higher magnification. This coincides with the XRD results where no diffraction peaks of RuO_2 were observed for the RuO_2-Ta_2O_5 coatings. It should be noted that the mixture of 80 mol% Ru and 20 mol% Ta has extremely uniform RuO_2 dispersed in amorphous Ta_2O_5 matrix.

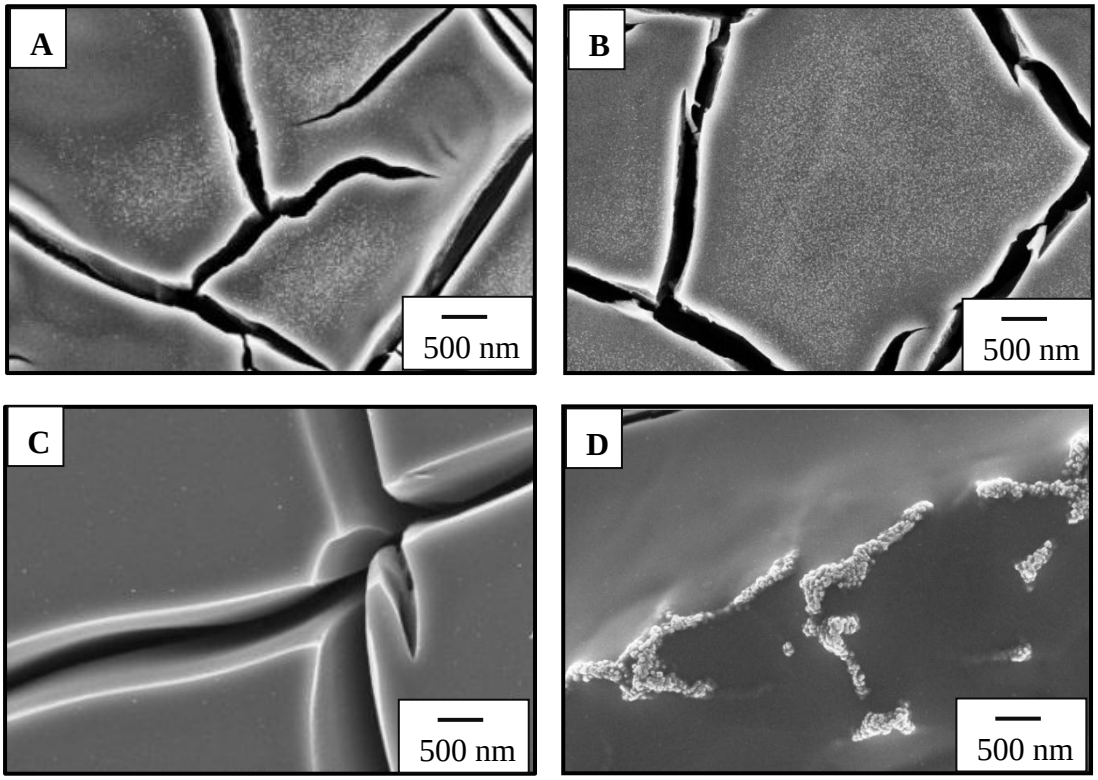

Figure 4.5 Surface morphologies of RuO_2-based coatings prepared at various Ru ratio: 30 mol% (A), 50 mol% (B), 80 mol% (C) and 100 mol% (D). Thermal decomposition temperature: 260 ^{o}C. Magnification: ×20,000.

4.2.3 Double layer charge

Double layer charge measurements were conducted similarly to those in Chapter 3 for the RuO_2/Ti and RuO_2-Ta_2O_5/Ti anodes in 2.0 mol dm^{-3} H_2SO_4 solution. Figure 4.6 shows the voltammograms recorded in the potential range from 0.85 V to 1.05 V at 5 mV s^{-1}, and the double layer charge, Q_{dl}, calculated from the

voltammograms are presented in Figure 4.7, in which the data of the anodes prepared at 500 ^{o}C are also given for comparison.

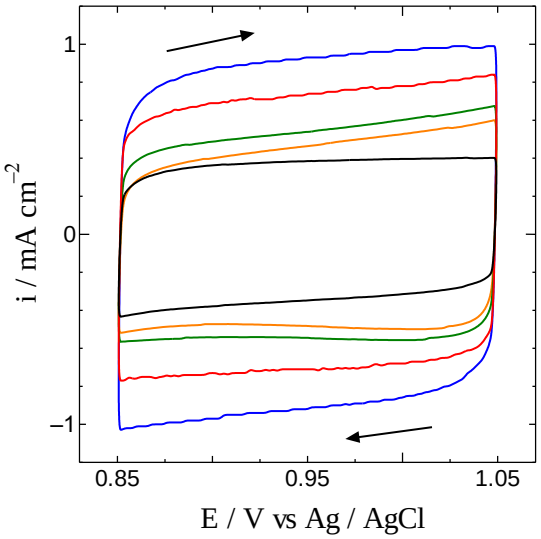

Figure 4.6 Cyclic voltammograms of RuO_2/Ti (black) and RuO_2-Ta_2O_5/Ti anodes prepared at various Ru ratio: 80 mol% (blue), 70 mol% (red), 50 mol% (green) and 30 mol% (orange) in 2.0 mol dm^{-3} H_2SO_4 solution at 40 ^{o}C. Thermal decomposition temperature: 260 ^{o}C. Scan rate: 5 mV s^{-1}.

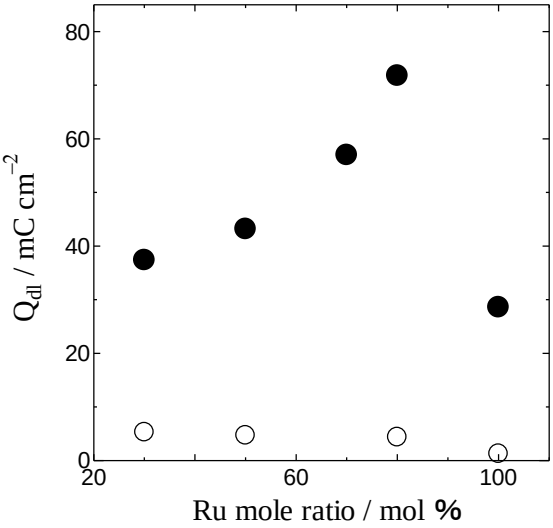

Figure 4.7 Dependence of the double layer charge of RuO_2/Ti and RuO_2-Ta_2O_5/Ti anodes in 2.0 mol dm^{-3} H_2SO_4 solution at 40 ^{o}C on Ru ratio. Thermal decomposition temperature: 260 ^{o}C (●) and 500 ^{o}C (○) .

The Q_{dl} of amorphous coatings prepared at 260 ^{o}C increased as the Ru ratio increased from 30 mol% to 80 mol%, and the Q_{dl} decreased markedly from 71.8 mC cm^{-2} to 28.6 mC cm^{-2} from 80 mol% to 100 mol% (*i.e.*, RuO_2 only); the highest Q_{dl} was obtained at 80 mol% Ru, and the Q_{dl} of the RuO_2/Ti anode was smaller than that of RuO_2-Ta_2O_5/Ti anode even at 30 mol% Ru. The results seem to be related with the surface morphologies of the coatings observed by SEM as follows. The increase in Ru ratio from 30 mol% to 80 mol% made RuO_2 particles smaller and RuO_2 dispersed homogeneously in amorphous Ta_2O_5 matrix so that the Q_{dl} increased. The Q_{dl} of the RuO_2 coating was small because RuO_2 particles of 50-80 nm existed on the coating, indicating that the coating is not amorphous structure as same as the amorphous RuO_2-Ta_2O_5 coatings. Figure 4.7 further revealed that Q_{dl} significantly increased irrespective of Ru ratio for all the anodes when the decomposition temperature was reduced from 500 ^{o}C to 260 ^{o}C. This is due to reducing particle size and the appearance of nano RuO_2 particles on the amorphous coatings, as already mentioned in Chapter 3.

4.2.4 Polarization curve

Figure 4.8 shows the voltammograms obtained of the anodes prepared at 260 ^{o}C in the potential range up to 1.32 V in 2.0 mol dm^{-3} H_2SO_4 solution. As the Ru ratio increased from 30 mol% to 80 mol%, oxygen evolution current increased, indicating that the RuO_2-Ta_2O_5/Ti anode at 80 mol% Ru has the highest catalytic activity for oxygen evolution. This is in good agreement with the results of the Q_{dl}. However, the RuO_2/Ti anode showed higher catalytic activity than the RuO_2-Ta_2O_5/Ti anode at 30 mol% Ru and 50 mol% Ru, which is contrary to the expected ones from the results of the Q_{dl}.

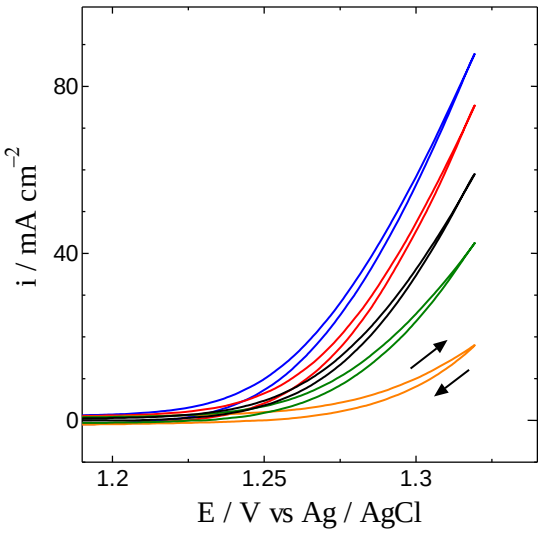

Figure 4.8 Cyclic voltammograms of RuO_2/Ti (black) and RuO_2-Ta_2O_5/Ti anodes prepared at various Ru ratio: 80 mol% (blue), 70 mol% (red), 50 mol% (green) and 30 mol% (orange) in 2.0 mol dm^{-3} H_2SO_4 solution at 40 ^{o}C. Thermal decomposition temperature: 260 ^{o}C. Scan rate: 5 mV s^{-1}.

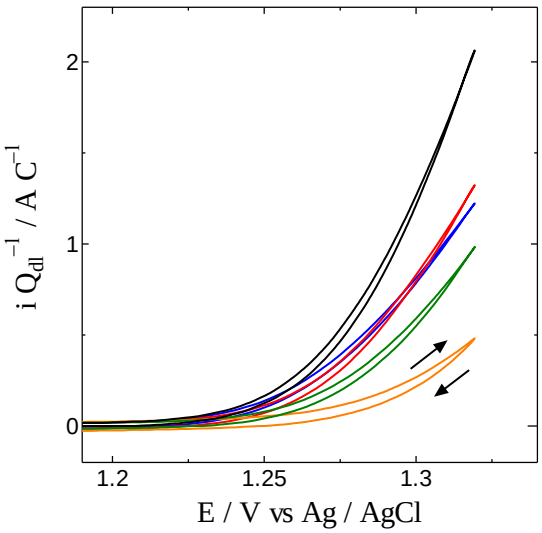

Figure 4.9 Cyclic voltammograms constructed from those shown in Figure 4.8 by dividing the current density by corresponding double layer charge. Ru ratio: 100 mol% (black), 80 mol% (blue), 70 mol% (red), 50 mol% (green) and 30 mol% (orange).

As described in Chapter 3, the catalytic activity for oxygen evolution is dependent of not only the effective surface area but also the electron transfer rate, and the normalized current density, i/Q_{dl}, is one of the tools to know their effects. Figure 4.9 shows the normalized polarization curves constructed from Figure 4.8. The normalized polarization curves are not overlapped, which means that the difference in catalytic activity does not caused only by an increase in effective surface area.

For more analysis, Tafel slope was evaluated for the anodes by linier sweep voltammetry at 0.5 mV s^{-1} in 2.0 mol dm^{-3} H_2SO_4 solution at 40 ^oC. The results are shown in Figure 4.10, in which a linear Tafel region was observed for all anodes, and the order of the overpotential of oxygen evolution is in good agreement with the results of the polarization curves shown in Figure 4.8.

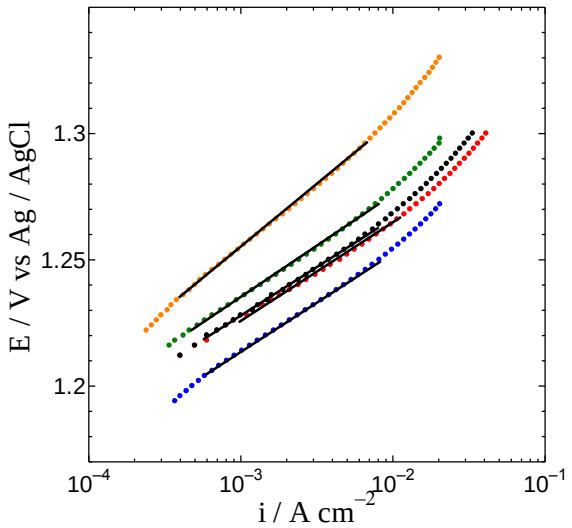

Figure 4.10 Polarization curves of RuO_2/Ti (black) and RuO_2-Ta_2O_5/Ti anodes prepared at various Ru ratio: 80 mol% (blue), 70 mol% (red), 50 mol% (green) and 30 mol% (orange) in 2.0 mol dm^{-3} H_2SO_4 solution at 40 ^oC. Thermal decomposition temperature: 260 ^oC. Scan rate: 0.5 mV s^{-1}.

Figure 4.11 shows a summary of Tafel slopes obtained from Figure 4.10, and the Tafel slope decreased when the Ru ratio increased from 30 mol% to 50 mol%, then was almost constant from 50 mol% Ru to 100 mol% Ru. The results suggest that the change of Ru ratio have little effect on the rds of oxygen evolution for the amorphous RuO_2-Ta_2O_5/Ti anodes. This also means the variation in the size of RuO_2 particles within a range of $\leq$ 30 nm has no considerable change in Tafel slope, while it induces a large increase in effective surface area. On the other hand, the dependence of Tafel slope on the Ru ratio seems to be independent of the trend in i/Q_{dl} shown in Figure 4.9, implying that the difference of the catalytic activity is difficult to explain in term of Tafel slope.

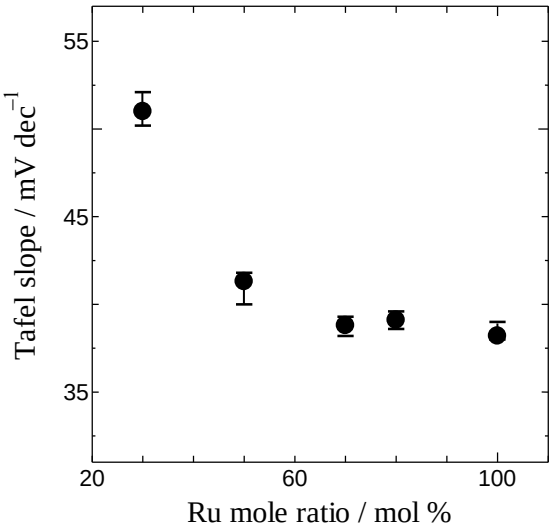

Figure 4.11 Dependence of the Tafel slope on of RuO_2/Ti and RuO_2-Ta_2O_5/Ti anodes in 2.0 mol dm^{-3} H_2SO_4 solution at 40 ^oC on Ru ratio. Thermal decomposition temperature: 260 ^oC.

Here, it is focused on i/Q_{dl} in Figure 4.9 again, and the dependence of i/Q_{dl} recorded at a fixed potential of 1.32 V on Ru ratio is presented in Figure 4.12. In the case, i/Q_{dl} is linear to Ru ratio, which means that the catalytic activity for oxygen evolution on the anodes prepared at 260 ^oC strongly depends on the coating composition

even with discussion based on the normalized current density; *i.e.*, in Figure 4.12, the catalytic activity of RuO_2 decreases significantly with more Ta_2O_5, and the nano RuO_2 observed on the RuO_2 coating seems to have higher catalytic activity than nano RuO_2 of 20-30 nm observed on the RuO_2-Ta_2O_5 coatings at 30 mol% Ru and 50 mol% Ru, even though no distinct difference is seen in Figure 4.11.

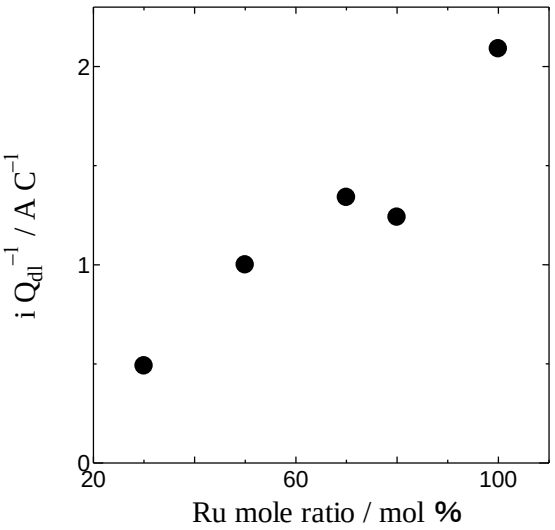

Figure 4.12 Dependence of i/Q_{dl} recorded at 1.32 V in Figure 4.9 on Ru ratio. Thermal decomposition temperature: 260 ^{o}C.

As mentioned above, linear relation between i/Q_{dl} and Ru ratio was only observed when the anode was prepared at 260 ^{o}C, *i.e.*, with the coatings comprising amorphous RuO_2, in this work. On the other hand, it was described in Section 4.2.3 that many researchers have demonstrated experimentally that the double layer charge is proportional to the effective surface area of the oxide coating, from which the double layer charge represents the number of electrochemically active sites. However, these conclusion was for IrO_2-based or RuO_2-based coatings prepared at a high temperature that can produce the coatings containing crystalline IrO_2 or RuO_2. The crystallographic structure and surface morphology are quite different from those in this study, and such crystalline IrO_2-based or RuO_2-based coatings seem to be simple to understand their

catalytic activity, compared to the amorphous oxide coatings.

Based on the above discussion, it can be concluded that mixing Ta_2O_5 to RuO_2 coating at the temperature, at which the amorphous RuO_2-Ta_2O_5 coating is produced, decreases the intrinsic catalytic activity of RuO_2 for oxygen evolution, but increases the effective surface area, so that the total balance governs the catalytic activity of the coatings. Consequently, the amorphous RuO_2-Ta_2O_5/Ti anode at 80 mol% Ru has the highest catalytic activity for the oxygen evolution among the anodes at different Ru ratios.

4.2.5 Oxygen overpotential

The onset potential and overpotential for oxygen evolution measured with the anodes prepared at 260 ^oC are summarized in Table 4.1 and Figure 4.13, of which the potential data were obtained in the same way as explained in Chapter 3. The oxygen overpotential decreased from 0.224 V to 0.182 V at the Ru ratio of 30 mol% to 80 mol%, which seems to be linear to the Ru ratio, then increased to 0.198 V on pure RuO_2 coating. The data proves again that the amorphous RuO_2-Ta_2O_5/Ti anode at 80 mol% Ru possesses the highest electrocatalytic activity for oxygen evolution.

Table 4.1 Onset potential and overpotential for oxygen evolution on RuO_2/Ti and RuO_2-Ta_2O_5/Ti anodes prepared at 260 ^oC in 2.0 mol dm^{-3} H_2SO_4 solution at 40 ^oC.

Ru ratio	30 mol%	50 mol%	70 mol%	80 mol%	100 mol%
Onset potential	1.267 V	1.245 V	1.234 V	1.225 V	1.241 V
Overpotential	0.224 V	0.202 V	0.191 V	0.182 V	0.198 V

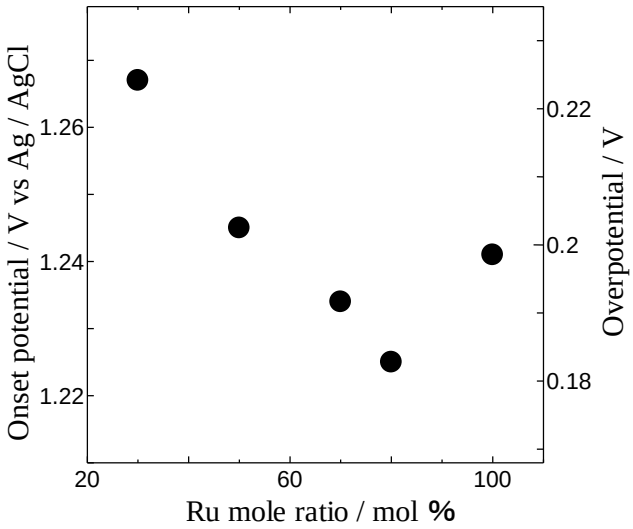

Figure 4.13 Dependence of the onset potential and overpotential of oxygen evolution on RuO_2/Ti and RuO_2-Ta_2O_5/Ti anodes in 2.0 mol dm^{-3} H_2SO_4 solution at 40 ^oC on Ru ratio. Thermal decomposition temperature: 260 ^oC.

4.2.6 Oxygen evolution potential

Figure 4.14 shows the chronopotentiograms of amorphous RuO_2-Ta_2O_5/Ti anodes recorded in 2.0 mol dm^{-3} H_2SO_4 solution at 100 A m^{-2}, 250 A m^{-2} and 500 A m^{-2}, and the oxygen evolution potentials at the end of the electrolysis are summarized in Table 4.2. The oxygen evolution potential showed a clear order like Ru = 80 mol% < Ru = 50 mol% < Ru = 30 mol% irrespective to the current density and was reduced by 0.04 V, 0.06 V and 0.08 V with the anode at 80 mol% Ru compared to that at 30 mol% Ru at 100 A m^{-2}, 250 A m^{-2} and 500 A m^{-2}, respectively.

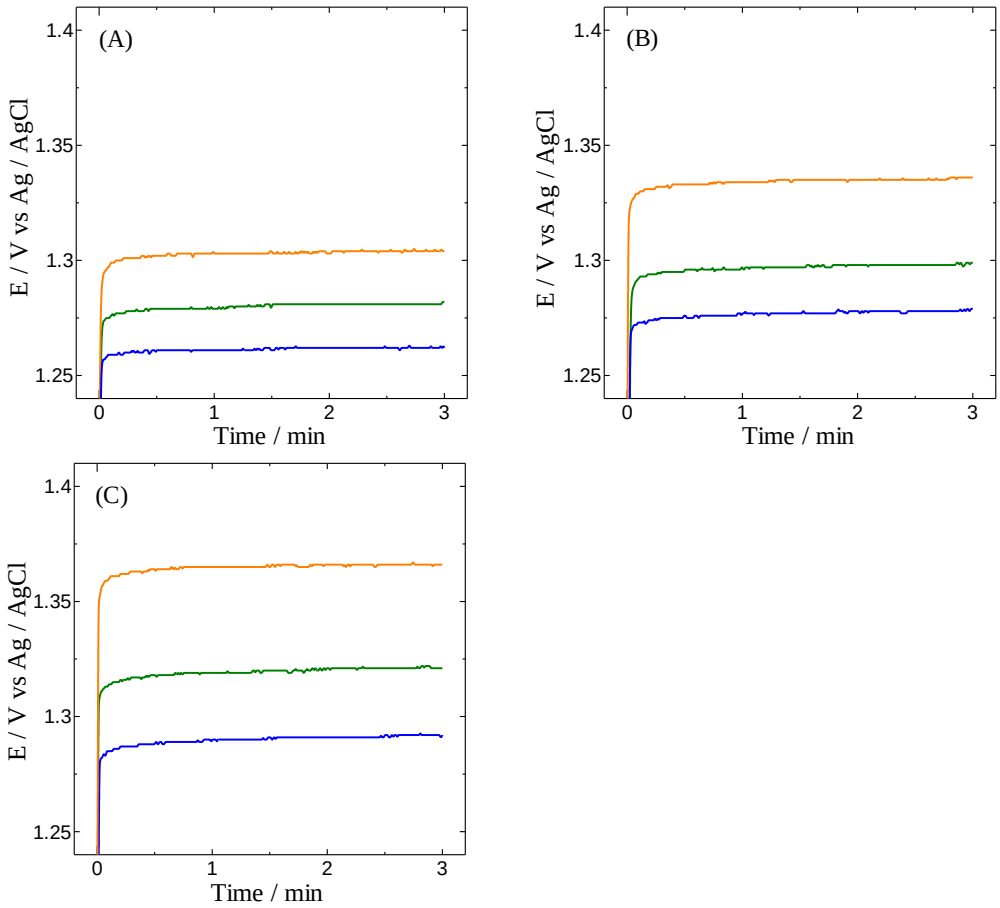

Figure 4.14 Potential variations of RuO_2-Ta_2O_5/Ti anodes prepared at various Ru ratio: 80 mol% (blue), 50 mol% (green) and 30 mol% (orange) during in constant current electrolysis at 100 A m^{-2} (A), 250 A m^{-2} (B) and 500 A m^{-2} (C) in 2.0 mol dm^{-3} H_2SO_4 solution at 40 ^oC. Thermal decomposition temperature: 260 ^oC.

Table 4.2 Oxygen evolution potentials on RuO_2-Ta_2O_5/Ti anodes at various current densities. Thermal decomposition temperature: 260 ^oC.

	100 A m^{-2}	250 A m^{-2}	500 A m^{-2}
Ru = 30 mol%	1.30 V	1.34 V	1.37 V
Ru = 50 mol%	1.28 V	1.30 V	1.32 V
Ru = 80 mol%	1.26 V	1.28 V	1.29 V

4.3 Conclusion

The RuO_2-Ta_2O_5/Ti and RuO_2/Ti anodes calcined at 260 ^oC comprising nano RuO_2 particles, and of which the size decreased with increasing Ru ratio from 30 mol% to 80 mol%. The nano structured surface including RuO_2 particles of 10 nm or less was formed on the whole coating at 80 mol% Ru, and this induced the highest effective surface area for oxygen evolution. The electrocatalytic activity of RuO_2 decreased with increasing Ta_2O_5 ratio in the coating, thereby the RuO_2 coating seemed to have the highest intrinsic activity based on the discussion with the normalized polarization curve. However, the effective surface area of the RuO_2/Ti anode was half or less than that of the RuO_2-Ta_2O_5/Ti anode at 80 mol% Ru, and the amorphous RuO_2-Ta_2O_5/Ti anode at 80 mol% Ru was found to be the best electrocatalyst for oxygen evolution.

4.4 References

[1] M. Morimitsu, "Polarization curve・Cyclic voltammetry", Electrochemistry, **77** (2009) 838-843.

[2] J. Gaudet, A.C. Tavares, S. Trasatti, D. Guay, "Physicochemical characterization of mixed RuO_2- SnO_2 solid solutions", **17** (2005) 1570-1579.

[3] S. Ardizzone, G. Fregonara, S. Trasatti, "Inner" and "outer" active surface of RuO_2 electrodes, Electrochimica Acta, **35** (1990) 263-267.

[4] O.R. Camara, S. Trasatti, "Surface electrochemical properties of Ti/(RuO_2+ZrO_2) electrodes", Electrochim. Acta, **41** (1996) 419-427.

[5] C.P. de Pauli, S. Trasatti, "Composite materials for electrocatalysis of O_2 evolution: IrO_2+SnO_2 in acid solution", J. Electroanal. Chem., **538-539** (2002) 145-151.

[6] A.J. Terezo, E.C. Pereira, "Preparation and characterization of Ti/RuO_2-Nb_2O_5 electrodes obtained by polymeric precursor method", Electrochim. Acta, **44** (1999) 4507-4513.

[7] J.F.C. Boodts, S. Trasatti, "Effect of composition on the electrocatalytic activity of the ternary oxide $Ru_{0.3}Ti_{(0.7-x)}Sn_xO_2$", J. Electrochem. Soc., **137** (1990) 3784-3789.

[8] L.M. Da Silva, J.F.C. Boodts, L.A. De Faria, "Oxygen evolution at $RuO_2(x)+Co_3O_4(1-x)$ electrodes from acid solution", Electrochim. Acta, **46** (2001) 1369-1375.

Chapter 5

Suppression of anodic PbO_2 deposition

5.1 Introduction

As described in Chapter 1, the electrowinning solutions of copper and nickel contain Pb(II) ions as a impurity, which is easily oxidized to PbO_2 on lead alloy anodes or commercially available IrO_2-Ta_2O_5/Ti anodes composing crystalline IrO_2 during oxygen evolution. This causes the increase in oxygen overpotential, the decrease in the anode's lifetime, and the production of hazardous byproducts and wastes.

Prof. Morimitsu has previously reported that amorphous IrO_2-Ta_2O_5/Ti anodes obtained at low thermal decomposition temperature have a low overpotential for oxygen evolution, but a high overpotential for PbO_2 deposition, with which the voltage reduction for copper electrolysis can be possible with a complete suppression of anodic deposition of PbO_2 [1-4]. On the other hand, little is known about the suppression effects to anodic PbO_2 deposition with RuO_2-Ta_2O_5/Ti anodes. In this Chapter, the performance of RuO_2-Ta_2O_5/Ti anodes for oxygen evolution in acid aqueous solutions with and without Pb(II) ions, and the effects of the amorphization of RuO_2 on suppression of anodic PbO_2 deposition are discussed.

5.2 Results and discussion

5.2.1 Overpotential for oxygen evolution and PbO_2 deposition

Cyclic voltammetry was carried out to investigate the oxygen evolution behavior of the RuO_2-Ta_2O_5/Ti anodes prepared at 260 ^oC, 280 ^oC or 500 ^oC (Ru = 80 mol%) in HNO_3 solutions, and the results are shown in Figure 5.1. The oxygen evolution current increased and the onset potential of oxygen evolution shifted negatively when the decomposition temperature decreased. This is in good agreement with the result obtained in the H_2SO_4 solution mentioned in Chapter 3. Therefore, the results indicated that the amorphous RuO_2-Ta_2O_5/Ti anode is more catalytic and shows lower oxygen overpotential in the HNO_3 solution than the crystalline RuO_2-Ta_2O_5/Ti

anode as well as in the H_2SO_4 solution.

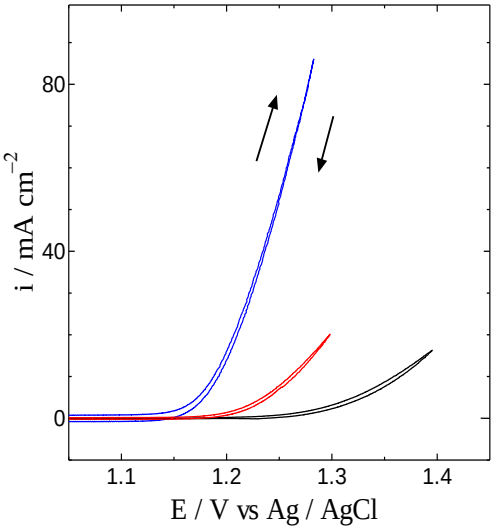

Figure 5.1 Cyclic voltammograms of RuO_2-Ta_2O_5/Ti anodes prepared at 500 ^oC (black), 280 ^oC (red) and 260 ^oC (blue) in HNO_3 solution (pH=0.7) at 30 ^oC. Ru ratio: 80 mol%. Scan rate: 5 mV s^{-1}.

The onset potentials of PbO_2 deposition on the RuO_2-Ta_2O_5/Ti anode were determined by the combined measurements of constant potential electrolysis and liner sweep voltammetry (cathodic scan) in HNO_3 solutions containing 30 wt% $Pb(NO_3)_2$, as shown in Figure 5.2. Constant potential electrolysis at a certain potential was conducted in the $Pb(NO_3)_2$ solution for 60 s, and immediately after that, the cathodic scan at 1 mV s^{-1} was performed. In the case, the reduction wave of PbO_2 produced during the constant potential electrolysis is observed, when the potential is more positive than the onset potential of PbO_2 deposition. The measurement was repeated until the cathodic wave was observed with changing the controlled potential to determine the onset potential of PbO_2.

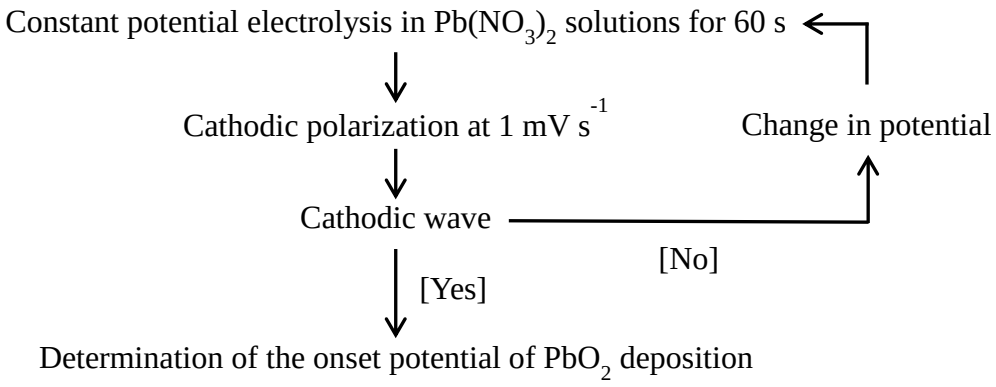

Figure 5.2 Determination procedure of the onset potential of PbO_2 deposition.

Figure 5.3 shows the obtained results; in the case of the anode prepared at 500 ^{o}C, no reduction wave was observed when the holding potential was 1.37 V, while the cathodic wave corresponding to the reduction of PbO_2 produced during the constant potential electrolysis was observed when the holding potential was 1.38 V, from which the onset potential of PbO_2 deposition was determined to be 1.38 V. These experiments were also performed using the other two anodes. The obtained data were summarized in Figure 5.4 and Table 5.1. The onset potentials of oxygen evolution were obtained from Figure 5.1, and it was defined as the same way as explained in Chapter 3. The results clearly indicate the overpotential of oxygen evolution decreases, while that of PbO_2 deposition increases, as thermal decomposition temperature becomes low. Consequently, the difference between the onset potentials of oxygen evolution and PbO_2 deposition becomes larger with lower decomposition temperature; the difference on the amorphous anode prepared at 260 ^{o}C is 0.58 V, while that on the crystalline anode at 500 ^{o}C is 0.18 V.

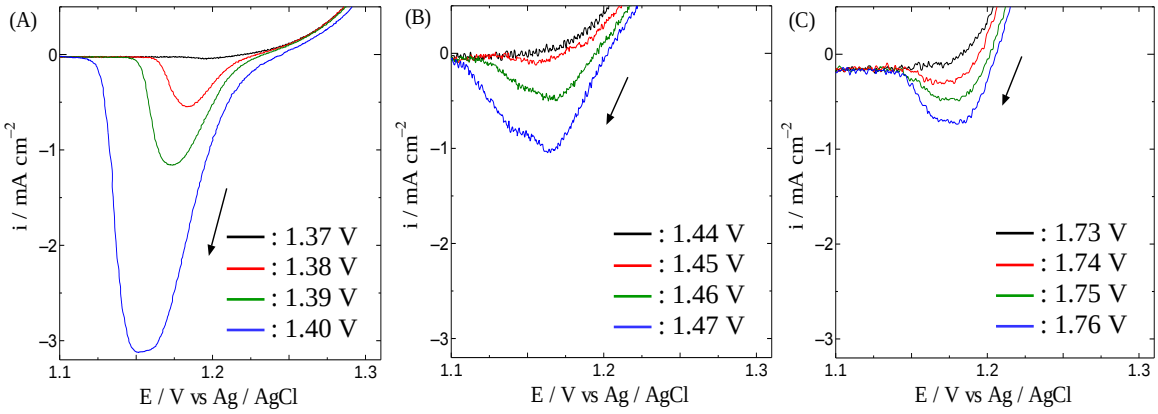

Figure 5.3 Cathodic polarization curves of RuO_2-Ta_2O_5/Ti anodes after the electrolysis at various potential for 60 s in 30 wt% $Pb(NO_3)_2$ (pH=0.7) at 30 ^oC. Thermal decomposition temperature: 500 ^oC (A), 280 ^oC (B) and 260 ^oC (C). Ru ratio: 80 mol%. Scan rate: 1 mV s^{-1}.

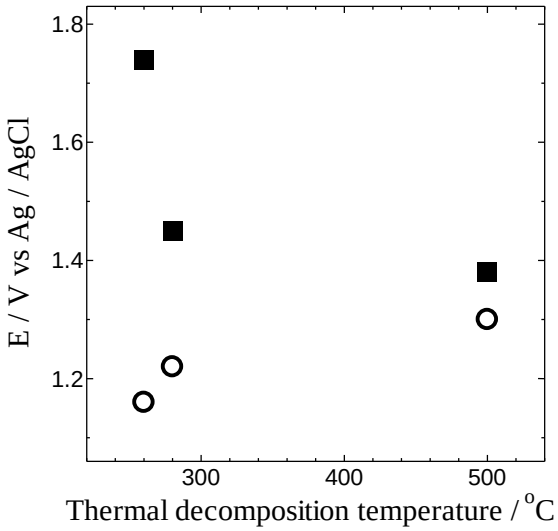

Figure 5.4 Onset potentials of oxygen evolution (○) and PbO_2 deposition (■) on RuO_2-Ta_2O_5/Ti anodes prepared at 500 ^oC, 280 ^oC and 260 ^oC in HNO_3 solution with and without 30 wt% $Pb(NO_3)_2$ (pH=0.7) at 30 ^oC. Ru ratio: 80 mol%.

Table 5.1 Onset potentials of oxygen evolution and PbO_2 deposition on RuO_2-Ta_2O_5/Ti anodes prepared at 500 ^oC, 280 ^oC and 260 ^oC. Ru ratio: 80 mol%.

	Oxygen evolution	PbO_2 deposition	Potential difference
500 ^oC	1.30 V	1.38 V	0.18 V
280 ^oC	1.22 V	1.45 V	0.23 V
260 ^oC	1.16 V	1.74 V	0.58 V

The dependence of the onset potentials of oxygen evolution and PbO_2 deposition on the Ru ratio is also given in Figure 5.5 and Table 5.2. The thermal decomposition temperature was 260 ^oC, so that all anodes comprised amorphous RuO_2.

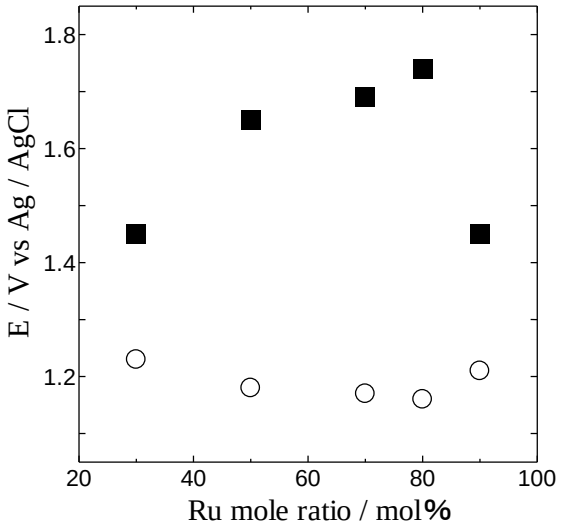

Figure 5.5 Onset potentials of oxygen evolution (○) and PbO_2 deposition (■) on RuO_2-Ta_2O_5/Ti anodes prepared at various Ru ratio in HNO_3 solution with and without 30 wt% $Pb(NO_3)_2$ (pH=0.7) at 30 ^oC. Thermal decomposition temperature: 260 ^oC.

Table 5.2 Onset potentials of oxygen evolution and PbO_2 deposition on RuO_2-Ta_2O_5/Ti anodes prepared at various Ru ratio. Thermal decomposition temperature: 260 ^oC.

	Oxygen evolution	PbO_2 deposition	Potential difference
Ru = 30 mol%	1.23 V	1.45 V	0.22 V
Ru = 50 mol%	1.18 V	1.65 V	0.47 V
Ru = 70 mol%	1.17 V	1.69 V	0.53 V
Ru = 80 mol%	1.16 V	1.74 V	0.58 V
Ru = 90 mol%	1.21 V	1.45 V	0.24 V

As shown in Figure 5.5, the onset potential of PbO_2 deposition increases as the Ru ratio increase up to 80 mol%, and then exhibited a drastic decrease when the Ru ratio changes from 80 mol% to 90 mol%. On the other hand, the onset potential of oxygen evolution is a minimum at 80 mol% Ru. Therefore, it is clear that the amorphous anode at 80 mol% Ru is the most effective to suppress PbO_2 deposition.

5.2.2 Active sites for PbO_2 deposition

Figure 5.6 depicts the surface of the crystalline RuO_2-Ta_2O_5/Ti anode before and after electrolysis at 400 A m^{-2} in the 30 wt% $Pb(NO_3)_2$ solution for 10 s. The SEM images indicated well-developed and aggregated RuO_2 particles of *ca*. 200 nm and flat areas on the surface of the anode before the electrolysis. However, after the electrolysis, these well-developed RuO_2 particles became invisible by being covered with the other particles which were confirmed to be deposited PbO_2 by EDX analysis, although the flat area remained unchanged and without such PbO_2. The results demonstrate that PbO_2

particles are selectively deposited on the well-developed and aggregated RuO_2 particles. This is reasonable, because PbO_2 and RuO_2 have similar lattice parameters due to the same crystallographic structure (rutile structure), so that the nucleation of PbO_2 is easier on crystalline RuO_2 than on the flat area. Therefore, it can be concluded that active sites for PbO_2 deposition are the well-developed RuO_2 particles. This is in good agreement with the result of the onset potentials of PbO_2 deposition (Figure 5.4); the amorphization of RuO_2, *i.e.*, the disappearance of well-developed RuO_2 particles, results in the decrease in active site for PbO_2 deposition, thereby the onset potential of PbO_2 deposition increases with decreasing thermal decomposition temperature.

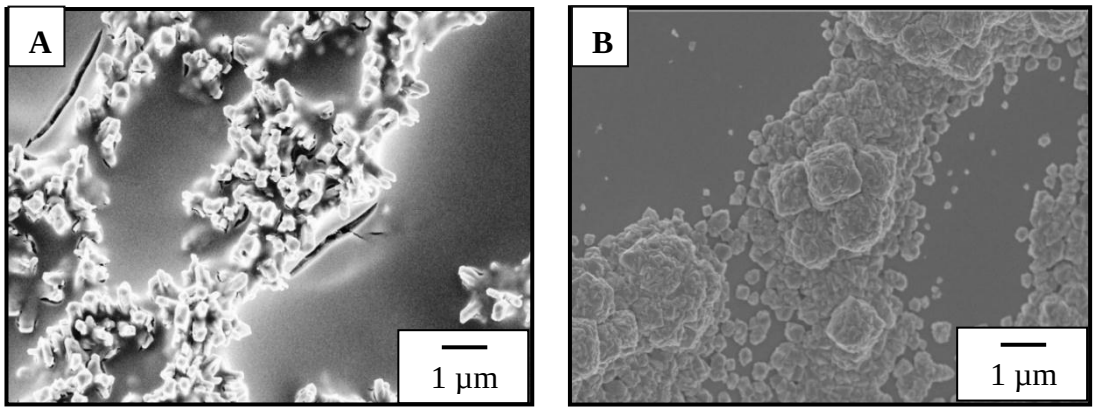

Figure 5.6 Surface morphologies of RuO_2-Ta_2O_5 coatings prepared at 500 ^oC before (A) and after (B) electrolysis at 400 A m^{-2} in 30 wt% $Pb(NO_3)_2$ (pH=0.7) for 10 s at 30 ^oC. Magnification: ×10,000.

5.2.3 Suppression of PbO_2 deposition

Constant current electrolysis at 400 A m^{-2} in HNO_3 solution with 30 wt% $Pb(NO_3)_2$ at 70 ^oC was further done to compare the anode potentials. As shown in Figure 5.7, the RuO_2-Ta_2O_5/Ti anodes prepared at 260 ^oC and 280 ^oC showed constant anode potential during the electrolysis, while the anode potential increased with the anode prepared at 500 ^oC, suggesting that anodic PbO_2 deposition occurs on this anode.

The anode potentials of the RuO_2-Ta_2O_5/Ti anodes prepared at 260 ^oC, 280 ^oC and 500 ^oC were 1.21 V, 1.29 V and 1.46 V at the end of the electrolysis, which reveals that the anode potential can be reduced by 0.25 V if the crystalline RuO_2-Ta_2O_5/Ti anode is replaced with the amorphous anode even in the solution containing Pb(II) ions.

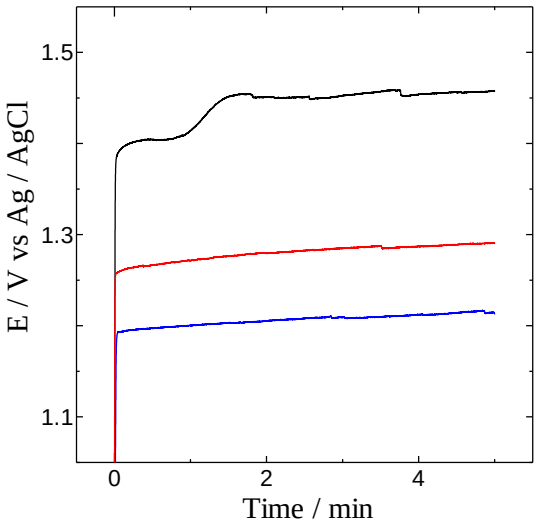

Figure 5.7 Potential variations of RuO_2-Ta_2O_5/Ti anodes prepared at 500 ^oC (black), 280 ^oC (red) and 260 ^oC (blue) during in constant current electrolysis at 400 A m^{-2} in 30 wt% $Pb(NO_3)_2$ (pH=0.7) at 70 ^oC. Ru ratio: 80 mol%.

Figure 5.8 shows the XRD pattern of each anode after the electrolysis. The anodes prepared at 260 ^oC and 280 ^oC indicated no PbO_2 deposit because the XRD patterns before and after the electrolysis are the same, while PbO_2 was detected on the anode prepared at 500 ^oC, with which the diffraction peaks of RuO_2 disappeared after the electrolysis. Consequently, the anode prepared at 260 ^oC and 280 ^oC can prevent the anodic PbO_2 deposition, while PbO_2 covers the surface of the anode prepared at 500 ^oC.

The amount of PbO_2 deposits was calculated from the mass change of the anode before and after the constant current electrolysis. Figure 5.9 shows the relationship between thermal decomposition temperature and the amount of PbO_2. The

amount of PbO_2 decreased with the decrease in thermal decomposition temperature, and the anodic deposition of PbO_2 never occurs at thermal decomposition temperature of 260 ^oC. This is because the amorphization of RuO_2 strongly accelerates oxygen evolution and simultaneously suppresses PbO_2 deposition. Therefore, the anode potential in copper and nickel EW can be significantly reduced with no possibility of PbO_2 deposition on the amorphous RuO_2-Ta_2O_5/Ti anode.

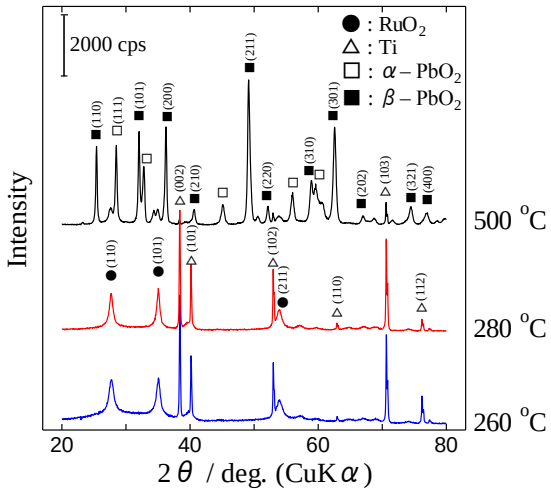

Figure 5.8 XRD patterns of RuO_2-Ta_2O_5/Ti anodes prepared at 500 ^oC, 280 ^oC and 260 ^oC after electrolysis at 400 A m^{-2} for 5 min in 30 wt% $Pb(NO_3)_2$ (pH=0.7) at 70 ^oC.

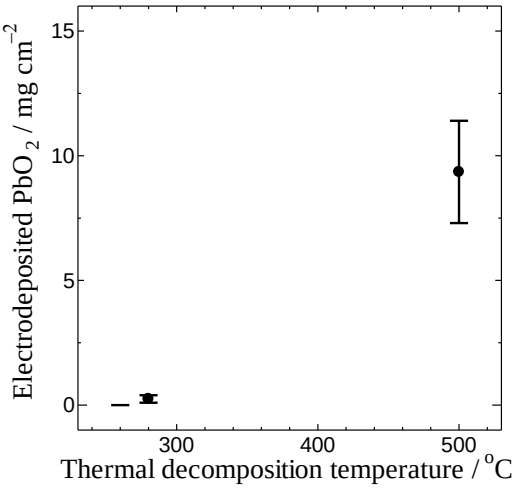

Figure 5.9 Amount of PbO_2 deposited on RuO_2-Ta_2O_5/Ti anodes prepared at 500 ^oC, 280 ^oC and 260 ^oC during the electrolysis 400 A m^{-2} for 5 min in 30 wt% $Pb(NO_3)_2$ (pH=0.7) at 70 ^oC.

5.3 Conclusion

The amorphization of RuO_2 induced the reduction in overpotential of oxygen evolution and the increase in that of PbO_2 deposition, so that less noble anode potential and no possibility of PbO_2 deposition were achieved with amorphous RuO_2-Ta_2O_5/Ti anodes. This is because well-developed RuO_2 particles which are the active sites for PbO_2 deposition are disappeared by the amorphization, and nano RuO_2 particles which are highly active for oxygen evolution, but non-active for PbO_2 deposition are uniformly dispersed in the coatings. These excellent properties are valuable to improve the purity of electrowon metal, prolong the anode's lifetime, reduce the maintenance of electrolysis process, decrease the production cost of EW, and make a low impact to environment.

5.4 References

[1] M. Morimitsu, N. Oshiumi, N. Wada, "Smart anodes for electrochemical processing of copper production", Proc. of Copper 2010, Electrowinning and –refining, **4** (2010) 1511-1520.

[2] M. Morimitsu, "Performance and commercialization of the smart anode, MSA™, for environmentally friendly electrometallurgical process", Proc. Electrometallurgy 2012, TMS (2012) 49-54.

[3] K. Kawaguchi, G.M. Haarberg, M. Morimitsu, "Control of amorphization of IrO_2-Ta_2O_5/Ti electrodes to suppress unwanted side reactions", ECS Transactions, **16** (2009) 41-47.

[4] K. Kawaguchi, G.M. Haarberg, M. Morimitsu, "Suppression of PbO_2 deposition on nano-structure surface of IrO_2-Ta_2O_5/Ti anodes in acidic solutions", ECS Transactions, **50** (2013) 75-85.

Chapter 6

Durability of amorphous RuO_2-Ta_2O_5/Ti anode

6.1 Introduction

The lifetime of the anode is extremely important for the practical use in EW processes. Despite the high catalytic activity of RuO_2 for oxygen evolution, it has been mentioned that none of RuO_2-based anodes have a sufficient lifetime for the practical use due to serious corrosion of RuO_2 in the coatings, and IrO_2-based anodes have been used for oxygen evolution in the last a few decades because of its good catalytic activity for oxygen evolution and better stability than other precious metal oxides [1-6]. It is also well known that the stability of IrO_2 is enhanced significantly by the addition of Ta_2O_5. IrO_2-Ta_2O_5/Ti anodes for oxygen evolution have been extensively investigated, in which some of them have been conducted to clarify the deterioration mechanism for oxygen evolution in acidic media [7-23]. In general, the deterioration of oxide coated titanium anodes is considered to the consumption of the active component in the coating and/or the formation of non-conductive titanium oxide layer on titanium. For this, various approaches have been examined to improve the lifetime of the anode, in which the durability of the anode has been revealed to be influenced by the surface morphology, the coating composition, the coating's amount, the densification of coating, the pretreatment of titanium, thermal decomposition temperature, and the other preparation procedures and conditions [1-4,7-27]. For example, the lifetime of the anode prolonged as the amount of the oxide coating increased [18,24,25], and the surface morphologies of titanium substrate affected those of the catalytic coatings and affected the durability of the anode [28]. The insertion of corrosion-resistant interlayer between the titanium substrate and the oxide coating prevented the electrolyte penetrating to the titanium substrate, which protects the substrate from corrosion [10,16,23].

Although the durability of RuO_2 for oxygen evolution seems to be lower than that of IrO_2, there is still a possibility of the development of non-iridium oxide based oxygen evolution anodes, and there are many researches which have been trying to prolong the lifetime of RuO_2-based anodes in different ways [29-42]. The RuO_2-ZrO_2/Ti anode prepared from nitrate salts showed better properties than those obtained from

chloride ones [40], and the RuO_2/Ti anode obtained by thermal decomposition of $RuCl_3$ using polymeric precursor method gave higher durability than those prepared from isopropanol solution method [41]. It was also demonstrated that the lifetime of the RuO_2-Ta_2O_5/Ti anodes increased with increasing Ru ratio from 10 atom% to 80 atom%, and the durability of RuO_2-Ta_2O_5/Ti anode was much higher than that of RuO_2-TiO_2/Ti anode [42]. From the above background, this Chapter presents the durability of amorphous RuO_2-Ta_2O_5/Ti anodes and the improvement by a novel method.

6.2 Results and discussion

6.2.1 Durability of RuO_2-Ta_2O_5/Ti anode

Accelerated life tests of the crystalline and amorphous RuO_2-Ta_2O_5/Ti anodes at 80 mol% Ru were carried out to evaluate the durability of the anodes for oxygen evolution. Figure 6.1 shows the variation in cell voltage between the RuO_2-Ta_2O_5/Ti anode and the platinum counter electrode with time during continuous electrolysis at 5,000 A m^{-2}. In the measurements, the RuO_2-TiO_2/Ti anode (Ru = 30 mol%, 280 ^oC) was also used as the anode for comparison. It should be noted that the amount of the catalytic coating of the anodes used in this measurement was small to enable to rapidly determine the lifetime.

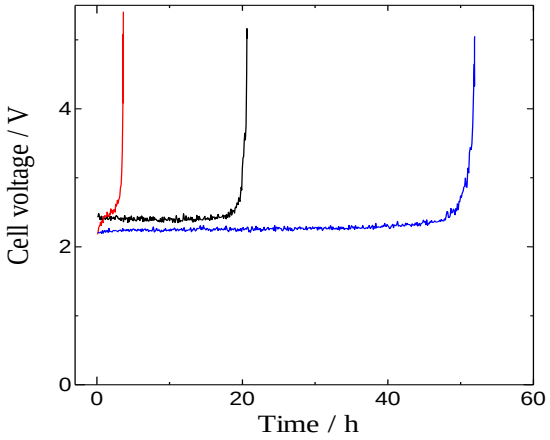

Figure 6.1 Variation in cell voltage during accelerated electrolysis of amorphous (blue) and crystalline (black) RuO_2-Ta_2O_5/Ti anodes and RuO_2-TiO_2/Ti anode (red) at 5,000 A m^{-2} in 2.0 mol dm^{-3} H_2SO_4 solution at 40 ^oC.

As shown in Figure 6.1, the cell voltage was almost stable for a certain time and finally increased abruptly, which was independent of the crystallographic structure of RuO_2-Ta_2O_5/Ti anodes, suggesting that the anode was deactivated within a short time, although the cell voltage with the amorphous anode was lower than that with the crystalline anode. However, amazingly, the amorphous RuO_2-Ta_2O_5/Ti anode showed a longer lifetime than the crystalline anode, which is more than double of the crystalline anode, even though the literatures reported that durability of the anode decreased with decreasing thermal decomposition temperature [26,27]. The results revealed that the crystallographic structure of the coating is one of the significant factors, as well as the oxide composition and amount of the coating, for the lifetime of the anode, and that the amorphous RuO_2-Ta_2O_5/Ti anode prepared by this work showed a superior durability to the crystalline anode.

The results also indicated that the amorphous RuO_2-Ta_2O_5/Ti anode had much higher durability than the RuO_2-TiO_2/Ti anode. The cell voltage with RuO_2-TiO_2/Ti anode was gradually increased within a few hours from the current loading, although the initial cell voltage with RuO_2-TiO_2/Ti anode was close to that with the amorphous RuO_2-Ta_2O_5/Ti anode. The photographs of the RuO_2-TiO_2/Ti anode and the amorphous RuO_2-Ta_2O_5/Ti anode before and after the accelerated life test (ALT) are shown in Figure 6.2. After the electrolysis, the coating of the RuO_2-TiO_2/Ti anode was completely consumed and the titanium substrate was exposed. However, the amorphous RuO_2-Ta_2O_5/Ti anode showed no change in surface morphology. The results implies that the deterioration mechanism of these two anodes was quite different and that the consumption of catalytic coating was much suppressed by adding Ta_2O_5 to RuO_2 even in the amorphous phase. This is because Ta_2O_5 has a high durability for oxygen evolution in acid aqueous solutions and is effective to hold and stabilize RuO_2 in the coating.

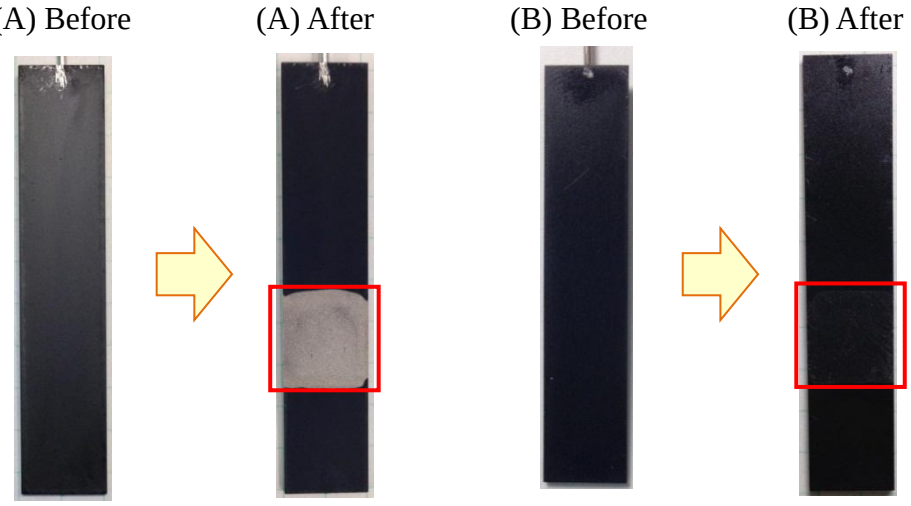

Figure 6.2 Overview images of RuO_2-TiO_2/Ti anode (A) and amorphous RuO_2-Ta_2O_5/Ti anode (B) before and after the accelerated life tests at 5,000 A m^{-2} in 2.0 mol dm^{-3} H_2SO_4 solution at 40 ^oC.

One of the major reasons for why the lifetime of the amorphous RuO_2-Ta_2O_5/Ti anode has longer lifetime in the ALT than the crystalline on is related to the effective surface area for oxygen evolution. As explained in Chapter 3, the effective surface area of the amorphous anode was more than 10 times higher than that of crystalline anode, so that the high effective surface area of the amorphous coating can make the actual current density smaller than the crystalline coating even when the same current density based on the geometrical surface is applied. For example, when the applied current density is 5,000 A m^{-2}, the actual current density would be 1/10 or less of the applied one for the amorphous anode compared to the crystalline one.

Figure 6.3 depicts the SEM images of the coating surface before and after the ALT. About the degradation mechanism of the amorphous RuO_2-Ta_2O_5/Ti anode, the SEM images show that the fresh coating consisted of the flat areas and the cracks of *ca*. 200 nm width, while the width of crack was greatly extended and reached to 500 nm or more after the ALT. However, no significant change was observed for the flat areas.

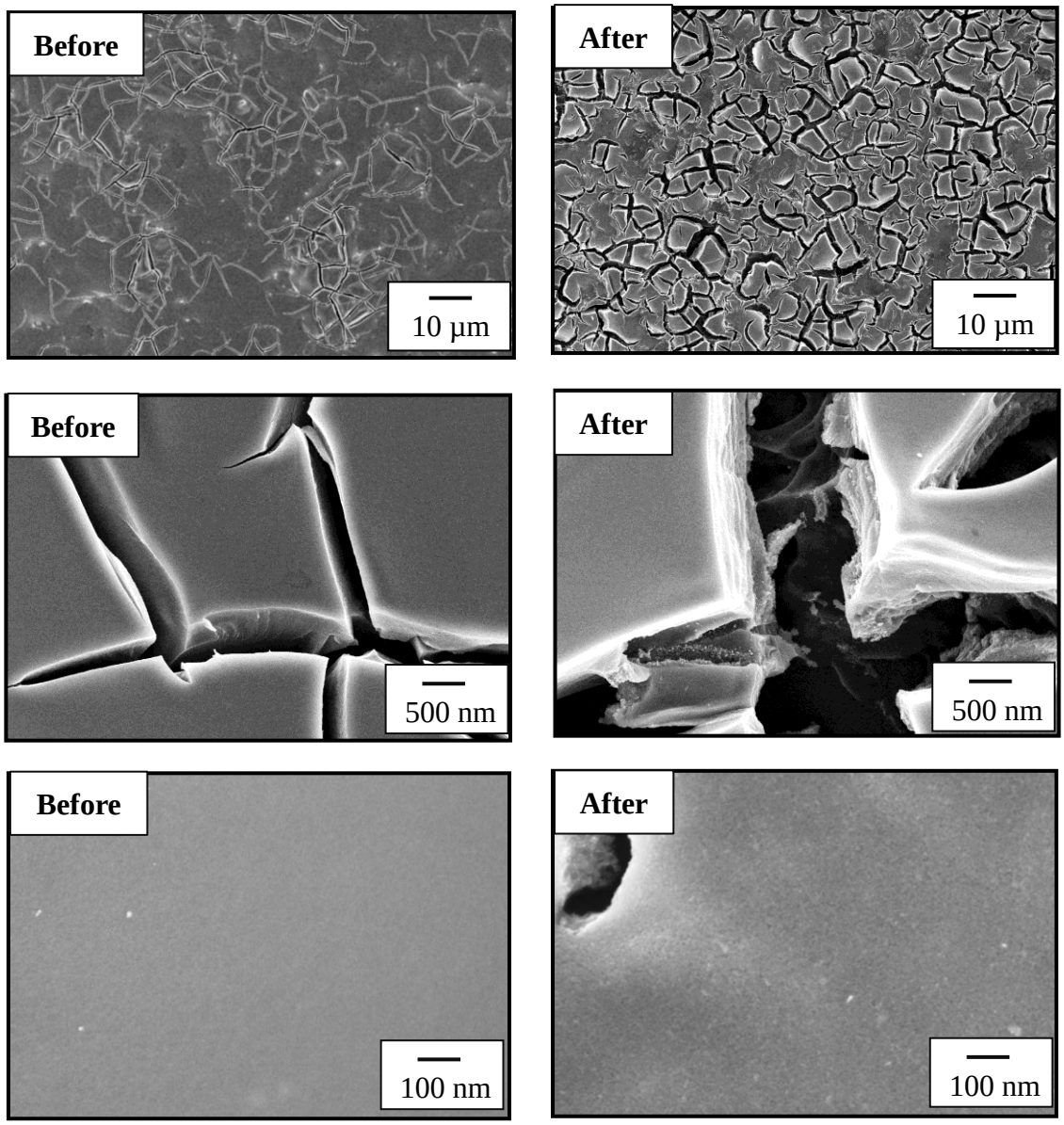

Figure 6.3 Surface morphologies of amorphous RuO_2-Ta_2O_5 coating before (left) and after (right) the accelerated life test at 5,000 A m^{-2} in 2.0 mol dm^{-3} H_2SO_4 solution at 40 ^oC. Magnification: ×1,000 (top), ×20,000 (middle) and ×100,000 (bottom).

More detailed analysis of the coatings before and after the ALT was performed by EDX and the results are discussed below. The EDX analysis of the amorphous

RuO_2-Ta_2O_5/Ti anode after the electrolysis at 5,000 A m^{-2} till the end of lifetime was carried out. Figure 6.4 depicts the SEM image and the elemental mapping images of ruthenium, tantalum, oxygen and titanium.

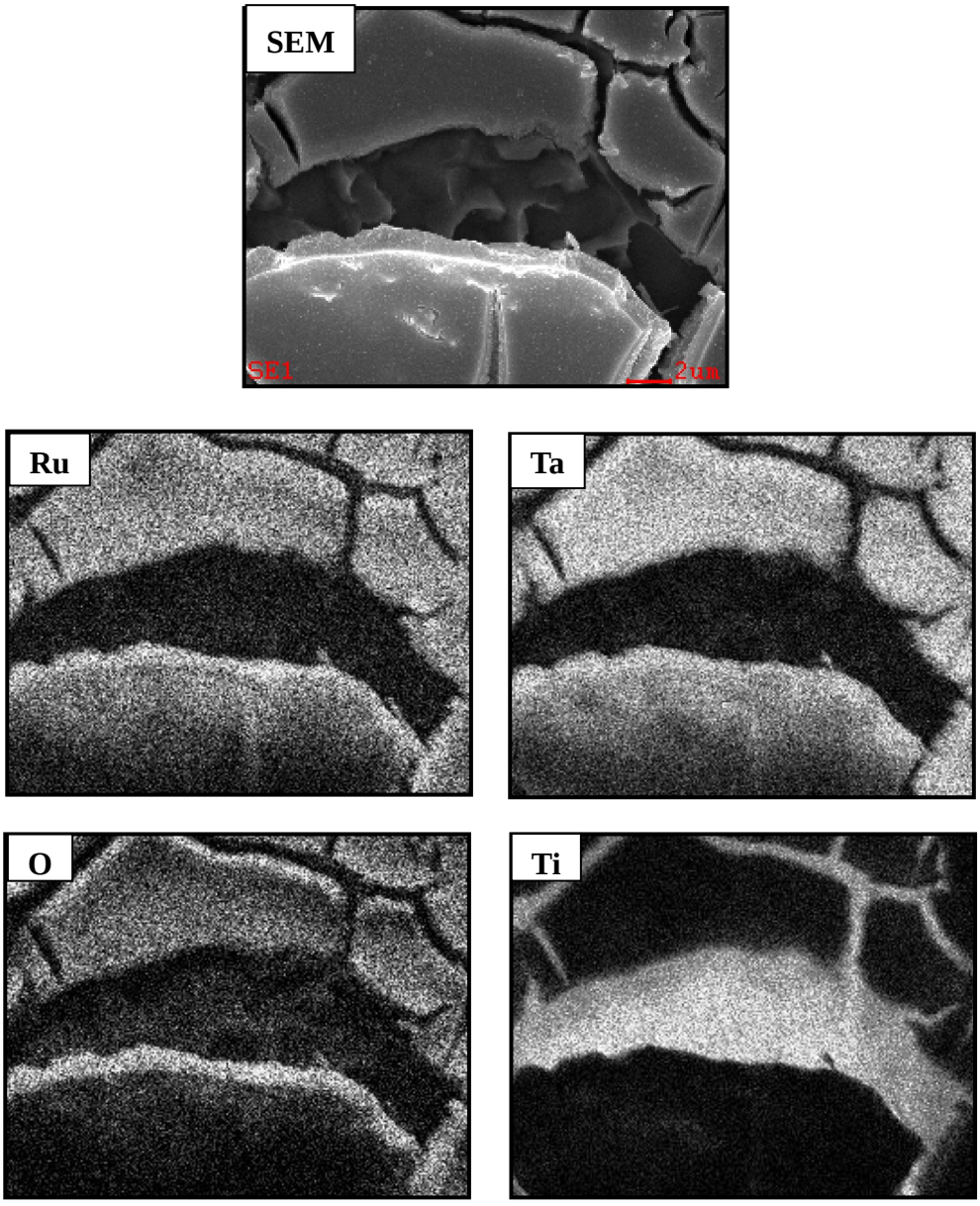

Figure 6.4 SEM image and mapping images for ruthenium, tantalum, oxygen and titanium on amorphous RuO_2-Ta_2O_5/Ti anode after the accelerated life test.

The SEM image shows the wide and deep crack of *ca.* 2 μm width in maximum, and the EDX images clearly indicate that titanium substrate is exposed through the wide crack, implying that non-conductive TiO_2 layer is formed during the electrolysis. On the other hand, it is also revealed that Ru and Ta still exist on the coating surface even after the ALT. These results suggest that the lifetime of the anode is governed by the corrosion of the titanium substrate rather than the consumption of the coating. The wide and deep cracks on the coating induce the electrolyte penetration to titanium surface, which results in the formation of non-conductive TiO_2 layer between the coating and the titanium substrate, *i.e.*, the passivation of the titanium substrate occurs, causing the rapid increase in the cell voltage which is the indicator of the anode's lifetime. Therefore, the prevention of the titanium substrate from corrosion will be helpful to obtain more lifetime of the amorphous anode.

6.2.2 Improvement of durability for oxygen evolution

To improve the lifetime of the amorphous RuO_2-Ta_2O_5/Ti anode, the pretreatment of titanium substrates were investigated in two ways; Sample A was etched in 10 wt% oxalic acid solution at 90 ^oC for 60 min followed by washing in distilled water, which is the basic method in this study, and Sample B was etched in 10 wt% oxalic acid solution at 90 ^oC for 10 min and then immersed into 5.0 mol dm^{-3} NaOH solution at 95 ^oC for 60 min, followed by washing with 0.1 mol dm^{-3} HNO_3 solution and distilled water. Sample B was prepared with the similar procedure reported by Miyauchi and his co-authors [43-45].

Figures 6.5 and 6.6 depict the typical SEM images of the substrate surface of Samples A and B, respectively. The low magnification images at ×1,000 and ×10,000 presented roughed titanium surface for both samples (Figure 6.5A, B and Figure 6.6A, B). However, there were a significant difference between these two samples on high magnification images; Sample A (Figure 6.5C, D) showed a smooth surface, while a

porous structure with nano-fibers of less than 100 nm in diameter was observed for Sample B (Figure 6.6C, D). ALT was conducted for the samples, and the results showed that the lifetime of Sample B was longer than that of Sample A. A high adhesion between the coating and the substrate (Sample B) is thought to be the reason for the durability enhancement.

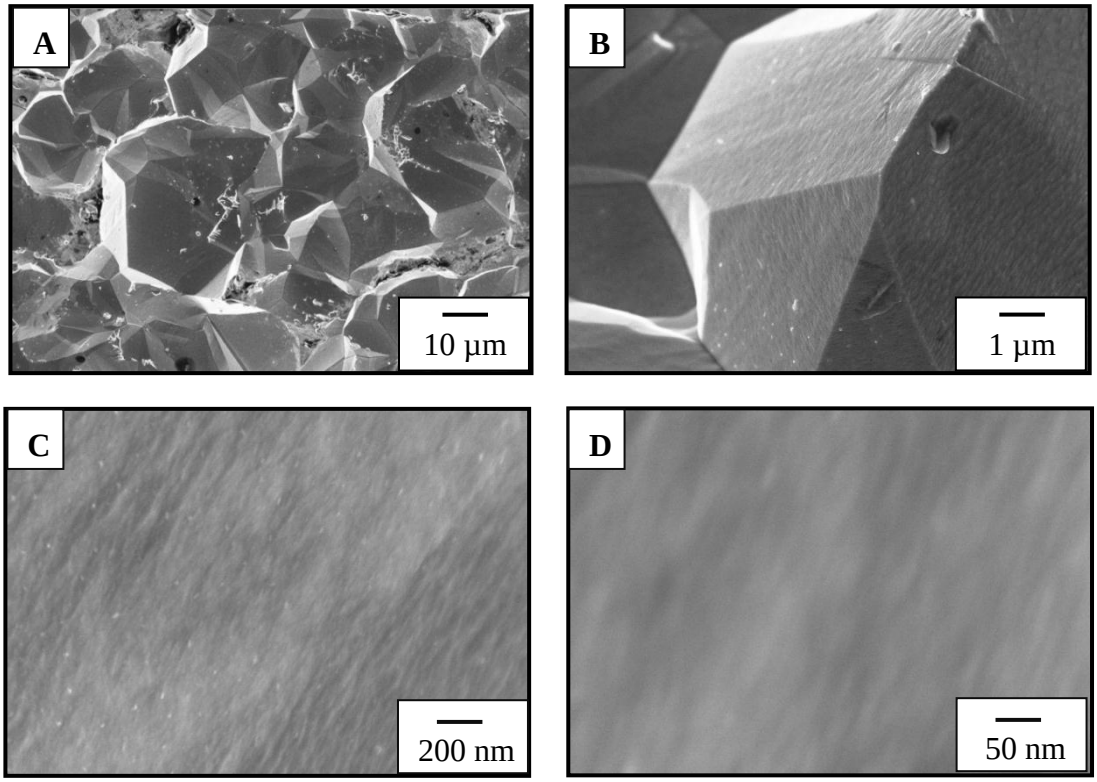

Figure 6.5 Surface morphologies of titanium plate (Sample A). Magnification: ×1,000 (A), ×10,000 (B), ×50,000 (C) and ×200,000 (D).

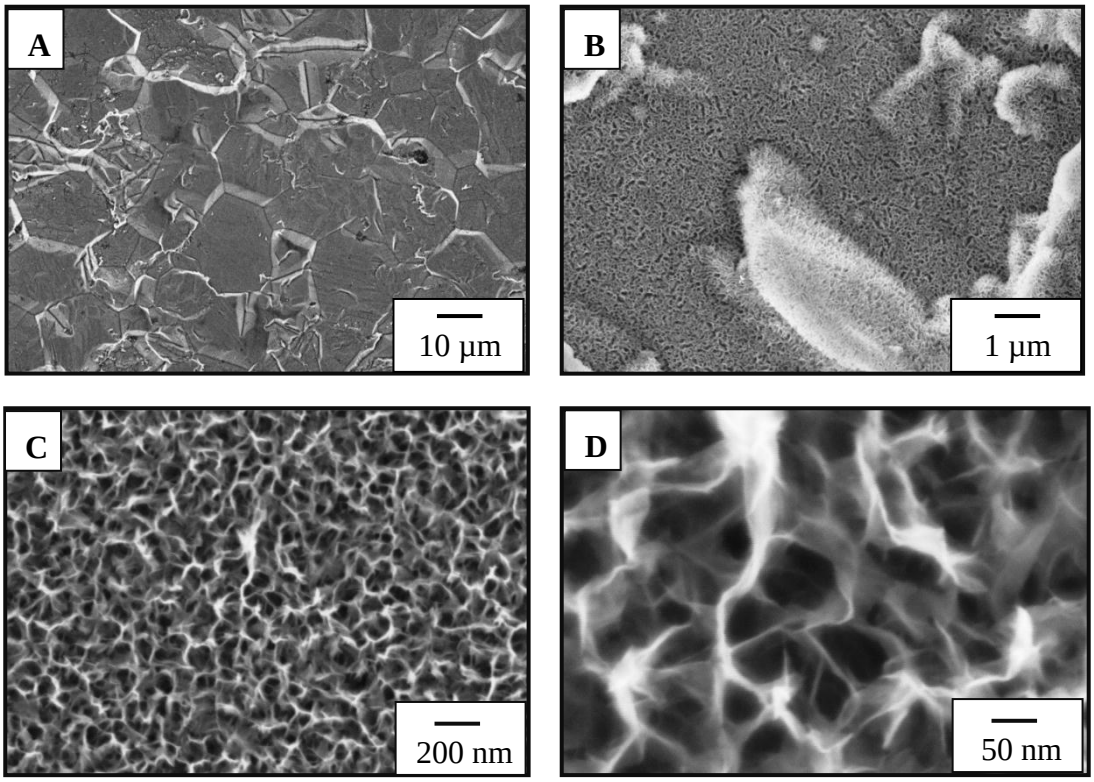

Figure 6.6 Surface morphologies of titanium plate (Sample B). Magnification: ×1,000 (A), ×10,000 (B), ×50,000 (C) and ×200,000 (D).

Figure 6.7 shows the cell voltage of the improved amorphous RuO_2-Ta_2O_5/Ti anode during constant current electrolysis at 500 A m^{-2}, a typical value of current density for Zn EW. In this figure, the cell voltages of the Pb-5%Sb alloy and amorphous IrO_2-Ta_2O_5/Ti anode are also shown for comparison. The cell voltage measured with the amorphous RuO_2-Ta_2O_5/Ti anode and the amorphous IrO_2-Ta_2O_5/Ti anode showed constant voltage during the electrolysis, while that with the lead alloy anode increased in the first 100 h and then slightly decreased, and became almost constant. This cell voltage change with the Pb alloy anode is reasonable, because PbO_2 is formed on the surface of the Pb alloy anode in parallel with oxygen evolution, by which the cell voltage increases due to the increase in the resistance of the anode.

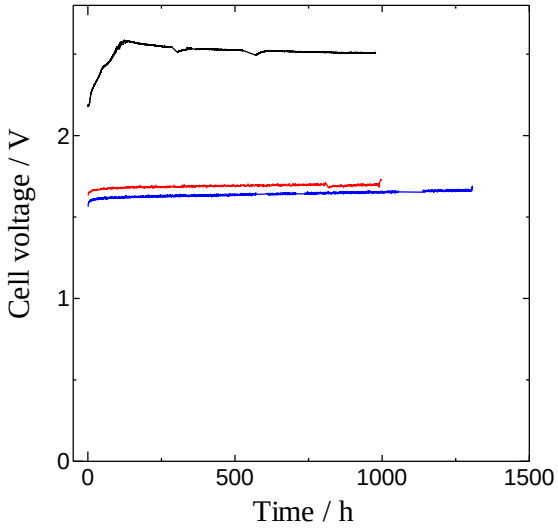

Figure 6.7 Variation in cell voltage during constant current electrolysis of amorphous RuO_2-Ta_2O_5/Ti anode (blue), amorphous IrO_2-Ta_2O_5/Ti anode (red) and Pb-5%Sb anode (black) at 500 A m^{-2} in 2.0 mol dm^{-3} H_2SO_4 solution at 40 ^oC.

The cell voltage measured with the amorphous RuO_2-Ta_2O_5/Ti anode or the amorphous IrO_2-Ta_2O_5/Ti anode was much lower than that of the Pb alloy anode. In addition, the amorphous RuO_2-Ta_2O_5/Ti anode showed lower cell voltage than the amorphous IrO_2-Ta_2O_5/Ti anode. For example, the cell voltages with the Pb alloy, the amorphous IrO_2-Ta_2O_5/Ti and amorphous RuO_2-Ta_2O_5/Ti anode at 1,000 hours were 2.51 V, 1.75 V and 1.65 V, respectively. Especially, the cell voltage with amorphous RuO_2-Ta_2O_5/Ti anode was 0.86 V lower than that with the lead alloy anode and was still 0.10 V lower than that with amorphous IrO_2-Ta_2O_5/Ti anode. Therefore, the results demonstrate that the improved amorphous RuO_2-Ta_2O_5/Ti anode has high durability for oxygen evolution and can keep low oxygen evolution potential for long time operation.

Figure 6.8 shows the photographs of the Pb alloy anode and the improved amorphous RuO_2-Ta_2O_5/Ti anode before and after the electrolysis at 500 A m^{-2}. After 1,000 hours electrolysis, Pb alloy anode was apparently consumed, and the amorphous RuO_2-Ta_2O_5/Ti anode showed no change.

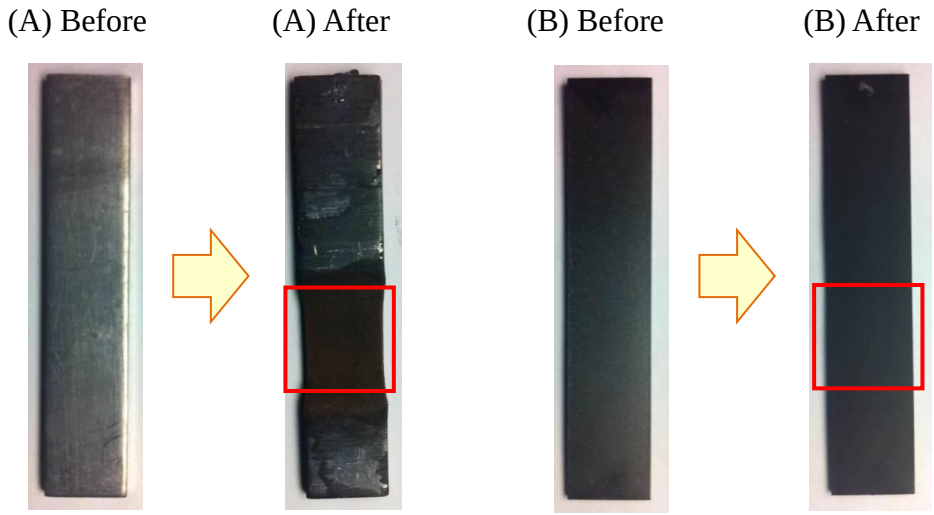

Figure 6.8 Overview images of Pb-5%Sb alloy anode (A) and amorphous RuO_2-Ta_2O_5/Ti anode (B) before and after the electrolysis at 500 A m^{-2} in 2.0 mol dm^{-3} H_2SO_4 solution at 40 ^oC.

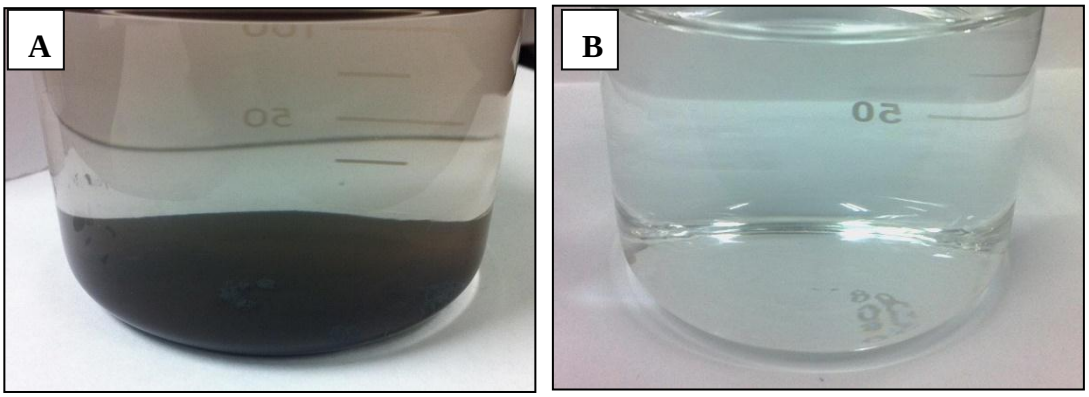

Figure 6.9 Electrolyte after the electrolysis at 500 A m^{-2}. Anode: Pb-5%Sb alloy (A), amorphous RuO_2-Ta_2O_5/Ti (B).

Figure 6.9 shows the photographs of the electrolytes used with each anode after the electrolysis, which clearly presents a significant difference that a large amount of sludge is observed with the Pb alloy anode, while the electrolyte was clear and no

sludge with the amorphous RuO_2-Ta_2O_5/Ti anode. From the results, it is concluded that less anode maintenance and no production of hazard byproducts are possible by replacing Pb alloy anode with the amorphous RuO_2-Ta_2O_5/Ti anode.

The cell voltage during ALT of the improved amorphous RuO_2-Ta_2O_5/Ti anode at a current density of 5,000 A m^{-2} is shown in Figure 6.10. The lifetime of the amorphous anode before the improvement was *ca.* 52 hours in Figure 6.1. Under the same electrolytic condition, the cell voltage of the improved anode was stable for *ca.* 2,000 hours, from which the amorphous anode can inhibit the substrate corrosion so as to prolong the lifetime drastically. It should be noted again that while the anode's lifetime depends on the preparation procedure and conditions such as pretreatment of titanium substrate, Ru:Ta ratio, the coating's amount, and the solvent and the additive to the precursor solution, this study has proven that the resulted surface morphology of the coatings, especially the generation and distribution nano-size of RuO_2 in amorphous Ta_2O_5 matrix, is quite important for the durability. As mentioned above, the amorphous RuO_2-Ta_2O_5/Ti anode is possible to reduce the number of cracks generated on the coating surface by the modification of the preparation procedure, so that there would be still a room to further enhance the durability of the amorphous anode.

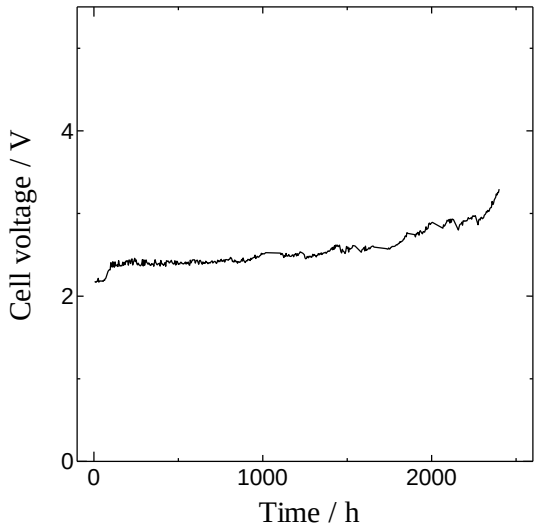

Figure 6.10 Variation in cell voltage during accelerated electrolysis of amorphous RuO_2-Ta_2O_5/Ti anode at 5,000 A m^{-2} in 2.0 mol dm^{-3} H_2SO_4 solution at 40 ^oC.

6.3 Conclusion

This chapter describes the degradation and lifetime improvement of the amorphous RuO_2-Ta_2O_5/Ti anode, in which the main reason for the degradation is not the consumption of the oxide coating and is the formation of non-conductive TiO_2 layer on the substrate caused by the penetration of the acidic solution to the substrate. A long lifetime of the amorphous anodes was successfully realized by modification of the preparation procedure to prevent the penetration of the electrolyte, and the lifetime more than 2,000 hours in ATL was demonstrated. The results also proved that low temperature thermal decomposition was possible to produce high catalytic and highly durable amorphous RuO_2-Ta_2O_5/Ti anodes for oxygen evolution.

6.4 References

[1] S. Trasatti, "Electrocatalysis in the anodic evolution of oxygen and chlorine", Electrochim. Acta, **29** (1984) 1503-1512.

[2] S. Trasatti, "Physical electrochemistry of ceramic oxides", Electrochim. Acta, **36** (1991) 225-241.

[3] Ch. Comninellis. G.P. Vercesi, "Characterization of DSA®-type oxygen evolving electrodes: choice of a coating", J. Appl. Electrochem., **21** (1991) 335-345.

[4] S. Trasatti, "Electrocatalysis: understanding the success of DSA®", Electrochim. Acta, **45** (2000) 2377-2385.

[5] C.P. de Pauli, S. Trasatti, "Composite materials for electrocatalysis of O_2 evolution: IrO_2+SnO_2 in acid solution", J. Electroanal. Chem., **538-539** (2002) 145-151.

[6] J. Melsheimer, D. Ziegler, "The oxygen electrode reaction in acid solutions on RuO_2 electrodes prepared by the thermal decomposition method", Thin Solid Films, **163** (1988) 301-308.

[7] R. Otogawa, K. Soda, S. Yamauchi, Y. Nagatoishi, M. Morimitsu, M. Matsunaga, "Morphological deterioration of iridium oxide-tantalum oxide anode by oxygen evolution", Denki Kagaku, **65** (1997) 987-991.

[8] R. Otogawa, K. Soda, H. Shimizu, T. Ikeda, M. Morimitsu, M. Matsunaga, "Effects of cathodizing on the durability of an IrO_2-based anode in an electrogalvanizing", Tetsu to Hagane, **84** (1998) 785-789. (in Japanese)

[9] H. Meng, M. Morimitsu, M. Matsunaga, R. Otogawa, "Effects of SnO_2 on the oxidation of PSA on IrO_2-based anodes", Denki Kagaku, **66** (1998) 1148-1149.

[10] R. Otogawa, H. Shimizu, T. Inoue, M. Morimitsu, M. Matsunaga, "Improved properties of IrO_2-based anodes for HCD electroplating", Proc. of 9th Continuous Steel Strip Plating Symp., AESF (1999) 11-16.

[11] T. Kunihiro, M. Morimitsu, M. Matsunaga, "Comparison of platinum with IrO_2-Ta_2O_5 system for the stannous ion consumption in methane sulfonic acid baths with and without catechol", J. Appl. Electrochem., **30** (2000) 359-364.

[12] R. Otogawa, M. Morimitsu, M. Matsunaga, "Development of a highly durable anode for electrogalvanizing lines", Nippon Kagaku Kaishi, **5** (2000) 299-350. (in Japanese)

[13] M. Morimitsu, R. Otogawa, M. Matsunaga, "Effects of cathodizing on the morphology and composition of IrO_2-Ta_2O_5/Ti anodes", Electrochim. Acta, **46** (1997) 401-406.

[14] H. Higobashi, "Highly-durable iridium oxide anode", J. Surface Finishing Soc. of Japan, **66** (2015) 3-5. (in Japanese)

[15] J.M. Hu, H.M. Meng, J.Q. Zhang, C.N. Cao, "Degradation mechanism of long service life Ti/IrO_2-Ta_2O_5 oxide anodes in sulphuric acid", Corrosion Science., **44** (2002) 1655-1668.

[16] Y. Kamegaya, K. Sasaki, M. Ogumi, T. Asaki, H. Kobayashi, T. Mitamura, "Improved durability of iridium oxide coated titanium anode with interlayers for oxygen evolution at high current densities", Electrochim. Acta, **40** (1995) 889-895.

[17] L.K Xu, J.D Scantlebury, "A study on the deactivation of an IrO_2-Ta_2O_5 coated titanium anode", Corrosion Science, **45** (2003) 2729-2740.

[18] J.Y. Lee, D.K. Kang, K.H. Lee, D.Y. Chang, "An Investigation on the electrochemical characteristics of Ta_2O_5-IrO_2 anodes for the application of electrolysis process", Mater. Sci. Appl., **2** (2011) 237-243.

[19] Z. Yan, H. Meng, "Effect of Different shapes of the titanium based IrO_2-Ta_2O_5 coatings anode on electrochemical properties", Rare Metal Materials and Engineering, **41** (2012) 772-775.

[20] S. Kulandaisamy, J.P. Rethinaraj, S.C. Chockalingam, S. Visvanathan, K.V. Venkateswaran, P. Ramachandran, V. Nandakumar, "Performance of catalytically activated anodes in the electrowinning of metals", J. Appl. Electrochem., **27** (1997) 579-583.

[21] X. Chen, G. Chen, "Investigation of Ti/IrO_2-Sb_2O_5-SnO_2 electrodes for O_2 evolution: calcination temperature and precursor composition effects", J. Electrochem. Soc., **152** (2005) J59-J64.

[22] B.S. Li, A. Lin, F.X. Gan, "Preparation and electrocatalytic properties of Ti/IrO_2-Ta_2O_5 anodes for oxygen evolution", Trans. Nonferrous Met. Soc. China, **16** (2006) 1193-1199.

[23] H.B. Xu, Y.H. Lu, C.H. Li, J.Z. Hu, "A novel IrO_2 electrode with iridium-titanium oxide interlayers from a mixture of TiN nanoparticle and H_2IrCl_6 solution", J. Appl. Electrochem., **40** (2009) 719-727.

[24] J. Krysa, L. Kule, R. Mraz, I. Rousar, "Effect of coating thickness and surface-treatment of titanium on the properties of IrO_2-Ta_2O_5 anodes", J. Appl. Electrochem., **26** (1996) 999-1005.

[25] J. Krysa, J. Maixner, R. Mraz, I. Rousar, "Effect of coating thickness on the properties of IrO_2-Ta_2O_5 anodes", J. Appl. Electrochem., **28** (1998) 369-372.

[26] G.P. Vercesi, J.Y. Salamin, Ch. Comninellis, "Morphological and microstructural study of the Ti/IrO_2-Ta_2O_5 electrode: effect of the preparation temperature", Electrochimica Acta, **36** (1991) 991-998.

[27] A.L. Antozzi, C.W. Brown, Jr., A. Calderara, "Novel DSA® anode for electrowinning of non-ferrous metals", Proc. of Electrometallurgy 2012, TMS (2012) 3-27.

[28] R. Otogawa, M. Morimitsu, M. Matsunaga, "Effects of microstructure of IrO_2-based anodes on electrocatalytic properties", Electrochim. Acta, **44** (1998) 1509-1513.

[29] F.I. Mattos-Costa, P. de Lima-Neto, S.A.S. Machado, L.A. Avaca, "Characterisation of surfaces modified by sol-gel derived $Ru_xIr_{1-x}O_2$ coatings for oxygen evolution in acid medium", Electrochim. Acta, **44** (1998) 1515-1523.

[30] Lj.M. Gajić-Krstajić, T.Lj. Trišović, N.V. Krstajić, "Spectrophotometric study of the anodic corrosion of Ti/RuO_2 electrode in acid sulfate solution", Corrosion Science, **46** (2004) 65-74.

[31] M.E.G. Lyons, S. Floquet, "Mechanism of oxygen reactions at porous oxide electrodes. Part 2-Oxygen evolution at RuO_2, IrO_2 and $Ir_xRu_{1-x}O_2$ electrodes in aqueous acid and alkaline solution", Phys. Chem. Chem. Phys., **13** (2011) 5314-5335.

[32] M. Vuković, D. Marijan1, D. Čukman, P. Pervan, M. Milun, "Electrocatalytic activity and anodic stability of electrodeposited ruthenium-rhodium coatings on titanium", J. Materials Science, **34** (1999) 869-874.

[33] R. Bertoncello, S. Cattarin, I. Frateur, M. Musiani, "Preparation of anodes for oxygen evolution by electrodeposition of composite oxides of Pb and Ru on Ti", J. Electroanalytical Chemistry, **492** (2000) 145-149.

[34] S.M. Hoseinieh, F. Ashrafizadeh, M.H. Maddahi, "A Comparative investigation of the corrosion behavior of RuO_2-IrO_2-TiO_2 coated titanium anodes in chloride solutions", J. Electrochem. Soc., **157** (2010) E50-E56.

[35] X. Chen, G. Chen, "Stable Ti/RuO_2-Sb_2O_5-SnO_2 electrodes for O_2 evolution", Electrochimica Acta, **50** (2005) 4155-4159.

[36] J.C. Cruz, S. Siracusano, V. Antonucci, A.S. Aricò, R. Ornelas, L. Ortiz-Frade, G. Osorio-Monreal, S.M. Durón-Torres, L.G. Arriaga, "Preparation and characterization of RuO_2 catalysts for oxygen evolution in a solid polymer electrolyte", Int. J. Electrochem. Sci., **6** (2011) 6607-6619.

[37] M.G. Pavlovic, A. Dekanski, "On the use of platinized and activated titanium anodes in some electrodeposition processes", J. Solid State Electrochem., **1** (1997)

208-214.

[38] V. Panić, A. Dekanski, S. K. Milonjić, R.T. Atanasoski, B.Ž. Nikolić, "RuO_2-TiO_2 coated titanium anodes obtained by the sol–gel procedure and their electrochemical behaviour in the chlorine evolution reaction", Colloids Surfaces A: Physicochem. Eng. Asp., **157** (1999) 269-274.

[39] V. Panić, A. Dekanski, S. Milonjić, R. Atanasoski, B. Nikolić, "The influence of the aging time of RuO_2 and TiO_2 sols on the electrochemical properties and behavior for the chlorine evolution reaction of activated titanium anodes obtained by the sol-gel procedure", Electrochimica Acta, **46** (2000) 415-421.

[40] O.R. Camara, S. Trasatti, "Surface electrochemical properties of Ti/(RuO_2+ZrO_2) electrodes", Electrochim. Acta, **41** (1996) 419-427.

[41] A.J. Terezo, E.C. Pereira, "Preparation and characterization of Ti/RuO_2 anodes obtained sol-gel and conventional method", Materials Letters, **53** (2002) 339-345.

[42] J. Ribeiro, A.R. de Andrade, "Characterization of RuO_2-Ta_2O_5 coated titanium electrode microstructure, morphology, and electrochemical investigation", J. Electrochem. Soc., **151** (2004) D106-D112.

[43] H. Tokudome, M. Miyauchi, "Electrochromism of Titanate-based nanotubes", Angew. Chem. Int., **44** (2005) 1974-1977.

[44] M. Miyauchi, H. Tokudome, Y. Toda, T. Kamiya, H. Hosono, "Electron field emission from TiO_2 nanotube arrays synthesized by hydrothermal reaction", Appl. Phys. Lett., **89** (2006) 043114.

[45] M. Miyauchi, H. Tokudome, "Super-hydrophilic and transparent thin films of TiO_2 nanotube arrays by a hydrothermal reaction", J. Mater. Chem., **17** (2007) 2095-2100.

Chapter 7 Summary

In this PhD thesis, a novel RuO_2-Ta_2O_5/Ti anode with low overpotential and high durability for oxygen evolution was developed by thermal decomposition with the detailed investigation on the preparation conditions such as thermal decomposition temperature and the oxide composition in order to replace Pb alloy anodes which have been employed in commercial EW processes despite its quite low oxygen evolution activity and stability.

The decrease in thermal decomposition temperature, *e.g.*, at 280 ^oC, lead to the amorphization of RuO_2 in the coating for a wide range of Ru:Ta mole ratio, and nano RuO_2 particles, which are highly active for oxygen evolution, were uniformly dispersed in amorphous Ta_2O_5 matrix. Such nano RuO_2 particles induced the increase in effective surface area for oxygen evolution and were more active than large and crystallized RuO_2 observed on the crystalline coating obtained at higher temperature. The unique surface morphology of the amorphous anode attributed to reduce the overpotential of oxygen evolution and resulted in a significant decrease in cell voltage for electrowinning of copper, zinc, nickel and cobalt. The amorphous RuO_2-Ta_2O_5/Ti anode at 80 mol% Ru calcined at 260 ^oC, which is the most active anode for oxygen evolution and superior to other anodes, demonstrated that the cell voltage of EW was reduced by 0.7 V compared to lead alloy anodes and a maximum voltage reduction of 37 % was achieved for copper EW. A simple calculation gave us that the cell voltage reduction in zinc and copper EW worldwide may equal to 13,900 GWh which corresponds to 1,280,000 households of electric energy consumption per year in U.S.A. Therefore, a significant energy saving will be possible, when the anode is changed from the Pb alloy to the amorphous RuO_2-Ta_2O_5/Ti anode developed in this study.

Another distinct feature of the amorphous RuO_2-Ta_2O_5/Ti anodes is that nano RuO_2 particles reduces the overpotential of oxygen evolution, but increases that of the

unwanted side reaction on the anode, so that the anodic deposition of PbO_2 can be completely inhibited on the developed amorphous anode. This excellent achievement is valuable to improve the purity of electrowon metal, reduce the maintenance of electrolysis process, prolong the lifetime of the anode, and make a low impact to environment.

The enhancement of lifetime of the amorphous RuO_2-Ta_2O_5/Ti anodes was further achieved by modification of the preparation procedure and condition. The lifetime of the amorphous anode was more than 2,000 hours even at high current density of 5,000 A m^{-2}, which is the data enough for practical uses in EW. The new technique on production of the anode is a significant step for RuO_2-based anodes, which is not possible with other existing methods.

Furthermore, the research achievements of this thesis and the learning contents in relation to advanced doctoral program in Global Resource Management (GRM) are expected to help the establishment and development of industries and the national construction in least developed and disputed countries in the near future.

List of publications

Papers:

[1] M. Morimitsu, T. Yamaguchi, N. Oshiumi, T. Zhang, "Energy-Efficient Electrowinning Process with Smart Anode Comprising Nano-Oxide Catalyst", Proc. of European Metallurgical Conference 2011, GDMB (2011) 975-984.

[2] T. Zhang, M. Morimitsu, "A Novel Oxygen Evolution Anode for Electrowinning of Non-ferrous Metals", Proc. of Electrometallurgy 2012, TMS (2012) 29-34.

[3] M. Morimitsu, T. Zhang, Y. Yamada, "A State of The Art Anode Technology: Smart Anode, MSA®, For Copper Electrowinning", Proc. of Copper 2013, **5** (2013) 85-94.

[4] M. Morimitsu, T. Zhang, M. Ueda, "Amorphous Oxide Coated Titanium Anode, MSA®, for Energy-Efficient Zinc Electrowinning without Manganese Oxide Deposition, Proc. Pb-Zn 2015, **2** (2015) 771-777.

[5] T. Zhang, M. Morimitsu, "Effects of Amorphization of RuO_2-Ta_2O_5 Catalytic Coating (Ru=30 mol%) on Oxygen Evolution in Sulfuric Acid Solution", Journal of MMIJ, accepted.

Presentations – Oversea:

[1] T. Zhang, M. Morimitsu, "Highly Sensitive and Selective Oxide Catalyst to H_2O_2 Reduction for Biosensing Applications", The 218th ECS Meeting, Abs #12, Las Vegas, USA (2010).

[2] T. Zhang, N. Osada, K. Hashimoto, M. Morimitsu, "A Novel Method to Detect H_2O_2 with IrO_2-based Catalysts for Biosensing Applications", The 62nd ISE Meeting, Niigata, Japan (2011).

[3] M. Morimitsu, T. Yamaguchi, N. Oshiumi, T. Zhang, "Energy-Efficient Electrowinning Process with Smart Anode Comprising Nano-Oxide Catalyst",

EMC 2011, Hamburg, Germany (2011).

[4] T. Zhang, M. Morimitsu, "A Novel Oxygen Evolution Anode for Electrowinning of Non-ferrous Metals", TMS 2012, Orlando, USA (2012).

[5] T. Zhang, M. Morimitsu, "A Novel Amorphous Oxide Anode for O_2 Evolution in Electrometallurgy", The 63rd ISE Meeting, Prague, Czech Republic (2012).

[6] K. Izumi, T. Zhang, M. Morimitsu, "Gas Evolution Behaviors and Co(Ⅱ) Oxidation on RuO_2-based Catalytic Coatings", The 63rd ISE Meeting, Prague, Czech Republic (2012).

[7] M. Ueda, T. Zhang, M. Morimitsu, "A Novel Anode Using Nano RuO_2 for Zn Electrowinning: Catalytic to O_2 and Non-catalytic to Mn Oxide Deposition", The 63rd ISE Meeting, Prague, Czech Republic (2012).

[8] Y. Yamada, T. Zhang, M. Morimitsu, "Enhanced O_2 Evolution and Suppressed PbO_2 Deposition on Amorphous RuO_2-based Oxide Anodes", The 63rd ISE Meeting, Prague, Czech Republic (2012).

[9] T. Zhang, M. Morimitsu, "Characterization and Performance of Non-Iridium Oxide Based Oxygen Evolution Anodes", The 222nd ECS Meeting, Honolulu, USA (2012).

[10] N. Ohnishi, M. Matsuda, T. Zhang, M. Morimitsu, "Morphology of Self-ordered Nano Oxide Coatings for Oxygen and Chlorine Evolution", The 222nd ECS Meeting, Honolulu, USA (2012).

[11] M. Ueda, T. Zhang, M. Morimitsu, "Effects of Interferents on H_2O_2 Quantification by Electrochemical Reduction on IrO_2 Electrodes", The 222nd ECS Meeting, Honolulu, USA (2012).

[12] T. Zhang, M. Morimitsu, "Amorphous RuO_2-Ta_2O_5/Ti Anode for Oxygen Evolution: Voltage Reduction and Durability for Electrowinning", The 64th ISE Meeting, Santiago de Queretaro, Mexico (2013).

[13] Y. Yamada, T. Zhang, M. Morimitsu, "A Novel Copper Electrowinning Anode Using Amorphous RuO_2-Ta_2O_5", The 64th ISE Meeting, Santiago de Queretaro, Mexico (2013).

[14] M. Ueda, T. Zhang, M. Morimitsu, "A Novel Zinc Electrowinning Anode Comprising Amorphous RuO_2-Ta_2O_5 Catalyst", Materials Science & Technology, Quebec, Canada (2013).

[15] K. Izumi, T. Zhang, M. Morimitsu, "Development of RuO_2-Ta_2O_5/Ti Anode for Cobalt Electrowinning Using Acidic Chloride Solutions", Materials Science & Technology, Montreal, Quebec, Canada (2013).

[16] S. Unoki, T. Zhang, M. Morimitsu, "Effects of Crystallographic Structure of IrO_2-Ta_2O_5 Catalyst on Oxygen Evolution in Alkaline Solutions", The 224th ECS Meeting, San Francisco, USA (2013).

[17] T. Zhang, M. Morimitsu, "Development of Smart Anode for Energy Saving of Metal Electrowinning", The 8th Joint Symposium between Chonnam National University and Doshisha University, Kyoto, Japan (2013).

[18] M. Morimitsu, T. Zhang, Y. Yamada, "A State of The Art Anode Technology: Smart Anode, MSA®, For Copper Electrowinning", Copper 2013, Santiago, Chile (2013).

[19] T. Zhang, M. Ueda, Y. Yamada, M. Morimitsu, "Development of Amorphous Oxide Coated Anode for Electrowinning of Zinc and Copper", 225th ECS meeting, Orlando, USA (2014).

[20] T. Morishita, T. Zhang, M. Morimitsu, "Preparation of IrO_2-Ta_2O_5 Coatings on Ni Substrate and Oxygen Evolution in Alkaline Aqueous Solution", The 226th ECS Meeting, Cancun, Mexico (2014).

[21] K. Kawaguchi, T. Zhang, M. Morimitsu, "Ordered Nano Oxide Particles in Amorphous Non-catalytic Oxide Matrix of Smart Anode for Oxygen Evolution", 10th International Symposium on Electrochemical Micro & Nanosystem Technologies, Okinawa (2014).

[22] T. Zhang, M. Morimitsu, "A Novel Anode Technology for Electrochemical Energy Conversion in Electrometallurgical Processes", 2015 MRS Spring Meeting, San Francisco, USA (2015).

Presentations – Japan:

[1] T. Zhang, M. Morimitsu, "Sensing Performance of H_2O_2 on IrO_2 Electrodes" , The 20th Symposium on Electrode Materials, Yokohama (2010).

[2] M. Morimitsu, T. Zhang, "Reduction of H_2O_2 on Amorphous Oxide Based Electrodes", The 123rd Meeting of the Surface Finishing Society of Japan, Yokohama (2011).

[3] T. Zhang, M. Morimitsu, "Development of Non-Iridium Oxide Based Oxygen Evolution Anodes for Electrowinning", MMIJ 2011, Osaka (2011).

[4] M. Ueda, T. Zhang, M. Morimitsu, "Suppression of Mn Oxide Deposition on the RuO_2-based Anode in Zinc Electrowinning", MMIJ 2012, Akita (2012).

[5] K. Izumi, T. Zhang, M. Morimitsu, "Anodic Reactions on RuO_2-based Anodes in Cobalt Electrowinning", MMIJ 2012, Akita (2012).

[6] N. Ohnishi, M. Matsuda, T. Zhang, M. Morimitsu, "Crystallographic Structure and Surface Morphology of RuO_2-based Catalyst for Electrowinning", MMIJ 2012, Akita (2012).

[7] Y. Yamada, T. Zhang, M. Morimitsu, "Prevention of Anodic PbO_2 Deposition on the Anode in Copper Electrowinning", MMIJ 2012, Akita (2012).

[8] T. Zhang, M. Morimitsu, "Electrolytic Performance of a Metal Electrowinning Anode Comprising a Nano/Amorphous Hybrid Structure of Catalyst Layer", The 9th Young Researchers' Symposium of Kansai Branch, MMIJ, Kyoto (2012).

[9] S. Unoki, T. Zhang, M. Morimitsu, "Effects of Crystallographic Structure of Catalytic Layer on Oxygen Evolution on IrO_2-Ta_2O_5/Ti Electrodes in Alkaline Solutions", The 23rd Symposium of Electrode Materials, Yamanashi (2013).

[10] T. Zhang, M. Morimitsu, "Oxygen Evolution Behaviors of RuO_2-Ta_2O_5/Ti Anodes in Sulfuric Acid Solutions: Effects of Composition and Structure", The 37th Symposium on Electrolysis Technology, Japan, Osaka (2013).

[11] H. Shobayashi, T. Zhang, M. Morimitsu, "Effects of Thermal Decomposition Temperature of RuO_2-Ta_2O_5 Catalytic Coatings on Oxygen Evolution Behaviors in Alkaline Solutions", The 37th Symposium on Electrolysis Technology, Japan,

Osaka (2013).

[12] K. Kumamoto, T. Zhang, M. Morimitsu, "Effects of Composition of IrO_2-Ta_2O_5 Catalyst for Oxygen Evolution in Alkaline Solution", The 24th Symposium on Electrode Materials, Yamanashi (2014).

[13] Y. Ishimura, T. Zhang, M. Morimitsu, "Oxygen Reduction Behaviors of RuO_2-Ta_2O_5 Mixed Oxide in Alkaline Solution", The 24th Symposium on Electrode Materials, Yamanashi (2014).

[14] T. Zhang, Y. Yamada, M. Ueda, K. Izumi, M. Morimitsu, "Voltage Reduction and Suppression of Side Reactions on Amorphous RuO_2-based Oxide Anodes for Electrowinning", MMIJ 2014, Kumamoto (2014).

[15] T. Morishita, T. Zhang, M. Morimitsu, "Preparation of IrO_2-Ta_2O_5 Coatings on Ni Substrate and Electrode Performance in Alkaline Aqueous Solution", The 130th Meeting of the Surface Finishing Society of Japan, Kyoto (2014).

[16] M. Yamamoto, T. Zhang, M. Morimitsu, "Sensing of Hydrogen Phosphate Ion with Iridium Oxide Based Catalysts", The 130th Meeting of the Surface Finishing Society of Japan, Kyoto (2014).

[17] R. Asami, T. Zhang, M. Morimitsu, "Anodic Reaction and Chronoamperometric Response of H_2O_2 on RuO_2-Ta_2O_5 Catalyst", 2014 Fall Meeting of Electrochemical Society of Japan, Sapporo (2014).

[18] T. Tsukuma, T. Zhang, M. Morimitsu, "Oxidation and Detection of HPO_4^{2-} on RuO_2-Ta_2O_5 Mixed Oxide", The 38th Symposium on Electrolysis Technology, Saitama (2014).

[19] H. Shobayashi, T. Zhang, M. Morimitsu, "Anodic Electrolysis Behaviors of Ru-based Oxide Coated Electrode in Alkaline Aqueous Solutions", The 34th Meeting of Hydrogen Energy Systems Society of Japan, Tokyo (2014).

[20] T. Zhang, M. Morimitsu, "Application of Catalytic Coating Comprising RuO_2 Nano-particles Dispersed in Amorphous Ta_2O_5 Matrix to Metal Electrowinning Anode", The 16th Forum on Surface Technology in Kansai, the Surface Finishing Society of Japan, Hyogo (2012).

[21] T. Tsukuma, T. Zhang, M. Morimitsu, “Effects of Composition and Structure of RuO_2-based Oxide Catalyst for Detection of Hydrogen Phosphate Ion”, The 16th Forum on Surface Technology in Kansai, the Surface Finishing Society of Japan, Hyogo (2012).

[22] M. Yamamoto, T. Zhang, M. Morimitsu, “Electrochemical Detection of Hydrogen Phosphate Ion by IrO_2-Ta_2O_5 Catalyst”, 2014 The 3rd Meeting of Kansai Branch of The Electrochemical Society of Japan, Osaka (2014).

[23] R. Asami, T. Zhang, M. Morimitsu, “Electrochemical Sensing of Hydrogen Peroxide by RuO_2-based Mixed Oxide Catalyst”, 2014 The 3rd Meeting of Kansai Branch of The Electrochemical Society of Japan, Osaka (2014).

[24] H. Shobayashi, T. Zhang, M. Morimitsu, “Polarization Behaviors of Ru-based Oxide Coated Electrode for Oxygen Evolution in Alkaline Solutions”, 2014 The 3rd Meeting of Kansai Branch of The Electrochemical Society of Japan, Osaka (2014).

[25] T. Morishita, T. Zhang, M. Morimitsu, “Oxygen Evolution Behaviors of IrO_2-Ta_2O_5 Coated Nickel Electrode in Alkaline Solutions”, 2014 The 3rd Meeting of Kansai Branch of The Electrochemical Society of Japan, Osaka (2014).

[26] K. Kumamoto, T. Zhang, M. Morimitsu, “Effects of Composition of IrO_2-Ta_2O_5 Coated on Titanium on Oxygen Evolution in Alkaline Solutions”, 2014 The 3rd Meeting of Kansai Branch of The Electrochemical Society of Japan, Osaka (2014).

Awards:

[1] The Outstanding Presentation Award at the 9th Young Researchers' Symposium of Kansai Branch, the Mining and Materials Processing Institute of Japan, Kyoto (2012)

- Paper title: Electrolytic Performance of a Metal Electrowinning Anode Comprising a Nano/Amorphous Hybrid Structure of Catalyst Layer
- Co-author: Professor Masatsugu Morimitsu

[2] The Outstanding Presentation Award at the 16th Forum on Surface Technology in Kansai, the Surface Finishing Society of Japan, Hyogo (2014)

- Paper title: Application of Catalytic Coating Comprising RuO_2 Nano-particles Dispersed in Amorphous Ta_2O_5 Matrix to Metal Electrowinning Anode
- Co-author: Professor Masatsugu Morimitsu

In relation to Advanced Doctoral Program in Global Resource Management (GRM) which is a program implemented by the Ministry of Education, Culture, Sports, Science and Technology (MEXT) of Japan, aimed at providing world-class graduate education.

Papers:

[1] T. Zhang, "Development of Infrastructure in the Kingdom of Cambodia: Export of Water Technology by Kitakyushu", Global Resource Management, **1** (2014) 151-159.

[2] X. Wang, T. Zhang, J. E. Lamas, K. Nakamura, "Electricity Supply to a Local/Isolated Area by Means of Renewable Energy", Global Resource Management, **1** (2014) 123-131.

[3] J. E. Lamas, T. Inui, K. Nakamura, X. Wang, T. Zhang, M. Taketani, N. Nishi, T. Moriyama, N. Nakao, R. Arakawa, K. Abdearahmanov, "Reconstruction of Syria's Electric Power Infrastructure using Renewable Energies", Global Resource Management, **1** (2014) 111-121.

Presentations – Oversea:

[1] X. Wang, T. Zhang, J. E. Lamas, K. Nakamura, "Electricity Supply to a Local/Isolated Area by Means of Renewable Energy", 2013 International Workshop on Renewable Energy, Hanoi, Vietnam (2013).

[2] J. E. Lamas, T. Inui, K. Nakamura, X. Wang, T. Zhang, M. Taketani, N. Nishi, T. Moriyama, N. Nakao, R. Arakawa, K. Abdearahmanov, "Reconstruction of Syrian Electric Power Infrastructures by Renewable Energy", 2013 International Workshop on Renewable Energy, Hanoi, Vietnam (2013).